

Kristoffer Tallhaug Sydnes
David Forrestad Swensen

Monocoque Optimization

of the DNV GL Fuel Fighter Car

Master's thesis in Mechanical Engineering
Supervisor: Knut Einar Aasland
June 2019



Kristoffer Tallhaug Sydnes
David Forrestad Swensen

Monocoque Optimization

of the DNV GL Fuel Fighter Car

Master's thesis in Mechanical Engineering
Supervisor: Knut Einar Aasland
June 2019

Norwegian University of Science and Technology
Faculty of Engineering
Department of Mechanical and Industrial Engineering

1 Abstract

In this thesis, generative design was applied in an effort to reduce the weight of the DNV GL Fuel Fighter car, by optimizing the shape and composite laminate of the car's monocoque. Topology optimization was used to locate the critical load paths in the car, in order to find the optimal shape and internal structure of the monocoque using a minimal amount of material. Composite optimization was used to find the optimal shapes, thicknesses, orientations and stack sequences of the composite laminate the car consists of, as well as discovering which areas required extra reinforcement from sandwich panels. By researching the latest composite material technology as well as utilizing an optimization software called Hyperworks, the monocoque of the DNV GL Fuel Fighter car experienced a weight reduction of 45%, while still retaining sufficient stiffness and structural integrity.

I denne masteren har generativt design blitt brukt til å redusere vekten til DNV GL Fuel Fighter sin fullelektriske bil. Denne vektreduksjonen ble oppnådd ved å optimalisere komposittstrukturen til bilens monocoque. Topologioptimalisering ble brukt til å lokalisere de større spenningene gjennom bilen, for så å finne den optimale formen og indre strukturen på monocoquen ved minimalt bruk av materiale. Komposittoptimalisering ble utnyttet for å finne optimal form, tykkelse, orientering og rekkefølge på komposittlaminatet som bilen består av, samt oppdage hvilke områder som trengte forsterkning av en sandwich-struktur. Ved å utforske moderne kompositteknologi, samt utnytte optimaliseringsprogrammet Hyperworks, ble vekten av monocoquen til DNV GL Fuel Fighter sin bil redusert med 45%, samtidig som den strukturelle styrken ble iveretatt.

Contents

1	Abstract	i
2	Acknowledgements	1
3	Introduction	2
4	Theory	3
4.1	Generative Design	3
4.2	Software	3
4.3	Monocoque	4
4.4	Model set-up	4
4.4.1	Mesh	4
4.4.2	Load cases	6
4.5	Optimization set-up	6
4.5.1	Design Variables	6
4.5.2	Responses	8
4.5.3	Constraints	8
4.5.4	Objectives	9
4.6	Composites	9
4.6.1	Carbon Fibre	10
4.6.2	Core Material	12
4.6.3	Resin	14
4.6.4	Manufacturing methods	15
5	Method	17
5.1	Load Cases	18
5.2	Topology Optimization	23
5.2.1	Model set-up	23
5.2.2	Optimization set-up	26
5.3	Free Shape Optimization	27
5.3.1	Model set-up	27

5.3.2	Optimization set-up	28
5.4	Composite Optimization	29
5.4.1	Model set-up	29
5.4.2	Optimization set-up	36
5.4.3	FEM-analysis	39
5.5	Topology optimization of the inner structure	39
5.5.1	Model set-up	39
5.5.2	Optimization set-up	41
5.6	Material testing	42
5.6.1	Resin	42
5.6.2	Core material	43
5.6.3	Carbon fibre	43
5.7	Production	43
6	Results	45
6.1	Topology optimization	45
6.1.1	Iteration 1	45
6.1.2	Iteration 2	47
6.1.3	Iteration 3	50
6.2	Free shape optimization	52
6.3	2D topology optimization	54
6.4	Composite optimization	56
6.4.1	Free-Size	56
6.4.2	Sizing	60
6.4.3	Shuffling	62
6.5	Topology optimization of the inner structure	64
6.6	Material selection	68
6.7	Production	70
7	Discussion	77
7.1	Load cases	77
7.2	Topology optimization	79
7.3	Free shape optimization	81

7.4	2D topology optimization	81
7.5	Composite optimization	81
7.5.1	Free-size optimization	82
7.5.2	Sizing	84
7.5.3	Shuffling	84
7.6	Topology optimization of the inner structure	86
7.7	Material selection	90
7.8	Production	92
8	Conclusion	99
	References	100
	Websites	101
	Appendices	103
A	Calculations for braking and turning forces	103
B	Stress contour plots after the first free-size optimization	108
C	Ply shapes	117
D	Displacements for the final design	124
E	Risk assessment	133

2 Acknowledgements

First of all we would like to thank our thesis advisor, professor Knut Einar Aasland of the Department of Mechanical and Industrial Engineering, NTNU. He has allowed us to be creative and explore a field outside of DNV GL Fuel Fighters usual operations, while providing invaluable guidance throughout the entire process. We would also like to thank the rest of the DNV GL Fuel Fighter team for all the time and effort they have put into making this project a reality. Lastly, we would like to thank Altair for providing us with both the software that has been the cornerstone to this thesis, as well as technical support during our work.

3 Introduction

DNV GL Fuel Fighter is a student organization dedicated to building the world's most energy-efficient car. During the summer of 2018, the team attended the Shell Eco-Marathon competition in London, an international competition where student teams from several nations across the world compete in energy efficiency. DNV GL Fuel Fighter managed to reach second place in the battery-electric class. The Fuel Fighter car, primarily composed of carbon fiber, weighed 88 kg. Approximately half of this weight originated from the car's monocoque, which is its load-carrying outer shell. For the 2019 competition, it was decided that DNV GL Fuel Fighter would commit additional resources into lowering the weight of the monocoque, in order to increase the energy efficiency of the car. To achieve this, several steps were taken, such as re-evaluating material choices and looking at different methods for producing composite laminates. The most critical step, however, was using topology and composite optimization software to find the optimal design for weight and stiffness.

Traditionally, when designing a car, one would have to sacrifice one mechanical property, e. g. strength, to improve on another, e. g. lower the mass. Using topology optimization, it is possible to find a design that meets both these criteria. It is a tool that utilizes Finite Element Analysis to create radically different designs that no human could have created on their own. In addition to topology optimization, composite optimization is used to obtain optimal thicknesses and shapes for every carbon fibre ply throughout the car. In this thesis, topology and composite optimization will be used to lower the weight of the Fuel Fighter car's monocoque, while retaining enough stiffness to be safely driven and meet the requirements for the Shell Eco-Marathon competition, set by Shell's rulebook.

It is assumed that the reader of this thesis possesses a basic understanding of composite terminology and finite element methods used in software.

4 Theory

4.1 Generative Design

Traditional product development is characterized by its use of educated guesses. No matter how many calculations are done beforehand, a human being still has to make the final decision of where to place the material in a structure and how much to use. This leaves room for guesswork. When a prototype is made, it might work for its intended use, but there is uncertainty regarding its optimality. Generative design is a way to circumvent this uncertainty. Using this method, the part is first modeled as a chunk of material using CAD software. The geometry is imported into a mesher, where it is discretized into elements that can be analyzed using FEM. The mesh is constrained and forces are applied in accordance with the stresses the part will be subjected to during its lifetime. Finally, it is run through the software's solver, where the entire solution space is searched in order to find the best geometry for the part. When the solver converges after a certain number of iterations, the resulting part will have the optimal design.

4.2 Software

Several types of software exist for generative design, such as ANSYS, Abaqus, Autodesk Fusion 360, etc. For this project, Altair Hyperworks was chosen for the analysis and optimization done on the DNV GL Fuel Fighter car. The reason for this choice is the fact that Hyperworks is the most comprehensive, open architecture CAE simulation platform in the industry, ensuring good and realistic results. It is also one of the few programs that offers finite element analysis and optimization processes on composite laminates. In addition, Altair offers live online courses on their software.

Hyperworks is a collection of many modules. Hypermesh is the module where the model set-up and optimization set-up is done, while Optistruct is the solver where the optimization itself occurs. The results are visualized in Hyperview. For making the CAD model of the car, DNV GL Fuel Fighter used Fusion 360. The software offers cloud-based storage, meaning every team member can access all the model files at any time and in any place.

4.3 Monocoque

When building a car, one central aspect of the design is the chassis. The chassis carries the weight of the car, as well as any loads the car is subjected to. It also affects the final design of the car, both aerodynamically and aesthetically. There are two main types of chassis: structural shell and structural frame[14]. A structural shell is what is commonly known as a monocoque, and is the chassis type used for the DNV GL Fuel Fighter car. In a monocoque type chassis, the loads and stresses are carried by the outer shell of the vehicle, as opposed to an inner framework. For a given vehicle shape, a monocoque will generally be lighter than other chassis types[15]. Hence, a monocoque chassis was a natural choice for DNV GL Fuel Fighter in order to make the car more fuel efficient. It is also easier to make a shell rather than a frame when building with carbon fiber, as the material consists of large, thin sheets. A drawback of using a monocoque chassis is that wear and tear on the outer shell of the car will weaken the entire structure. This was not a big hurdle for DNV GL Fuel Fighter, since the car was only designed for the annual Shell Eco-Marathon competition, as opposed to daily use. In reality, the chassis type of the DNV GL Fuel Fighter car is actually a monocoque hybrid, as there are some internal structural elements present, that support loads in combination with the outer shell.

4.4 Model set-up

4.4.1 Mesh

When the CAD model is imported into the meshing software, the model is a continuous body. To be able to perform FEM analysis on it, it needs to be divided into discrete elements. The collection of these elements is called a mesh. The parameters of the mesh are the element size and the element type. In the 3D case, the two main element types are tetrahedral (figure 1a) and hexahedral (figure 1b). Hexahedral elements generally provide more accurate results when applied in structural analysis, but the meshing process is time consuming and requires more experience to perform correctly[1]. Tetrahedral elements are faster to mesh, but provides less accuracy. However, making the elements second order tetrahedral will improve the mesh quality to comparable levels of a hexahedral mesh.

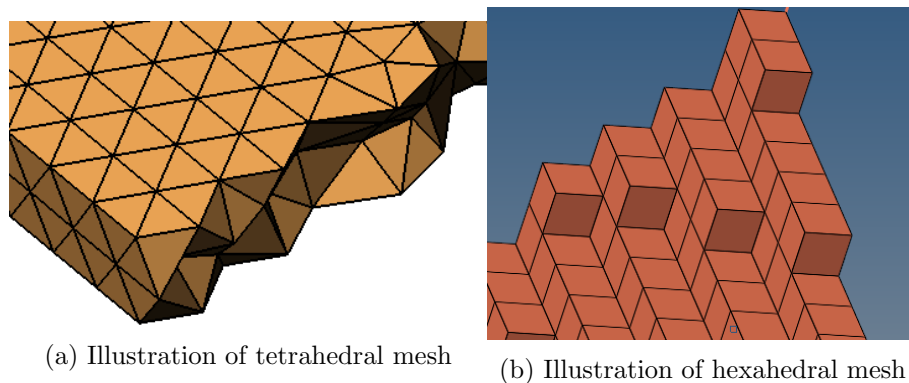


Figure 1

A 2D-shell model needs a 2D-mesh. A 2D-mesh can be constructed with different types of elements, just as a 3D-model. The most common ones are quadrilateral (figure 2a) and triangular (figure 2b). These are elements that have the shape of a square and a triangle, respectively. Triangular elements are inherently stiffer elements, and due to their shape and the underlying mathematical principles, triangular elements tend to result in larger errors than quadrilateral elements. Using triangular exclusively can often result in singularities, and should be avoided. For geometries with complex shapes, quadrilateral elements are harder to apply. With this in mind, a mix of quadrilateral and triangular are often preferred.

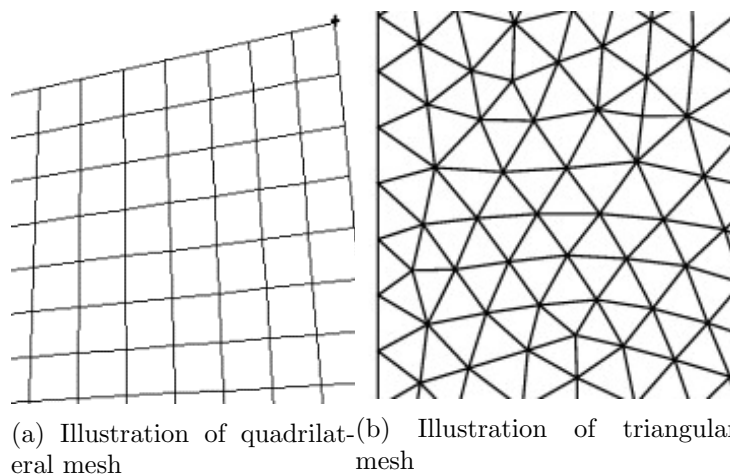


Figure 2

The meshing process includes adding point masses, in addition to 1D-

elements such as RBE2 and RBE3 elements. RBE means rigid body elements. These 1D-elements are used to connect two or more nodes in a meshed model. They are divided into two different groups, RBE2 and RBE3. For RBE2 elements, one node serves as a master node and the other(s) serve as slave nodes. The slave nodes follow the motion of the master node. They are often used to connect two dissimilar meshes, represent stiff beams in a structure, or to transfer loads. RBE2 elements are infinitely stiff, and tends to induce a stiffness to the model that might not be desired [16]. RBE3 elements do not induce undesired stiffness to the model, thus unsuitable for connecting meshes or act as stiff beams. However, RBE3 elements are suitable for cases where you want to have motion in a node as a function of the weighted average of other nodes[16].

4.4.2 Load cases

The most important part of the optimization process, is how loads and constraints are applied to the model. A load case consists of forces or pressures applied to the part, as well as the constraints that hold the part in place.

4.5 Optimization set-up

The optimization set-up consists of four steps that must be specified before the optimization can occur. These four steps are Design variables, Responses, Constraints and Objectives.

4.5.1 Design Variables

There are several different methods of optimization, called design variables, that can be applied in generative design. Design variables determine in what way the part will be affected by the optimization, and they each have their own uses. This thesis will focus on topology, free shape and composite optimization, as these are the methods utilized by DNV GL Fuel fighter for the optimization project.

Topology Optimization When running a part through a solver, topology optimization shows the densities of each element. The densities can be interpreted as how much stress each element is subjected to. The elements subjected to the least stresses will be the least essential elements and can be removed from the structure. The resulting part will often look alien and

unconventional but will be extremely light and stiff.

Free Shape Optimization Free shape optimization is an optimization process in the "Design Fine Tuning" category. It differs from topology and composite optimization in that it is generally not used by itself, but as a way to further improve upon an already optimized part. Free shape optimization works by moving individual elements on the surface of the part and thereby changing its shape without introducing any new topology to the structure. The process works extremely well for reducing high-stress concentrations.

Composite Optimization Composite optimization is an advanced analysis done on a composite laminate. A laminate consist of a stack of plies. The stack is often anisotropic, which makes the analysis particularly complicated. Ply thickness, stacking order and force translations between plies are some of the difficulties that arise in a composite laminate optimization. To solve these difficulties, the optimization is done in three different optimization steps: Free-size, sizing and composite shuffling. The figure below illustrates the process.

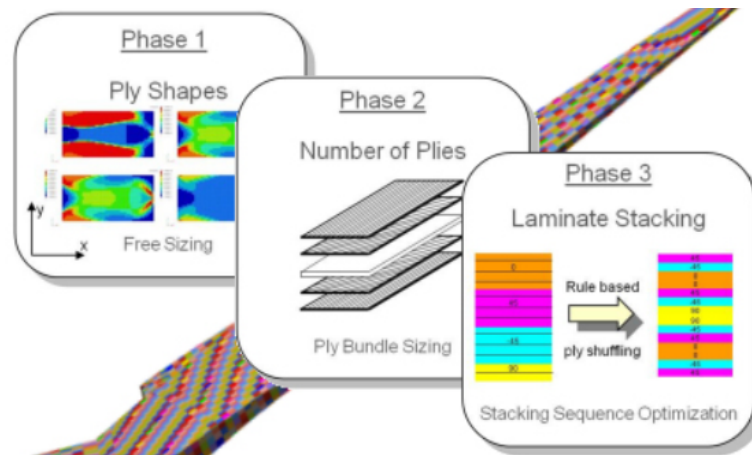


Figure 3: Composite optimization process [17]

Free-size optimization determines the optimum composite patch size, shape and location for a group of composite elements based on the responses and constraints associated with the specified objective. It works like a hybrid of topology and topography optimization. It is commonly used for identifying the optimal ply shape in composite laminates and for thickness

distribution in metal structures[2]. In this project, free-size optimization is used to identify laminate thicknesses and shapes in the monocoque of the car. The user determines ply angles, ply thicknesses, loads and boundary conditions, minimum and maximum laminate thickness and minimum and maximum thickness for any given angle. The result of analysis will be plies with different thicknesses throughout the structure, and a unique shape for each ply. This shape needs to be modified before manufacturing. This step alone does not yet have any practical value. To create discrete plies, so that each ply has a specific thickness, sizing optimization is required after a free-size optimization.

Sizing optimization is a tool that transforms the results from the free-size optimization into a practical solution. It optimizes the structure with the help of options that lets the user determine specific manufacturing thicknesses for each ply. The aim is to obtain feasible thicknesses that can be produced within normal standards[18]. The stacking order for the plies in the laminate at this stage is somewhat chaotic. Therefore a shuffling optimization is needed.

With the shuffling optimization, the program determines which ply should go where in the laminate. A specific stacking order for the plies in the laminate is often desired. With this optimization step, it is possible to set constraints for the stacking order. For example, for each ply that is oriented at 45 degrees, a second ply is placed on top with an orientation of -45 degrees. This is to ensure homogeneous strength. It is also possible to specify cover plies, and decide how many similarly oriented plies should be stacked on top of each other.

4.5.2 Responses

Responses are the characteristics that are relevant to the optimization problem. This could be parameters such as mass, volume, strength, compliance etc. Responses must be defined before the optimization can be carried out. When defining the objectives and constraints for the problem, the parameters must be chosen from these responses.

4.5.3 Constraints

When optimizing a structure, there are usually conflicting goals, e. g. minimize weight while also maximizing stiffness. Defining a target goal to reach for one parameter, makes it possible to improve on the other parameter. A constraint could, for example, be to lower the volume by 50% or

allow no more than 10 mm displacement in the part.

4.5.4 Objectives

The objective determines what to optimize once the constraints are set. A parameter is chosen, and it will either be minimized or maximized. A typical goal for structures is to maximize stiffness, however due to the mathematics involved in generative design, it is easier to minimize than to maximize. Therefore, minimizing compliance is a more common objective than maximizing stiffness.

Generative design is a valuable tool for creating optimal geometries, but building an optimal part requires choosing the optimal materials as well. Both topology and free-size optimization are strongly dependant on mechanical properties, and research of the different available composite materials is therefore crucial for the optimization process.

4.6 Composites

Composite materials are strong and lightweight, and for that reason they are well suited for structural problems. DNV GL Fuel Fighter is a project that benefits greatly from the use of these types of materials. Composites are made out of two or more constituents that together create a stronger laminate than each individual constituent[3]. Fibre-reinforced composites, like carbon fibre, is the type of composite used for the DNV GL Fuel Fighter car. They are characterized by high stiffness and outstanding strength-to-weight ratio (high specific strength). The reinforced fibres are embedded in a matrix, consisting of some sort of resin. The matrix enhances the mechanical properties, protect the fibres from environmental effects, such as humidity and dust particles bind the fibres together and redistribute stresses if a fibre breaks. In addition, the reinforced fibres are flexible, which makes it easy to manufacture complex parts. To increase the second moment of area of the structure, and thereby increase bending stiffness, a core is often inserted between fabrics[4]. Finding the right size and type of core is an important part of optimizing the DNV GL Fuel Fighter monocoque. Another important part is which manufacturing method to use when embedding the carbon fibre in a matrix. Possible methods include vacuum infusion, preimpregnated fibres and manual coating.

4.6.1 Carbon Fibre

Carbon fibre can be woven or sewed in different ways. Each type has its own unique specifications, and has to be researched for different uses. Woven fabrics have fibres that are woven into each other, creating one sheet. Some fabrics are sewn, meaning one sheet of carbon fibre oriented in one direction is laid on top of a sheet oriented in another direction, and both are sewed together. The carbon fibre types presented in this section are the most relevant types that Lindberg&Lund, a sponsor of DNV GL Fuel Fighter could offer. These paragraphs provide an overview of the different fabrics available. The focus has not been on material properties, as the loads acting on the carbon fibre cause stresses well below the materials yield strength [5]. In this project it was more important to explore the carbon fibres ability to drape around curves, its ease of manufacturing, the types of pattern available, and price.

1x1 Carbon Fibre pattern This pattern is also called a plain weave pattern. As figure 4 shows, the pattern is made by fibres that are woven over-under. The fabric is woven tight, meaning the fibres do not separate easily. A disadvantage of this pattern the large stiffness created by the tight weave. This makes it harder to create complex geometries. The mechanical properties are strongest in the horizontal and vertical direction, along the fibres[19].

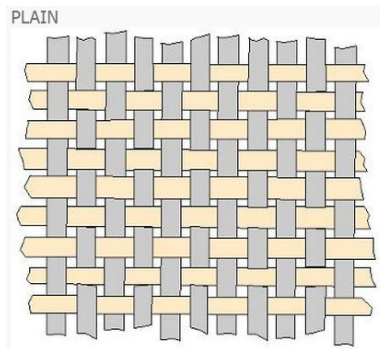


Figure 4: 1x1 Carbon fibre pattern [20]

Biaxial 45/-45 Biaxial carbon fibre fabric has one sheet with fibre oriented at 45 degrees and another oriented at -45 degrees. This is not a woven fabric, but sewn. It is commonly used in between woven carbon fibre fabrics

to increase strength and obtain quasi isotropic material properties. It is stiffer than most fabrics, but easy to handle because of seams that hold the fibres together[21].



Figure 5: Biaxial 45/-45 [21]

2x2 Twill weave This fabric follows a diagonal pattern where the fibres are braided over-over-under-under, hence the name 2x2. This woven fabric is looser than others, allowing the fabric to drape more easily around intricate geometries. 2x2 twill weave is commonly used when laminating on curved moulds. However, the loose pattern makes the fibres separate more easily. For that reason, the fabric must be handled carefully to maintain strength and a good cosmetic appearance[22].

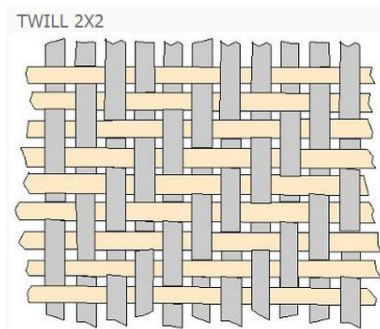


Figure 6: 2x2 Twill weave [20]

Unidirectional carbon fibre Unidirectional carbon fibre has its fibres oriented in a single direction. Only occasional strands of carbon fibre or polyester are placed 90 degrees to the fibres to hold them together. This fabric is used for specific cases where loads follow in a single direction, like

in an arrow. However, the unidirectional fibres can be positioned at angles and allow for any combination of bias. This makes it more flexible, since the fabric can be placed exactly where it is needed to withstand the subjected loads[22].

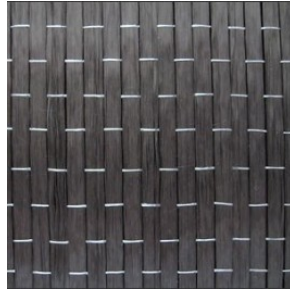


Figure 7: Unidirectional fibre [23]

4.6.2 Core Material

The bending stiffness of a part is proportional to the cube of the thickness of any panel [24]. Increasing the stiffness by thickening the laminate with a low-density core is, for this reason, a great way to achieve a severe increase in stiffness for a very small added weight. The laminate can be thought of as an I-beam, where the core works as the shear web and the plies at the top and bottom as the flanges. In the figure below it can be observed that the core is subjected to shear, while the plies are subjected to compression and tension when the part is put to a three-point bending test. In addition, the core must withstand compressive loading to keep the plies from wrinkling and buckling[25].

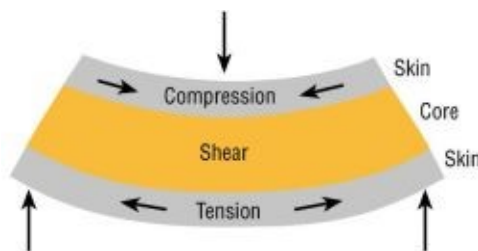


Figure 8: Illustration of core [25]

PVC foam This type of foam can be thermoformed in spite of the material being a thermoset, thus making it unique to other foams. It is compatible with most resins, yet resistant to solvents. The density can vary from 45

kg/m³ to 400 kg/m³, and it has good bonding strength to adhesives like epoxy. Another important property is its ability to resist moisture, which is critical in vacuum infusion. The core material can be ductile or rigid, depending on what is desired. The physical properties are 20-40% higher for rigid foams[26].

Honeycomb As with foams, there are different honeycombs. They can vary from cardboard with low strength and stiffness, to lightweight aluminum honeycomb with high strength and stiffness. Aluminum honeycomb has a high strength-to-weight ratio, making it one of the most favored honeycombs in the automotive and aerospace industry. It can corrode in salty conditions and have reduced mechanical properties on the impact of cored laminates. This is because the aluminum will deform plastically, whereas the fiber reinforced plies will deform elastically and move back to their original position. At these spots, there will be unbounded plies, which negatively impacts the mechanical properties of the composite material[27].

Nomex honeycomb is based on Kevlar, which is made of aramid fibre. It is a polymer that is proven to be five times stronger than steel and can withstand 400 degrees Celsius[6]. Nomex is highly resistant to both cold and hot weather, moisture and chemicals. It is a lightweight honeycomb material, and more expensive than most other honeycombs.

Polymer honeycomb tubes from Tubus-Waben is a lightweight honeycomb with good mechanical properties. The core is made of tubes instead of a honeycomb structure, making it a quasi-isotropic material. It can be thermoformed and, therefore, fitted to curves with ease. The core is available in three different variants; one with open tubes, one with laminated polyester fleece on both sides and one with polypropylene fleece on both sides together with polyester fleece on both sides. The figure below illustrates the three different types. The polypropylene film guarantees that the honeycomb tubes will be free of resin when working with liquid resins and honeycomb together.



Figure 9: Three variants of Tubus honeycomb [28]

4.6.3 Resin

When choosing resin systems, there are some material properties that has to be taken into account. The adhesive properties are important to ensure good adhesion between resin and fabric. This prevents debonding under stress. It also ensures that the loads are transferred uniformly throughout the composite laminate. Toughness is another important property of resins, which signifies the material’s resistance to crack propagation. If the resin can endure large deformations before fracture, it means it is tougher than those that fracture at lower deformations. The last important property to consider, is the resistance to environmental effects, such as humidity, chemicals, temperature, and sunlight[29]. The three most common resins are reviewed in this section.

Epoxy Epoxy resin is the most expensive resin Lindberg&Lund has to offer, but also the resin that is proven to be the strongest. It is widely used for fibre reinforced composites and protective coatings. Epoxy has exceptional surface properties, solvent and chemical resistance, good adhesion performance and ease of cure. It has the advantage of adhering to other resins as well as epoxy itself. This means it is possible to coat epoxy on both vinyl ester and polyester. The colors can vary from crystal clear to diffuse yellow[7].

Vinyl ester Vinyl ester is a type of plastic that replaces polyester in situations where there are higher requirements for durability and chemical resistance. Vinyl ester is not as tough as epoxy, and the resin adheres poorly to surfaces coated with epoxy [8].

Polyester Polyester provides weaker bonding compared to vinyl ester and epoxy. Polyester is cheap but possesses poorer mechanical properties and resistance to moisture[30].

4.6.4 Manufacturing methods

It can be hard to visually differentiate between pre-impregnated, infused and manually coated carbon fibre. However, the physical properties vary greatly with each method. In order to obtain the best results for a composite laminate, it is essential to know the benefits and the consequences of choosing either one. Strength, weight, price, and complexity of execution are important aspects of these methods.

Pre-impregnated With pre-preg, the fibres are bought pre-coted with resin. This allows the fibre to be saturated with the exact amount of resin required. Since the fibre already contains resin, the pre-preg needs to be stored in a cold environment with temperatures around -18 degrees Celsius to avoid curing. The fibre-resin ratio is 70-30, making it the lightest and strongest option compared to infusion and manual coating. However, the cost of pre-impregnated carbon fibre is higher than for other methods. In addition, the lay-up for pre-preg requires skilled personnel and is, in general, a more complex process than infusion. An autoclave is often needed to get the pre-preg to cure under pressure and high temperature, which makes the process even more expensive[9].

Infusion With infusion, the fabric is saturated with resin with the help of a vacuum pump. Resin is not introduced into the system before the component is vacuum bagged. At this point, atmospheric pressure forces the resin through the fibres and distributes it evenly throughout the component. The fibre-resin ratio usually ends up at about 60-40 if the process is done correctly. The strength is somewhat lower than for pre-preg due to higher amounts of epoxy and less homogeneity throughout the composite laminate[31].

Manual coating With this method, the resin is coated manually on the fabric. It is harder to control the amount of epoxy that is applied to the fibres since it is coated with a brush. The weight ratio between fibre and resin usually ends up at about 30-70, which indicates a heavy laminate due to high amounts of resin. Despite this, the composite laminate does not necessarily get any stronger. Resin is brittle, and therefore excess resin might weaken the part. The coating process is simple, and the composite can either cure with or without a vacuum.

5 Method

The process of optimizing the monocoque of the DNV GL Fuel Fighter car consisted of several iterating steps. It started with a 3D scan of a clay model car. This model featured no internal details, intending instead to leave a large design space for topology optimization to identify the most critical load paths throughout the structure. After conducting a topology optimization on the model, the results were analyzed. New considerations in design and ergonomics, in combination with the analysis of the topology optimization and aerodynamic simulations, resulted in a new, more detailed model of the car. More information on this interdisciplinary process can be obtained in Eirik Evjan Furuholmens ongoing master's thesis [10].



Figure 10: 3D-scanning of clay model

Through additional iterations of topology and free shape optimization, the model was further optimized, and the results were again analyzed. Lastly, a 2D model was created in order to utilize the differences in the topology optimization algorithms for 2D and 3D shapes. When the final design of the car was decided on, a 2D model was optimized using composite optimization. The composite optimization step calculates the exact number of plies the monocoque would consist of, in addition to the shape and stacking sequence of each ply. This optimization step was done to minimize the weight of the car while still keeping the required structural integrity. Lastly, a final topology optimization was conducted on a few internal components. Parallel to the optimization process, several material tests were carried out in order to evaluate which materials would be best suited for the monocoque.

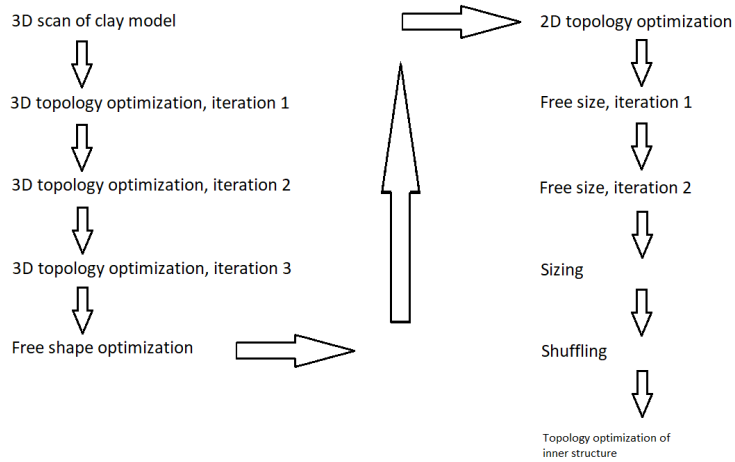


Figure 11: Optimization process overview

5.1 Load Cases

For optimizing the car, static load cases were used during the optimization process. The car is subjected to loads both when driving and when standing still. The challenge is picking out which load cases will contribute the most to an efficient design. For the topology optimization, forces were acting directly on the suspension systems, unlike the composite optimization where the forces were introduced as gravity loads with the use of a point mass (140 kg) centered at the position of the driver.

Another problem when choosing load cases in Hyperworks arose when subjecting the car to multiple loads. To illustrate the problem, imagine a box subjected to three forces of 5000N each (see the figure below).

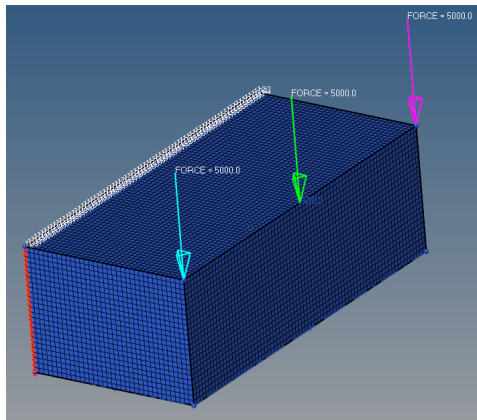


Figure 12: Box subjected to three forces

There are two alternative ways to simulate this scenario. One option is to make all three forces part of the same load case, where the software runs the optimization once. Another option is to make three different load cases, one for each force, and then take the weighted average of the results. An experiment was made to identify the differences that emerge in topology optimization, and gain information on what method should be used for the car. The results are shown below.

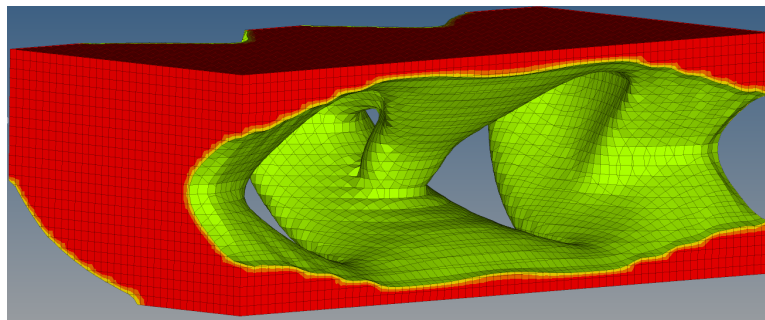


Figure 13: Optimization with one load case

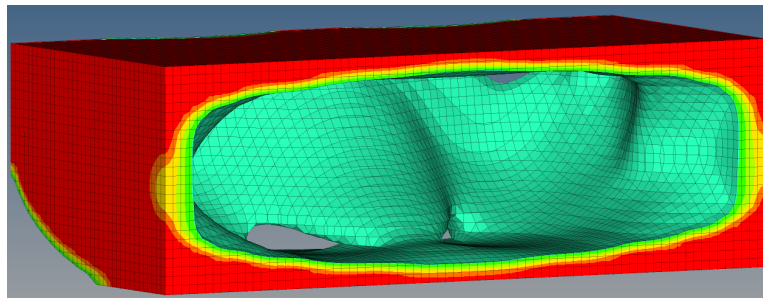


Figure 14: Optimization with three load cases

In both cases the boxes were subjected to the same total force, however, the results vary greatly.

For the topology and composite optimization, the method of weighted compliance was used. This is because some of the loads placed on the model would cancel each other out when applied in the same load case. Placing the loads in different load cases also makes large number of different loading schemes easier to manage.

Load Cases		
Load Type	Load Magnitude	Load Direction
Seat	700N (1G)	-y
Roof	700N	x, -x, z, -z, -y
Tow hook	700N	-z
Braking front	680N (0.5G)	-z
Braking rear	340N (0.25G)	-z
Braking all	960N (0.7G)	-z
Turning left	700N (0.5G)	x
Turning right	700N (0.5G)	-x
Step into car	700N	-y
Harness	700N	-z, x, -x

Constraints [translation/rotation]								
Load Type	Right Wheel	Front	Left Wheel	Front	Right Wheel	Rear	Left Wheel	Rear
Seat	x, y, z / - - -		x, y, z / - - -		x, y, z / - - -		x, y, z / - - -	
Roof	x, y, z / - - -		x, y, z / - - -		x, y, z / - - -		x, y, z / - - -	
Tow hook	x, y, z / - - -		x, y, z / - - -		x, y, z / - - -		x, y, z / - - -	
Braking front	x, y, z / x, y, z		- y, z / x, y, z		- y - / x, y, z		- y - / x, y, z	
Braking rear	- y, z / x, y, z		x, y, z / x, y, z		- y - / x, y, z		- y - / x, y, z	
Braking all	x, y, z / x, y, z		- y, z / x, y, z		- y, z / x, y, z		x, y, z / x, y, z	
Turning left	x, y, z / x, y, z		- y - / x, y, z		x, y - / x, y, z		- y - / x, y, z	
Turning right	- y - / x, y, z		x, y, z / x, y, z		- y - / x, y, z		x, y - / x, y, z	
Step into car	x, y, z / - - -		x, y, z / - - -		x, y, z / - - -		x, y, z / - - -	
Harness	x, y, z / - - -		x, y, z / - - -		x, y, z / - - -		x, y, z / - - -	

The orientation of the coordinate system is shown in figure 15. The load cases chosen for the topology and composite optimization of the car were as follows (a summary can be seen in the tables above where the forces in parenthesis applies to the composite optimization):

1. To simulate the driver sitting in the driver's seat, the weight of the driver (approximated as 700N), was spread out over the seat of the car via 1D-elements. For composite optimization, a gravitational load of 1G was used. All wheels of the car were constrained against translation in the x, y and z-direction.

2. According to the Shell Eco-Marathon rule book, the roof above the driver's head needs to withstand a force equal to the weight of the driver (approximated as 700N) in all directions[32]. Five load cases were constructed, placing loads in directions -y, +x, -x, +z, -z. All wheels of the car were constrained against translation in the x, y and z-direction.

3. According to the Shell Eco-Marathon rule book, the car needs to be able to be towed, should it break down on the track[32]. The chassis must, therefore, be able to withstand a pulling force at the front, equal to the weight of the vehicle, estimated to be around 700N. All wheels of the car were constrained against translation in the x, y and z-direction.

4. To simulate the car braking with its front wheels, a negative acceleration of 0.5G was used (Figure 112). A mass of 140kg was assumed (the mass of the driver is 70kg, the mass of the car was assumed to become 70kg, with a centre of mass at the same point as the driver). For the topology op-

timization, the resulting force was applied directly to the harness fastening points. For the composite optimization, gravity was simulated on a point mass centred at the position of the driver, with additional downwards gravity with a magnitude of 1G to simulate the weight of the car. The right front wheel was constrained against translation in the x, y and z-direction, the left front wheel was constrained against translation in the y and z-direction, and the rear wheels were constrained against translation in the y-direction. All wheels were constrained against rotation around all axes.

5. The load case for braking with the rear wheels is the same as for braking with the front wheels, except the constraints for the front and rear wheels are opposite, and the negative acceleration is now 0.25G (Figure 112).

6. The load case for braking with all wheels is the same as the above, except now both right wheels are constrained against translation in the x, y and z-direction, while both left wheels are constrained against translation in the y and z-direction. The negative acceleration is now 0.7G (Figure 112).

7. To simulate turning left, a centripetal acceleration of 0.5G was used (Figure 112) and a mass of 140kg was assumed. For the topology optimization, a force was applied to the harness fastening points, normal to the driving direction. For the composite optimization, gravity was simulated on the point mass in the driver's position, with additional downwards gravity with a magnitude of 1G to simulate the weight of the car. Both left wheels were constrained against translation in the y-direction, the front right wheel was constrained against translation in the x, y, and z-direction, and the rear right wheel was constrained against translation in the x and y-direction. All wheels were also constrained from rotation around all axes.

8. To simulate turning right, the load case for turning left was mirrored.

9. To simulate braking and turning simultaneously, the loads from braking and turning were added together into six separate load cases; 100% left turn + 50% braking, 100% left turn + 100% braking, 50% left turn + 100% braking, and vice versa for right turns. For the load cases where the centripetal force was the largest, the constraints from the left turn load case were used. For the load cases where the braking force was the largest, the constraints from the braking with all wheels load case were used.

10. To simulate someone stepping into the car, six separate loads of 700N directed downwards were placed at various areas in the car. The car was constrained against translation in all directions.

11. To simulate the forces acting on the harness during a crash, a force of 583 N was calculated by assuming the car would accelerate from 30 km/h to 0 km/h in 1 second (figure 113). A safety factor of 1.2 was added, resulting in a force of 700 N in the driving direction, to the right and to the left side. The car was constrained against translation in all directions. The force of 700N was placed at the centre point for the harness (where the point mass of 140 kg is located). The forces acting on each attachment point will therefore be one-fifth of 700N since it is evenly distributed on five fixed points.

5.2 Topology Optimization

5.2.1 Model set-up

The first 3D model of the car was created using a 3D scan of a clay model of the car as a baseline, which was then modified using Fusion 360 CAD software. The consecutive 2D and 3D models were created in Fusion 360 by analyzing the results of the topology optimizations in parallel with aerodynamic simulations and new considerations in ergonomics and design. Altair Hyperworks was used for meshing.

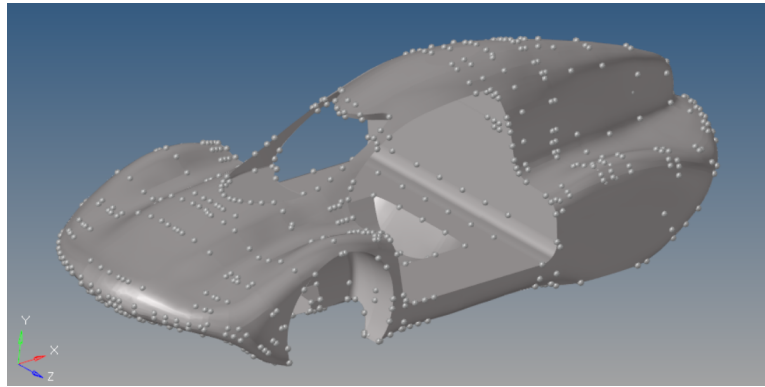


Figure 15: 3D CAD model

Meshing The 3D models were meshed using second order tetrahedral elements with an average element size of 20 mm, resulting in a total of 130.000 elements in the final model. The reason for choosing tetrahedral elements over hexahedral elements is because the latter requires more time and experience to mesh[1]. Over the years, the algorithm for tetra meshing has improved to the point where there is no longer much of a difference in quality between the two element types.

The 2D model was meshed using 50.000 elements of average size 15 mm. The element types were a mix of quadrilateral and triangular elements.

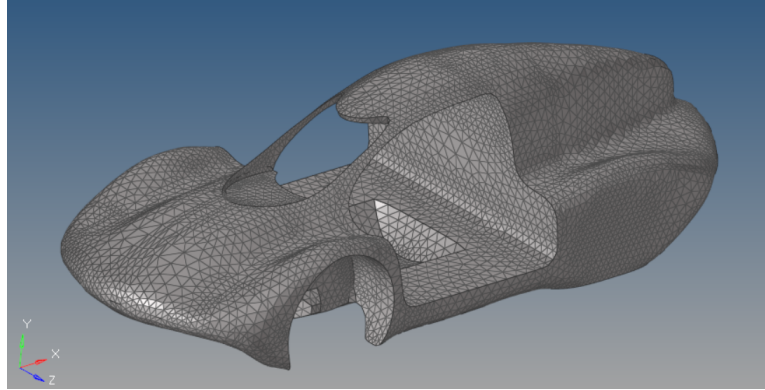


Figure 16: Meshed model

Constraints As previously stated, a load case consists of forces or pressures acting on the model, as well as constraints holding the model in place. Ideally the model would be constrained at the nodes where the wheel touches the ground. However, the wheels were cut out from the CAD-model, as they were not going to be optimized using generative design. For the first optimization iteration, the empty wheel hubs of the model were directly constrained instead.

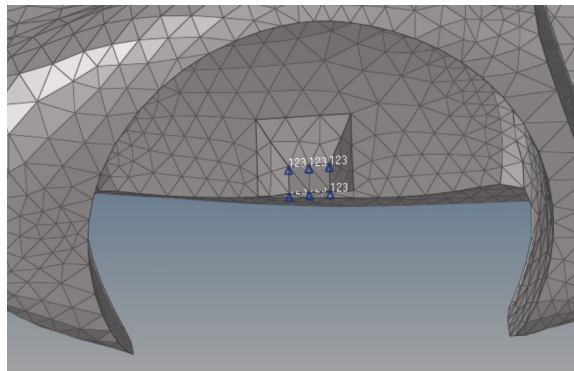


Figure 17: Constrained wheel hub

During the second optimization iteration, it was realized that the moment generated by friction between a wheel and the ground could not be accurately captured by constraining the wheel hubs directly. To properly

simulate the forces and moments from the wheels, front and back suspensions needed to be constructed. 1D elements (RBE2) were used for this task.

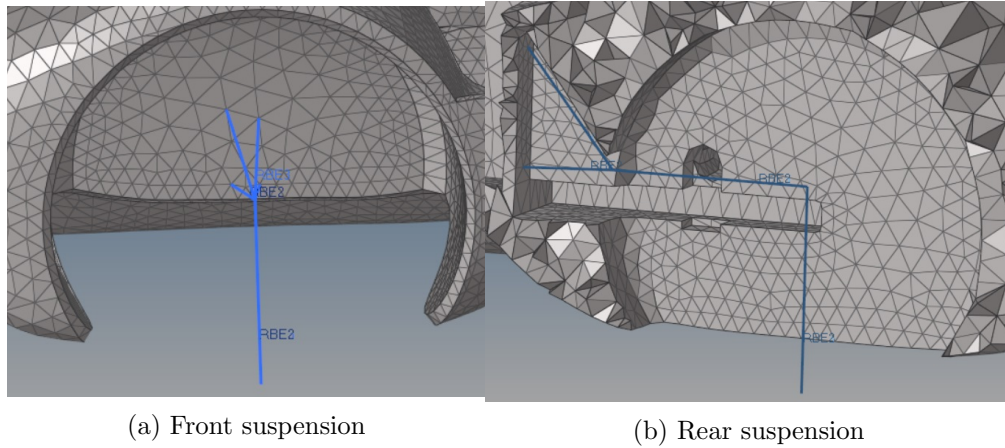


Figure 18

In the third optimization iteration, front and rear suspensions were a part of the CAD-model and could be meshed just like the rest of the car. Since the suspensions were going to be made out of metal, the corresponding elements got assigned different mechanical properties than the rest of the model. These elements were not a part of the design space of the optimization, as the task was to optimize the monocoque itself, and not the suspensions.

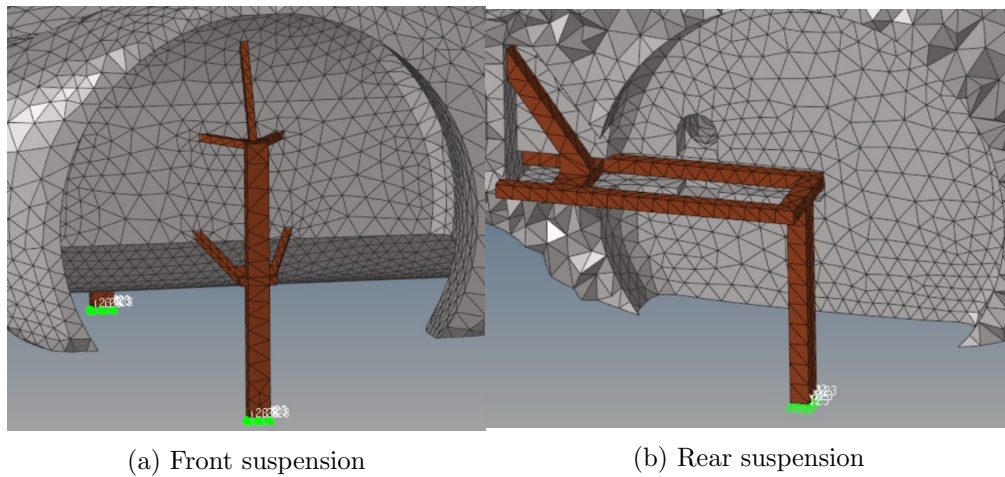


Figure 19

Material selection In Hyperworks, there are several material types to choose from, with different characteristics regarding mechanical and thermal properties. Even though the DNV GL Fuel Fighter car was to be made out of carbon fibre, a highly anisotropic material, the model needed to be simulated using an isotropic material. The 3D model of the car was a bulk solid, and during the topology optimization a truss-like structure would be created. Without knowing which direction these trusses would point, there would be no way to orient the carbon fibres in the correct direction beforehand. Therefore, a MAT1 material was chosen, which is used for linear, temperature-independent, isotropic materials. The following mechanical properties were used, taken from assumptions made by DNV GL Fuel Fighters R&D team during the 2017/18 project:

Young's modulus: 70 000 MPa

Poisson's ratio: 0.1

Density: 1115 kg/m³

Load cases During the first iteration of the topology optimization, gravitational forces were used to simulate braking and turning, as well as the weight of the driver and the vehicle. In later iterations, gravitational forces were removed in favor of braking and turning forces placed directly on the harness. These would simulate both the mass of the driver accelerating, as well as the vehicles centre of mass accelerating. This approach controlled exactly how large the forces from braking and turning would be.

5.2.2 Optimization set-up

After the model was meshed and load cases were determined, optimization parameters needed to be applied. Design variables, responses, objectives and constraints were all generated in Hyperworks. The model was then optimized using Hyperworks' solver.

Design variables For the first iterations of the optimization process, a topology design variable was chosen. Topology optimization creates a framework of material consisting of several interconnected beams. To avoid creating too thin beams, a MINDIM parameter with size 60 was applied to the design variable, ensuring no structures with a thickness smaller than 60 mm would be included in the final design. A MAXDIM parameter with size 120 was also applied, ensuring no structures with a thickness larger than 120

mm could be created. This was done to the design to obtain clearly defined beams instead of plates.

Objectives and constraints An FEM-analysis was carried out on the 3D model while subjected to the expected stresses of the race. The maximal observed displacement was set as the optimization constraint. The objective was originally set to minimize the volume fraction of the solid. The following results were poor, and provided little insight into where the critical load paths of the monocoque lay. The FEM-analysis had been carried out on a structure far more robust than the finished monocoque would be, and so the observed displacements were inaccurate. After consulting professor Jan Torgersen, the optimization constraint was changed from setting a maximum allowed displacement to setting a maximum allowed volume fraction of 5%, allowing the software to strip away superfluous material. The objective was changed to maximizing the models stiffness. The math behind the algorithms utilized in the solver favours minimizing a value as opposed to maximizing it. Therefore, the actual objective used was minimize compliance, which mathematically can be transformed into maximizing stiffness[11]. As the model was subjected to multiple separate load cases, weighted compliance was used.

5.3 Free Shape Optimization

5.3.1 Model set-up

The 3D model used for the free shape optimization process was created after three iterations of topology optimization. The resulting topology was imported back into Hyperworks using FEA reanalysis, in order to be refined using free shape optimization.

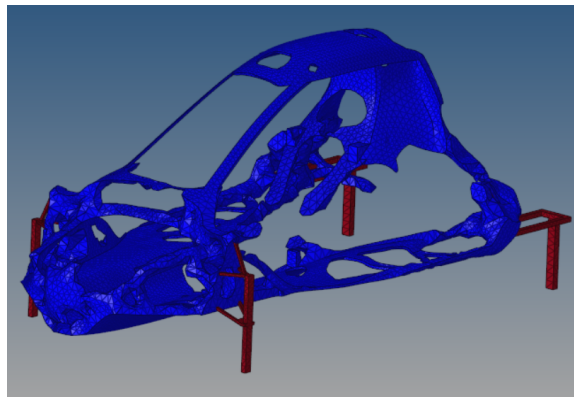


Figure 20: Car model after three topology optimization iterations

Meshing Since free shape optimization is a design fine tuning process, it is normally done following a different optimization type, e. g. topology. This means that creating a new CAD model in Fusion 360 could be skipped. Instead, FEA reanalysis was used to import the results of the previous optimization process directly back into the meshing software. FEA reanalysis retains the meshing properties of the previous mesh but reorganizes the elements in order to apply the same forces and constraints as before.

Material selection The mechanical properties used during the free shape optimization were identical to the mechanical properties used during the topology optimization.

Load cases The load cases used during the free shape optimization were identical to the load cases used during the topology optimization.

5.3.2 Optimization set-up

Design variables The free shape design variable contains five parameters that affect how the design region deforms during an optimization.

Direction Type was set to *Both* to make the grid unconstrained, and thus able to both shrink and grow.

Move Factor determines the allowed movement per iteration and was set to its default value of 0.5. Making this value larger would have sped up the optimization, but would also have introduced instability to the process.

NSMOOTH determines the size of the buffer zone, which counteracts mesh distortion. A larger buffer zone will result in less distortion, but longer computation times. *NSMOOTH* was set to its default value of 10.

MXSHRK and *MXGROW* defines a maximum distance the elements can move. These parameters were left unchecked to provide more freedom to the optimization.

NTRANS defines a transition zone between the design and non-design space. This parameter was not used as the entire structure was defined as design space.

Objectives and constraints The objective of the optimization was set to MINMAX compliance, meaning the elements with the largest values of compliance in the structure would be shifted in order to minimize this value. As previously stated, lowering compliance is the same as increasing stiffness. By using MINMAX, one is able to fine tune the design of the structure by only targeting certain elements. Free shape optimization requires no constraints. Instead it relies on the parameters defined in the design variables.

5.4 Composite Optimization

5.4.1 Model set-up

A 2D-shell model was made in Fusion 360 CAD software and imported into Hyperworks.

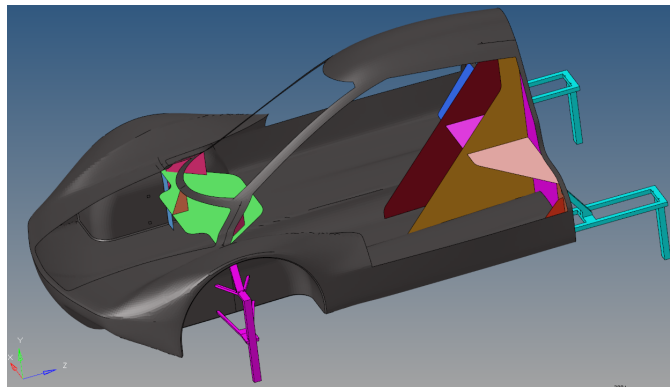


Figure 21: CAD model of the car

Meshing The 2D shell model was meshed with a mix of quadrilateral and triangular elements with an element size of 10 mm. Due to the complex shape of the car, a mesh with only quadrilateral elements was hard to obtain. The triangular elements adapt better to intricate shapes compared to quadrilateral, and was for that reason chosen in this case. A symmetrical mesh was preferred because it makes it a lot easier to add loads, constraints and other elements at the exact same locations on both sides of the car. It was not possible to achieve a fully symmetrical mesh by using quads and triangular when the model was meshed as one single model. For that reason, only one half of the car was meshed, and then mirrored at its centre line. The yellow points in the figure below shows elements that have bad quality, such as elements that are stretched out. All of these elements were edited individually to avoid singularities during the simulation process.

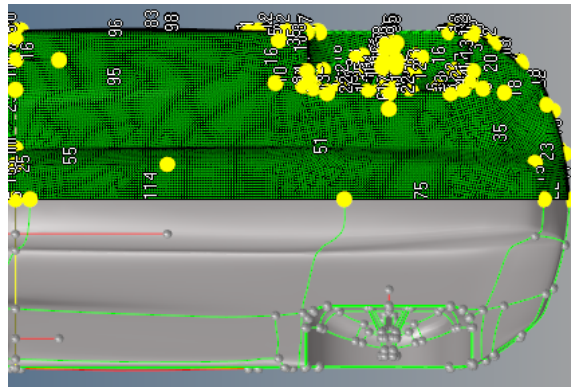


Figure 22: Half of the model is meshed

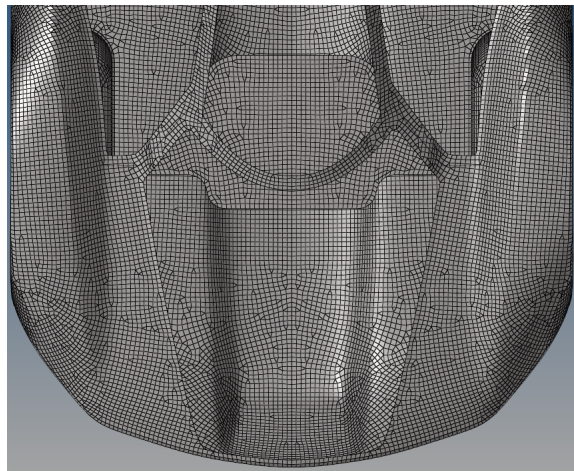


Figure 23: The mesh is fully symmetrical along the centre line of the car

A problem that often emerge when meshing is that not all surfaces are connected. If the mesh is not continuous, forces and displacements will not be transferred between elements, which gives incorrect results. This means that every element that is not stitched to all surrounding elements must be extended in order to obtain the proper results. This problem is especially prominent where one surface joins another surface, e. g. where the suspensions system meets the dashboard. The difference in the connectedness of the elements before and after stitching can be observed in the figures below.

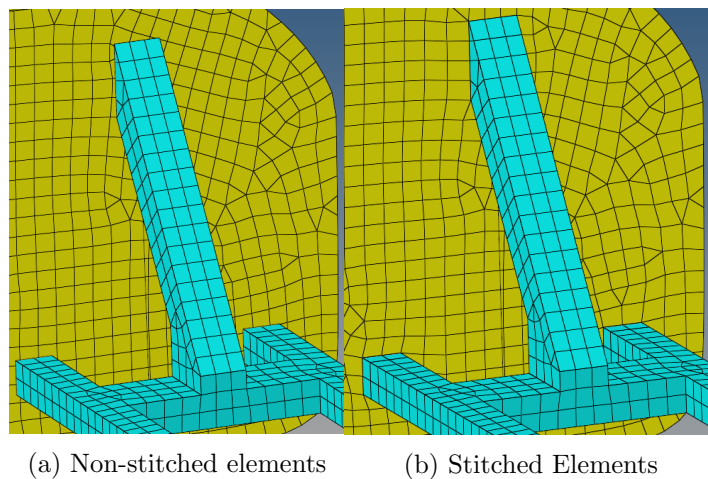


Figure 24

RBE2 elements (1D elements) were made to represent the seat belts and

tow hook in front. In addition, RBE2 elements were placed on the roof to evenly distribute the roof load. RBE2 elements were also used to simulate a person stepping into the car. The RBE2 elements can be seen as the thin lines in figure 25. The green lines that represent the seat belts were given a point mass of 140 kg at its master node in the middle. This simulated the weight of a 70 kg person, as well as the weight of the car (assumed to be 70 kg), which compensates for the fact that parts of the car was missing (doors, hood, rear hatch, electronics etc). The point mass was added to obtain more realistic results when using gravity loads.

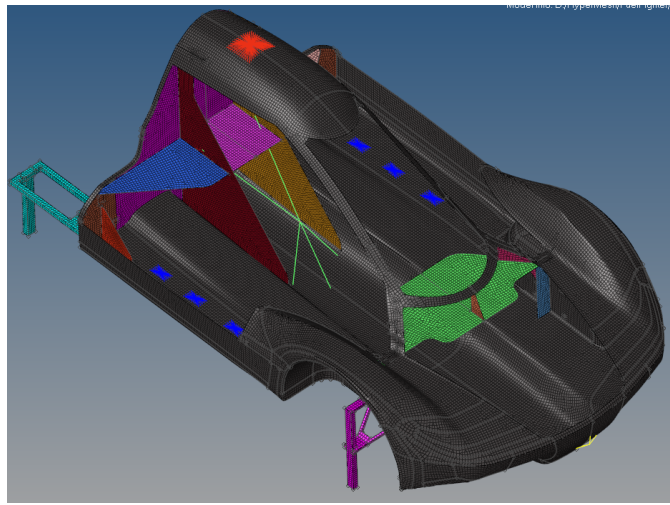
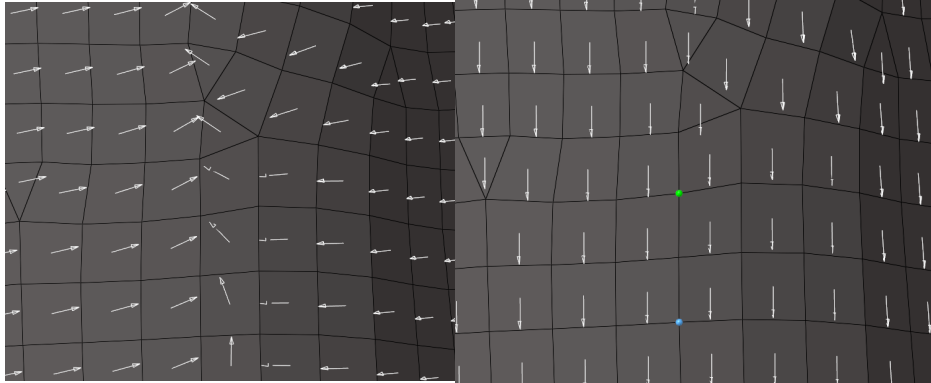


Figure 25: The RBE2 elements can be observed as the thin lines stretching from one master node in the middle to other slave nodes

It is a prerequisite that all the elements in the mesh are oriented in the same direction to be able to run a composite optimization (see figure 26a). The orientation of the elements defines the 0 degree orientation of the later created plies. If the elements point in different directions, a ply oriented at 45 degrees will vary for every element. This should be avoided. In this case, the 0 degree orientation was positioned along the driving direction. In addition, the element normals must point in the same direction, from bottom to top. These normals define the stacking sequence for each ply, and if these are not set up correctly the program will stack plies in random directions (figure 27).



(a) Elements with random orientation (b) Elements with uniform direction

Figure 26

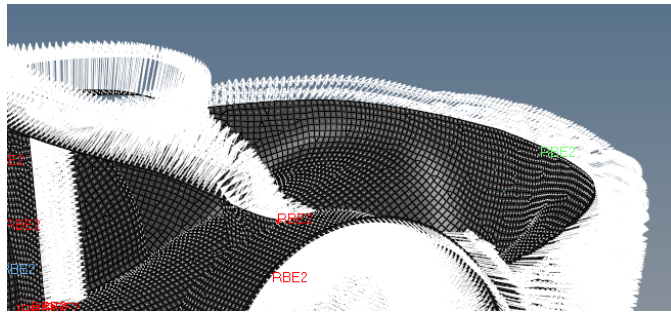


Figure 27: All the normals point from bottom to top for each element

Material selection A shell model was used for the 2D model in order to run a composite optimization. A composite optimization varies greatly from topology optimization because plies have to be considered in the optimization process. The carbon fibre type was chosen by testing different available fabrics from Lindberg&Lund, as well as the core material. The reason for the choice of material can be found in section 6. In this optimization, aerospace grade 2x2 carbon fibre twill pattern with a thickness of 0.3 mm was chosen, with material parameters listed in the table below. The core was chosen to be foam core Divinycell 45H, with material parameters also listed below.

Material Parameters	2x2 twill Carbon Fibre Pattern, 0.3 mm	Divinycell 45H
E-modulus x-direction [Mpa]	70000	50
E-modulus y-direction [Mpa]	70000	50
Poisson Ratio	0.1	0.4
Mass Density [ton/mm ³]	1.0*10 ⁻⁹	4.8*10 ⁻¹¹
Stress Tension x-direction [Mpa]	600	1.4
Stress Tension y-direction [Mpa]	570	1.4
Stress Compression x-direction [Mpa]	600	0.6
Stress Compression y-direction [Mpa]	570	0.6
In-plane Shear	90	0.56

Figure 28: Material parameters for carbon fibre and foam

Material	Orientation, degrees	Thickness [mm]
Carbon Fibre	0	0.15
Carbon Fibre	90	0.15
Carbon Fibre	45	0.15
Carbon Fibre	-45	0.15
Divinycell 45H	180	5

Figure 29: Orientation and thicknesses for foam and carbon fibre

Each ply represents one layer of fabric with a given material property and a given orientation. For this model, four carbon fibre plies were made, in addition to Divinycell PVC foam core ply on top, as the initial laminate design. A 0.3 mm 2x2 twill fabric has both 0 and 90 degree orientation in one single ply (see section 4.6.1). Hyperworks can only handle one orientation for each ply, hence one 0.3 mm ply in real life had to be simulated as two plies of 0.15 mm. One would have an orientation of 0 degrees while the other would have an orientation of 90 degrees. Together this creates a 0.3 mm ply with orientation 0 and 90 degrees. This applies to plies with 45 and -45-degree orientations as well. To ensure a symmetric shape before optimization, an option called "symmetric" is checked to create the same plies and core twice, see figure 31. The core was made 5 mm thick, and the symmetric option created two cores that in total had a thickness equal to 10 mm. These plies were then interrelated in a laminate. The laminate held all the plies, and the optimization focused on the laminate as a whole, as opposed to individual plies.

The initial carbon fibre plies were set to cover the whole monocoque, to be optimized later. For the core material, the shape was predetermined by first doing a free-size optimization on the whole model. The results were

then modified to match the practical manufacturing constraints. This was because the foam could not be placed where there was double curvature (due to the foams bending limits), which the optimization suggested. In addition, the core varied in thickness throughout the monocoque. Areas with great stresses got a core with a thickness of 20 mm, while the areas with less stresses got a core of 10 mm. The thickness variation was solved by creating a single core of 10 mm that covered the entire area where the optimization suggested core should be placed (figure 30a), and adding an additional 10 mm core on top of it wherever the stresses demanded it (figure 30b). For the 2D shell model, MAT8 was chosen for carbon fibre plies, which is used for linear orthotropic materials applied to 2D models. MAT1 was used for the core material.

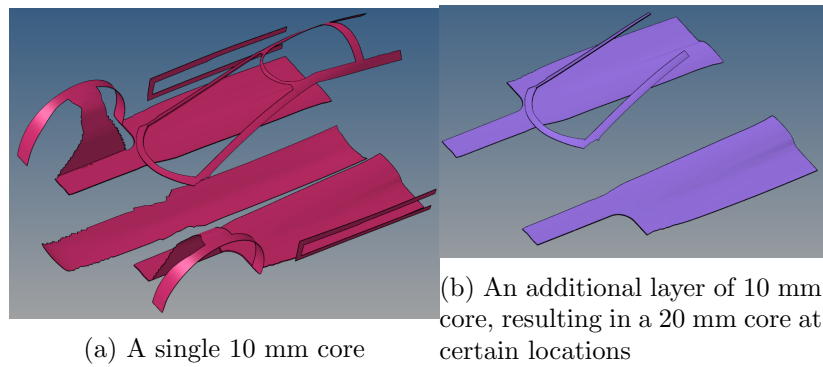


Figure 30

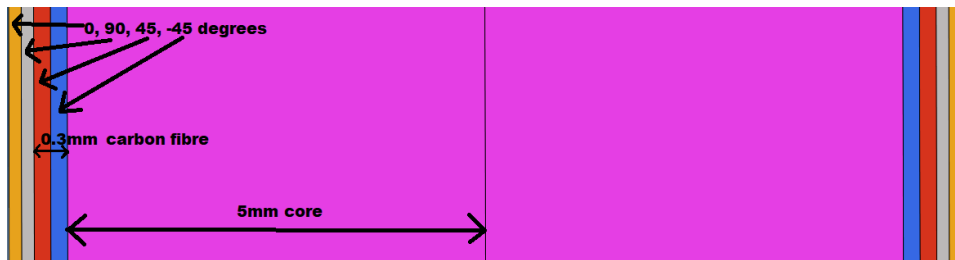


Figure 31: Initial laminate with four carbon fibre plies and one core ply mirrored along the symmetry line in the middle

Load cases The load cases in the composite optimization were based on gravity loads with a point mass simulating the weight of the car and driver. Before the optimization process began, a stress analysis was completed to get an analytical overview of the location of stresses and displacements in

the car, as well as their magnitudes. By doing this, the best placement of the carbon fibre ply patches and core material could be located and compared with the results from the composite optimization. The load cases had to be analyzed separately due to constraints in Hyperworks.

5.4.2 Optimization set-up

Design variables For the 2D shell model, three different design variables were used to individually obtain desired results. As mentioned in the theory section, a composite optimization is a comprehensive simulation that requires free-size, sizing and composite-shuffling optimization. The first design variable was free-size. This tells the program to create optimal thicknesses and shapes throughout the structure based on the objective and constraints. The initial laminate that was created had a total of eight carbon fibre plies and two core plies that covered the whole model. As mentioned above, the core material was modified after the first free-size simulation and then placed into the laminate with the initial carbon fibre plies. A new free-size simulation was done to the laminate with an updated core. The composite laminate was constrained to have a thickness between 0.6 mm and 30 mm. In addition, minimum member size control was set to a value of 30 mm. This caused Hyperworks to leave a minimum of three elements (with element size 10 mm) along the load paths. Some shapes from the free-size optimization are very hard to manufacture because of holes and single elements in the open air. For that reason, each ply was modified element by element to make the plies possible to manufacture. At this point, it was possible to see the total thickness for every element, but they varied from ply to ply. Since each ply could only have a thickness of 0.3 mm in practice, a sizing optimization was necessary. Figure 32 illustrates what a single ply might look like.

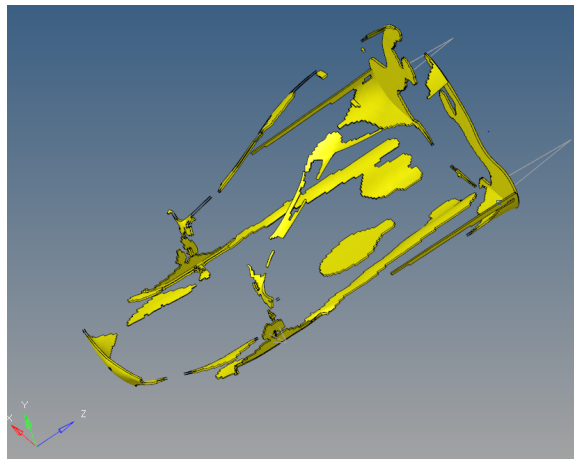


Figure 32: A raw ply from the free-size optimization

The sizing design variable was used to constrain the thicknesses. A manufacturing thickness of 0.15 mm was set to make sure every patch of the ply had the correct thickness. In addition, an upper bound of 0.3 mm was set for each ply. This allowed Hyperworks a third value to choose from in order to avoid locking the optimizer between only two values, 0 mm and 0.15 mm. The optimization does not consider the stacking sequence of the plies, which can result in a long sequence of plies with the same orientation. This led to the last design variable, composite-shuffling.



Name	Value	Name	Value
Solver Keyword	PLY	Solver Keyword	DESVAR
Name	PLYS_8200	Name	fstosz.5
ID	8200	ID	8200
Color		Include	[Master Model]
Include	[Master Model]	Config	size/shape
Card Image	PLY	Move Limit	
Thickness	0.0265696	Ddval Id	<Unspecified>
Orientation	90.0	Shape Id	<Unspecified>
Result request	<input checked="" type="checkbox"/>	Initial Value	0.0265696
Material	(1) Carbon Fibre	Lower Bound	0.001
Drape	<Unspecified>	Upper Bound	0.3
Shape	1 Sets	RAND	<input type="checkbox"/>
Ply system	<Unspecified>	RANP	<input type="checkbox"/>
List of base surfaces	0 Surfaces		
User Comments	Do Not Export		
TMANUF	0.15		
No of rows	1		
Data: ESID			

Figure 33: Parameters for ply 8200 (later referred to as ply 6) in the sizing optimization

It is desirable to have plies pointing in specific directions to ensure sufficient strength throughout the structure. At this point, plies might be pointing in multiple different directions, and have no specific order. The shuffling optimization was used to tell which sequence plies are stacked in. An option called Maximum Successful Plies was set to define the maximum number of plies with the same orientation allowed to be stacked after each other. To avoid two plies with the same orientation to follow each other, this option was set to 1. In addition, plies oriented at 45 and -45 degrees were paired together. Unfortunately, pairing plies oriented at 0 and 90 degrees together is not an option featured in Hyperworks. However, they tend to pair when 45 and -45 are constrained to pair. The core was constrained to always be in the middle of the carbon fibre plies.

<input checked="" type="checkbox"/> pairing constraint		
pair type:		
▼	same	
ply angle1 =	4 5 . 0 0 0	
ply angle2 =	- 4 5 . 0 0 0	

D S H U F F L E	2 S T A C K	1
	M A N G L E	M S U C C
M A X S U C C	0 . 0 0 0	1
M A X S U C C	9 0 . 0 0 0	1
M A X S U C C	4 5 . 0 0 0	1
M A X S U C C	- 4 5 . 0 0 0	1
	P A N G L E 1	P A N G L E 2

<input checked="" type="checkbox"/> MAXSUCC

Figure 34: Pairing constraints and MAXSUCC parameters for shuffling

Objectives and constraints For the free-size optimization, the objective was set to minimize compliance, which is the inverse of stiffness. The constraint set for the optimization was total mass. With this constraint, a lower and upper bound for the total mass was set. Using mass as a constraint made it easier to predict the total mass of the monocoque, and thereby improve the weight of the car from last year. The initial weight of the car before optimization (with modified core) was approximately 10 kg (without resin). The upper bound was set to 8 kg and the lower bound to 1 kg. The objectives and constraints were the same for the sizing and shuffling optimization as well.

5.4.3 FEM-analysis

The optimization made the model as light as possible, yet stiff enough to resist the acting loads. However, every optimization was controlled by doing FEM-analysis to observe the displacements and loads acting on the monocoque. If the stresses in the monocoque was found to be well below the yield limit of carbon fibre, or should the displacements on the car turn out to be very small, carbon fibre plies could manually be removed to save weight. A new FEM-analysis would then be performed on the new design. These FEM-analyses were done in parallel with every optimization process during the project.

5.5 Topology optimization of the inner structure

After the monocoque was finished, additional features in the car had to be optimized and built. An FEM-analysis revealed that the inner structure of the car contained some areas with zero stresses and small displacements. This dead mass could be removed to make the monocoque even lighter. These features included seat support, dashboard and general supporting beams.

5.5.1 Model set-up

As the monocoque was already optimized at this stage, it was not a part of the design space. The design space was chosen to be the firewall, seat support and dashboard, see figure 35.

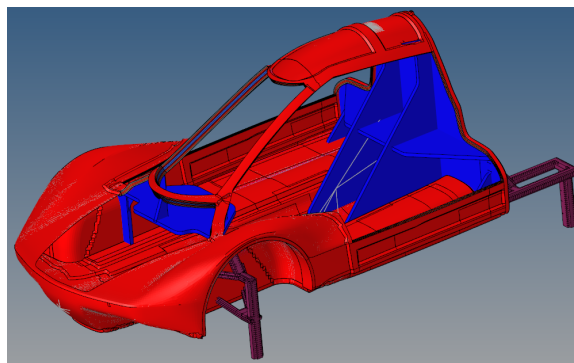


Figure 35: The design space is displayed as the blue area. Only these elements are affected by the topology optimization

Meshing The mesh from the composite optimization was reused for this model, as well as the RBE2 elements and the point mass.

Material selection As this optimization was carried out after the mono-coque was finished, there was more time to experiment and get used to the different materials available. It was found that using sandwich panels with foam in the core and one layer of 300 g carbon fibre at the top and bottom provided a strong, yet light material which was easy to manufacture and shape. The left and right side of the firewall, where the rear suspension was fixed, had a more dense foam core to avoid fracture under load. The same type of foam was used, but the density was increased from 45 kg/m³ to 200 kg/m³. This was done to make it easier to manufacture. Seeing as the laminate was already decided on, a composite optimization would not offer any new information. The problem with using topology optimization was that Hyperworks does not support composite materials for this type of optimization. Despite these limitations, a workaround was found. The most important factors for the optimization process was determined to be tensile stiffness and bending stiffness. If it was possible to create an isotropic material on paper that would have the same tensile and bending stiffness as the composite laminate, it could be used as a simulated material in place of the composite laminate, and could thereby be used in topology optimization.

The composite laminate had a core with a thickness of 10 mm, with a carbon fibre ply of 0.3 mm on each side. While Young's modulus of the core could be neglected, the carbon fibre had Young's modulus of

$$E_c = 140000MPa$$

The goal was to construct an isotropic material that had the same tensile and bending stiffness as this carbon fibre sandwich panel. To do so, the thickness and Young's modulus where these properties would be equal for both materials had to be found. Let "c" denote the properties of the sandwich panel, and "i" denote the properties of the isotropic material. The formula for tensile stiffness is

$$k = \frac{AE}{L}$$

$L_c = L_i$, and $k_c = k_i$ was desired. Let t denote the thickness of the isotropic

material. This leads to

$$A_c E_c = A_i E_i$$

$$E_i = \frac{0.6}{t} E_c$$

The formula for bending stiffness is

$$M = EI\kappa$$

where κ is the curvature of the beam. $M_c = M_i$ and $\kappa_c = \kappa_i$ was desired.

$$I_c = \frac{bt^3}{12} = 2 * \left(\frac{1 * 0.3^3}{12} + 0.3 * 1 * 5.15^2 \right) = 15.918 mm^4$$

$$I_i = \frac{t^4}{12}$$

$$E_i = \frac{I_c}{I_i} E_c = \frac{15.918}{\frac{t^3}{12}} E_c$$

There are now two equations with two unknowns.

$$t = \sqrt{\frac{15.818 * 12}{0.6}} = 17.84 mm$$

$$E_i = 4709 MPa$$

This means that setting the material thickness to 17.84 mm and Young's modulus to 4709 MPa would yield a material with similar stiffness properties as a sandwich panel.

Load cases The loads and constraints of the model were identical to the ones used in the composite optimization.

5.5.2 Optimization set-up

Design variables The topology optimization variables were identical to the ones used in the previous topology optimization.

Objectives and constraints The objective for this optimization was to minimize compliance in order to increase the stiffness. The constraint used was 50% volume fraction.

5.6 Material testing

As stated in the theory section, there were many different material choices available regarding both carbon fibre, core material and type of resin. By researching the different options and their advantages, in addition to determining what materials were available from suppliers, the list of materials was narrowed down. The remaining options were physically tested.

5.6.1 Resin

When consulting Lindberg&Lund about which resin type would be suitable for Fuel Fighter, they stated that epoxy was the only good and usable type of resin for the monocoque. However, each type of epoxy had some distinguishing features. Our interest lay in the epoxy's curing time. Two epoxy systems were tested several times at varying room temperatures.

The first system was Araldite ESR3 (epoxy) and ESH3 (hardener). The second system was Araldite LY1564 (epoxy) and XB3404 (hardener). The tests were carried out in a composite lab where other students worked on their own projects. For this reason, the temperature in the room could not be regulated as precisely as intended. However, a heating lamp was utilized in order to heat up the epoxy. The surface temperature of the test piece was adjusted by increasing or decreasing the distance between the heating lamp and the test piece. Three tests were done; at room temperature in the absence of a heating lamp, at 60 degrees Celsius and at 80 degrees Celsius.



Figure 36: Epoxy curing at approximately 60 degrees Celsius



Figure 37: Epoxy curing at approximately 80 degrees Celsius

5.6.2 Core material

Given the knowledge stated in the theory section, it was quickly discovered that the only core material Fuel Fighter had the budget for was PVC foam and Tubus honeycomb. These were further tested. The tests revolved around how well the core material could be permanently bent, as the geometry of the monocoque contained several curves. The tests were carried out by heating up and then bending the core material. Heating up the core was done using a heat gun as well as an oven set at different temperatures. The different core materials were also tested for how much epoxy was soaked into the core during vacuum infusion.

5.6.3 Carbon fibre

The material properties for the different types of carbon fibre were hard to obtain, and they appeared somewhat similar. The suppliers asserted that choice of fabric coincided with the production method. Accordingly, the carbon fibre was tested for how easily it draped around intricate shapes, how easy it was to handle under production, and thickness of the fabric.

5.7 Production

After all tests and simulations were completed, five team members of Fuel Fighter travelled to High-Performance Composites (HPC), located in Sarpsborg. By utilizing the previously gathered information, the physical product was made here. The process started with sending the finished CAD model to a CNC machinist at Eker Design, who milled and sanded three

moulds. These consisted of one top, one bottom and one rear mould for the car. The moulds were brought to HPC where they were first sprayed with a non-adhesive spray and then waxed. This was done to make the removal of the carbon fibre from the moulds after manufacturing easier. Then the process of laying the carbon fibre and core material started. To avoid epoxy-filled gaps between the core material and carbon fibre, every edge on the foam core was sanded with an angle that the carbon fibre could drape over with ease.

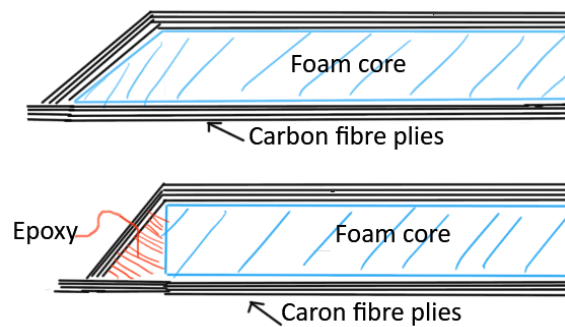


Figure 38: Figure illustrating the effect of sanding the edges to save weight

In addition, 3 mm holes were made at regular intervals across the foam core with a nail to let epoxy run through the foam. This was done to saturate the carbon fibre plies underneath the foam with epoxy. The fabric used was 0/90 twill weave that was cut with an angle of 45 degrees to create 45/-45 twill weave. With this method it was possible to use the same fabric for the whole monocoque. The plies were laid in an order specified by the simulations done beforehand. An adhesive spray was used to bind the carbon fibre and core material to the mould despite its steep curvatures. After the laminate was laid, vacuum infusion was used to run epoxy through the fibres. The epoxy cured overnight and the monocoque was removed from the mould. When the car was brought back to Trondheim, the inner structure and the firewall, was manufactured in the composite lab. These parts were later glued to the monocoque using a strong epoxy glue called Araldite 2048 from Lindberg&Lund. The bottom and the top of the monocoque was then glued together with a seam between the flanges. These flanges were later cut off, and the seam was reinforced with a layer of carbon fibre on the inside of the monocoque. After the upper and lower body was assembled, the doors, windows, hood and rear hatch were cut out. The monocoque was then left as a single body, with the cut out parts as detachable components.

6 Results

6.1 Topology optimization

The results of the topology optimization can be seen in the figures below. The contour plot shows the element densities of the mesh, ranging from 0% density (blue) to 100% density (red). The cutoff density can be regulated post simulation in order to get the clearest view of the results. The below figures show the optimization results with the most illustrative densities for that particular iteration.

6.1.1 Iteration 1

The results of the first topology optimization required 37 iterations before convergence was obtained. All elements with a density below 11% were removed. The results can be seen below.

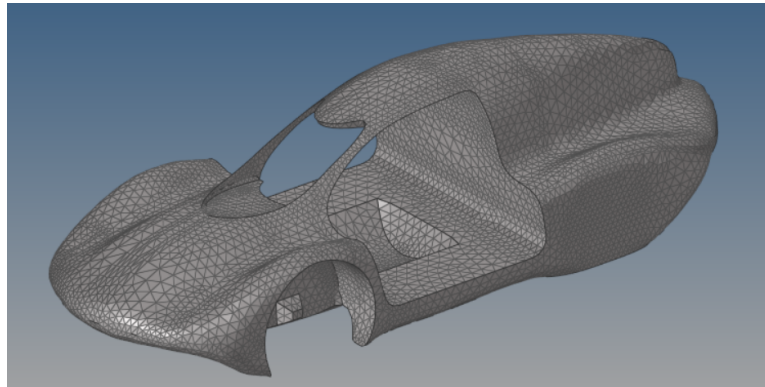


Figure 39: CAD model before optimization

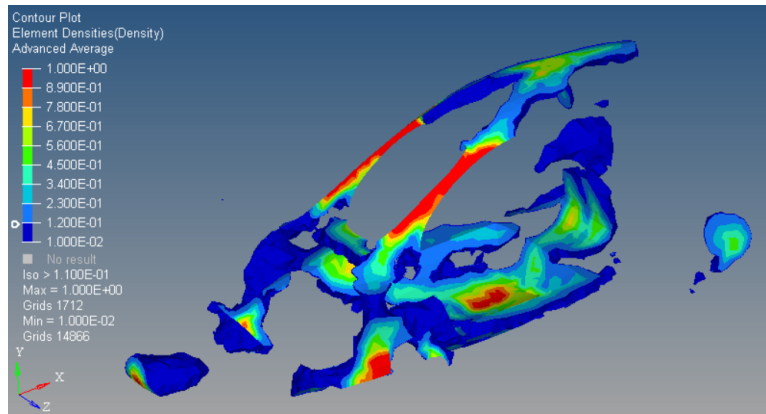
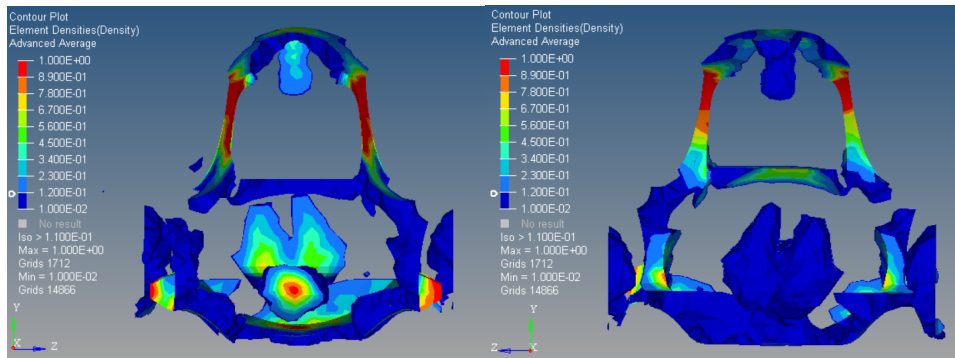


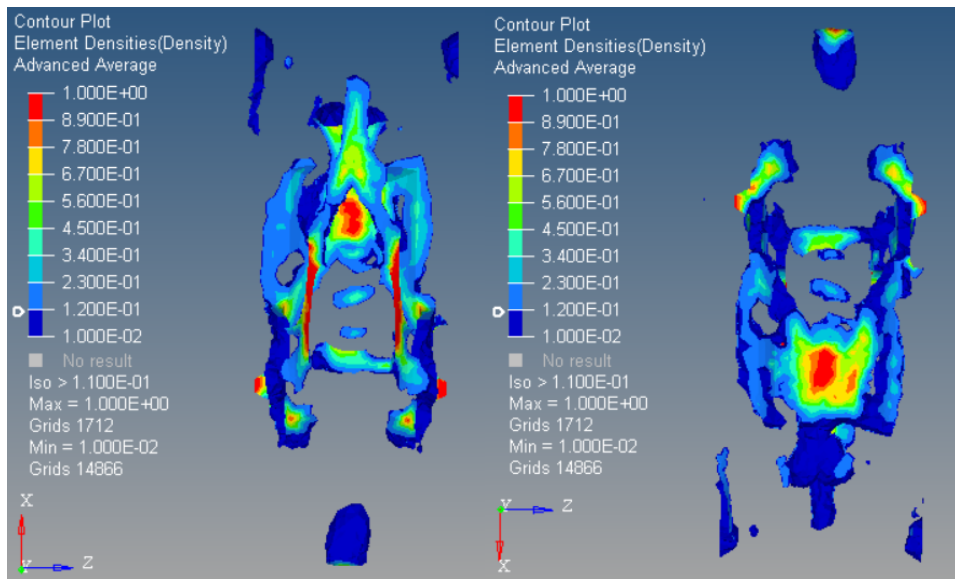
Figure 40: Topology optimization result



(a) Front view

(b) Rear view

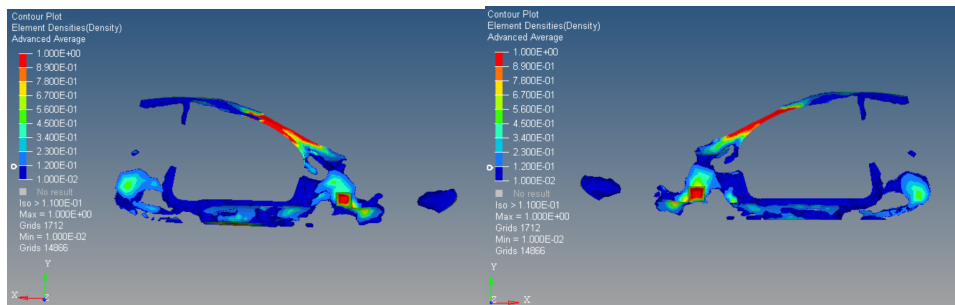
Figure 41



(a) Top view

(b) Bottom view

Figure 42



(a) Right side view

(b) Left side view

Figure 43

6.1.2 Iteration 2

The results of the second topology optimization required 37 iterations before convergence was obtained. All elements with a density below 50.5% has been removed. The results can be seen below.

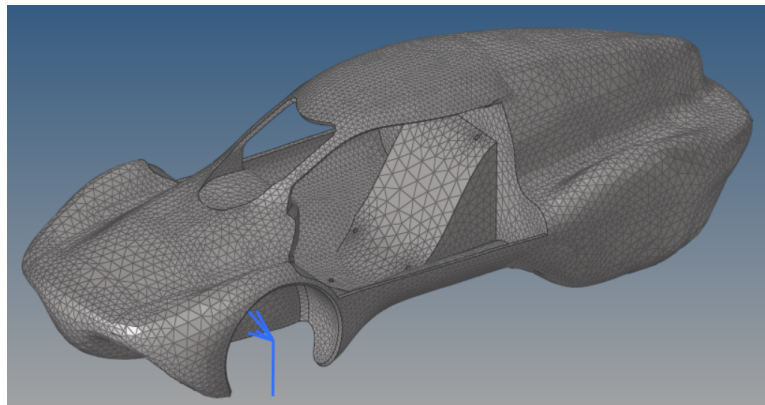


Figure 44: CAD model before optimization

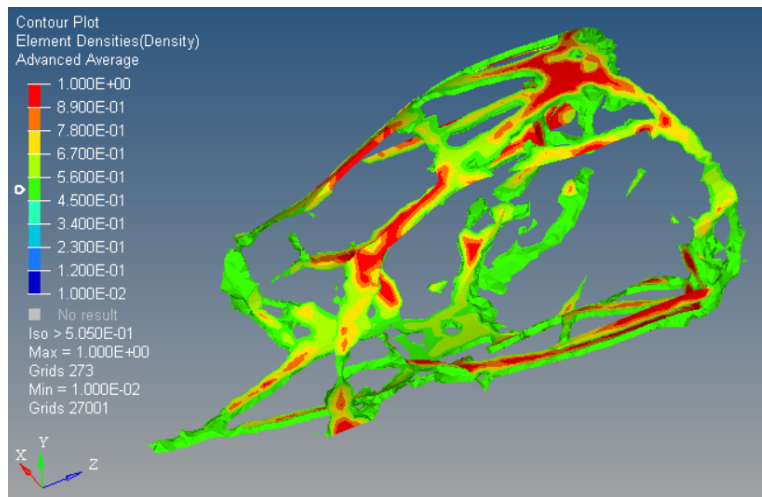
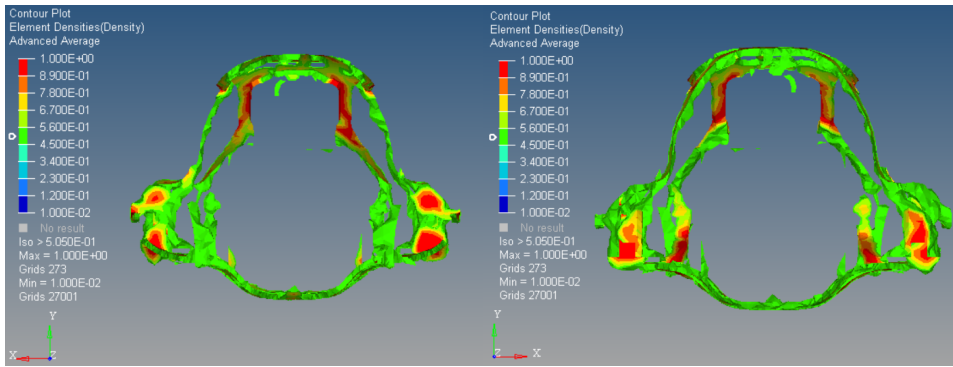


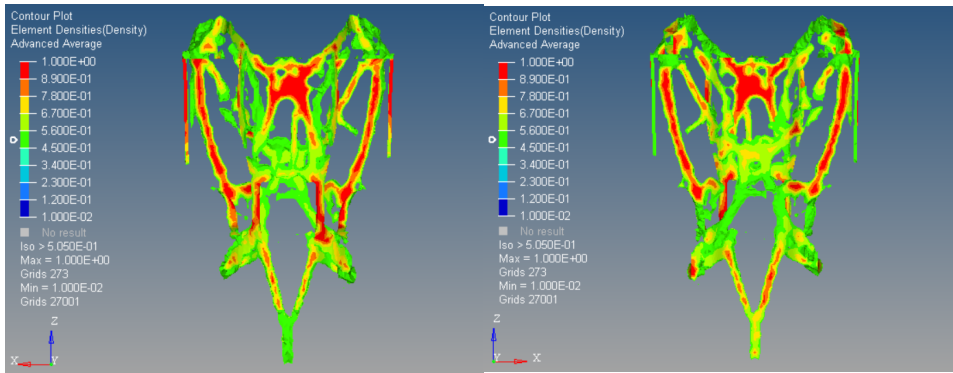
Figure 45: Topology optimization result



(a) Front view

(b) Rear view

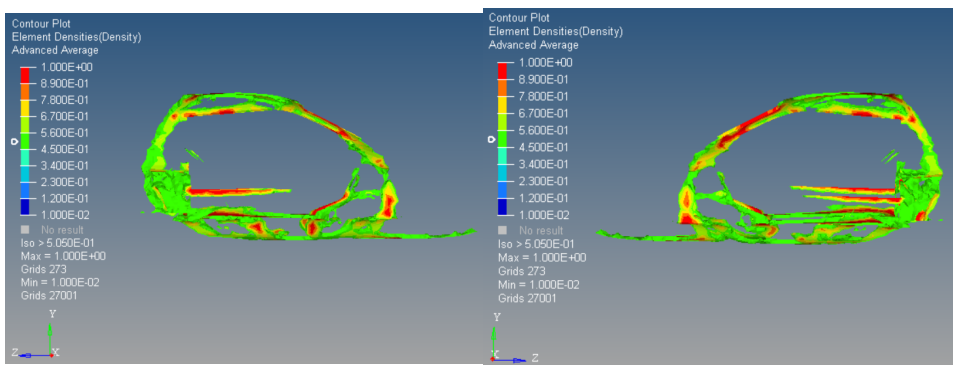
Figure 46



(a) Top view

(b) Bottom view

Figure 47



(a) Right side view

(b) Left side view

Figure 48

6.1.3 Iteration 3

The results of the third topology optimization required 42 iterations before convergence was obtained. All elements with a density below 30% were removed. The results can be seen below.

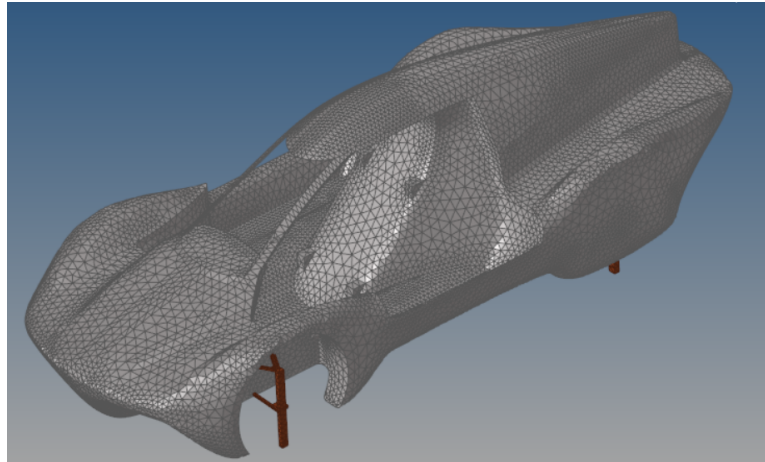


Figure 49: CAD model before optimization

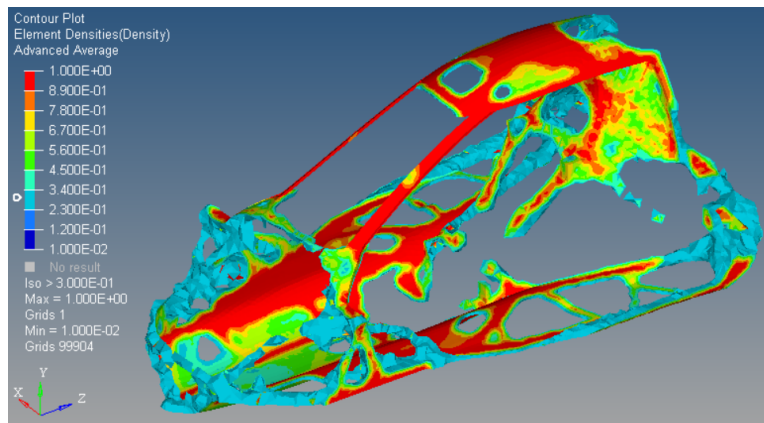
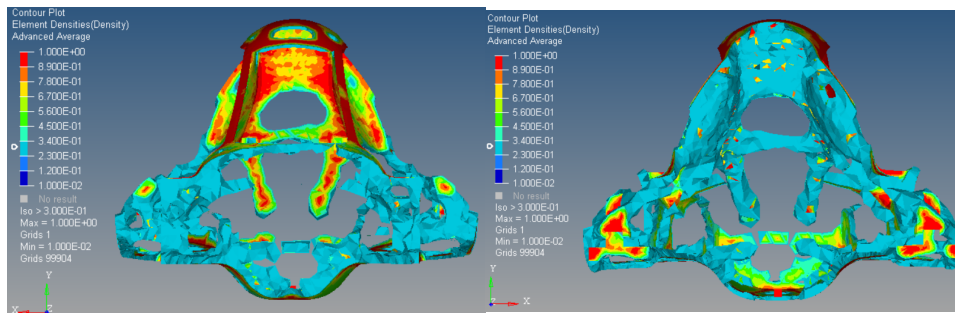


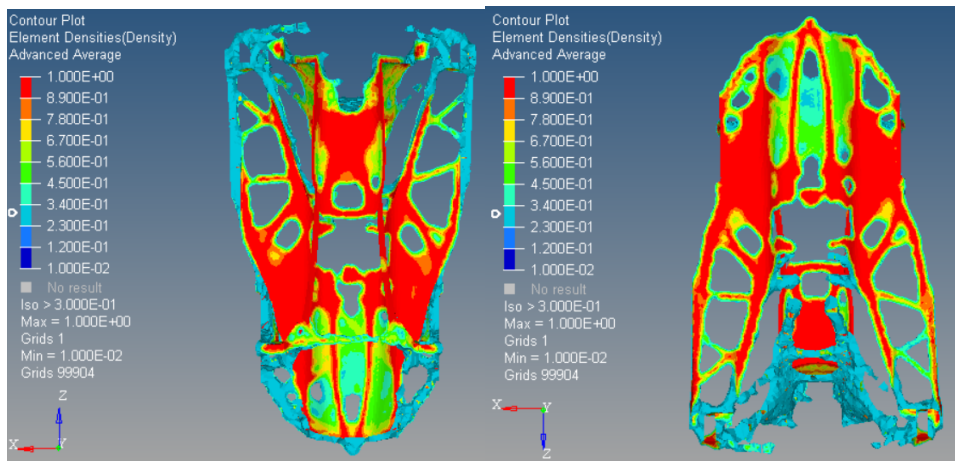
Figure 50: Topology optimization result



(a) Front view

(b) Rear view

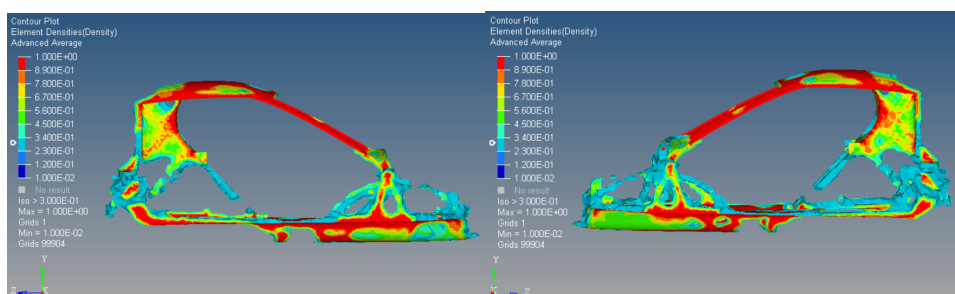
Figure 51



(a) Top view

(b) Bottom view

Figure 52



(a) Right side view

(b) Left side view

Figure 53

6.2 Free shape optimization

The result of the free shape optimization can be seen in the figures below. The optimization required 11 iterations before convergence was obtained. The contour plot shows a normalized value of the distance each element has grown (red) or shrunk (blue). The white wire frame surrounding the structure shows the placement of the original elements before the optimization.

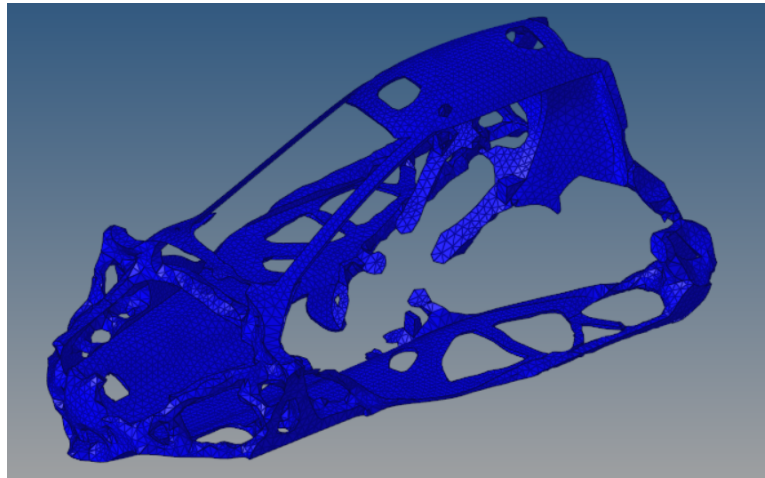


Figure 54: Topology optimized model before free shape fine tuning

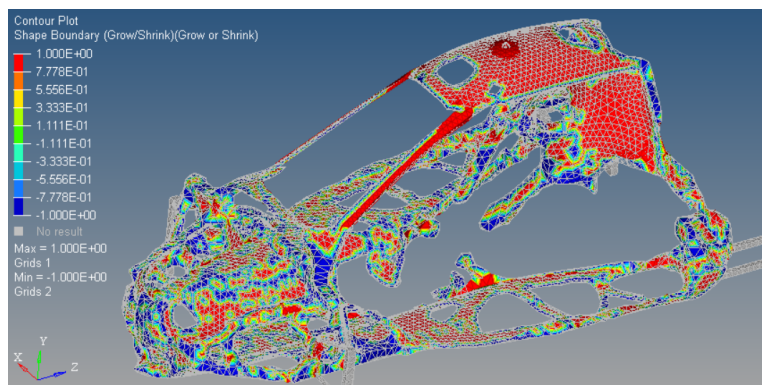
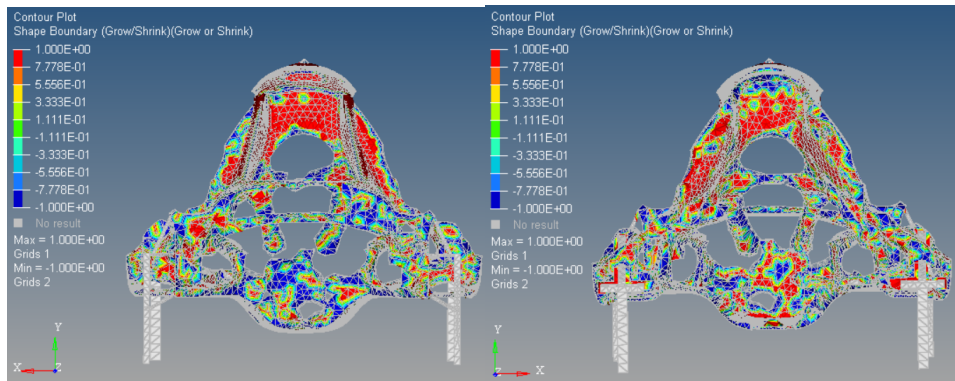


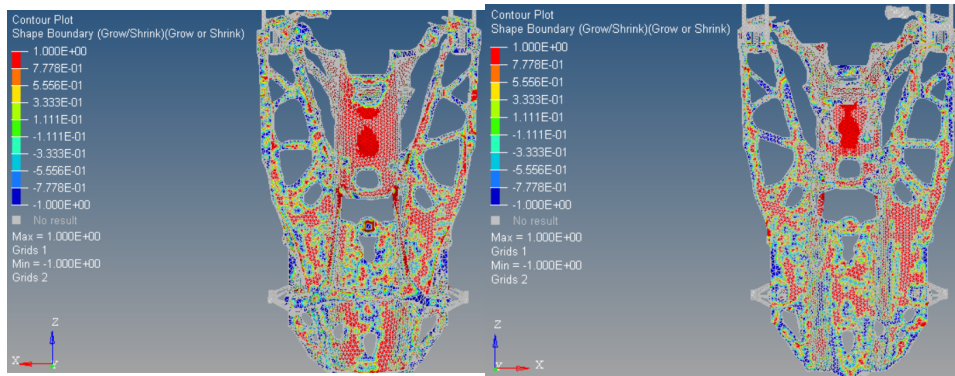
Figure 55: Free shape optimization result



(a) Front view

(b) Rear view

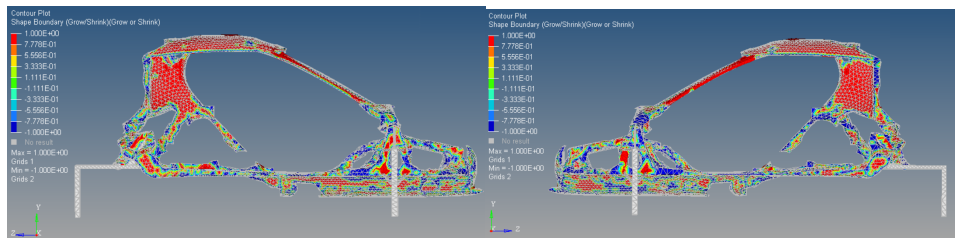
Figure 56



(a) Top view

(b) Bottom view

Figure 57



(a) Right side view

(b) Left side view

Figure 58

6.3 2D topology optimization

The result of the 2D topology optimization can be seen in the figures below. As with the previous topology optimization, the contour plot shows the element densities of the mesh, ranging from 0% density (blue) to 100% density (red). The optimization required 66 iteration before convergence was obtained. All elements with a density below 5% were removed.

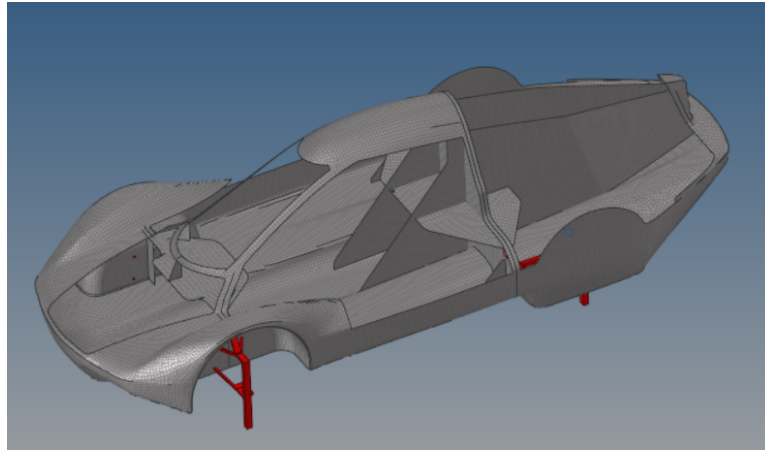


Figure 59: 2D CAD model before optimization

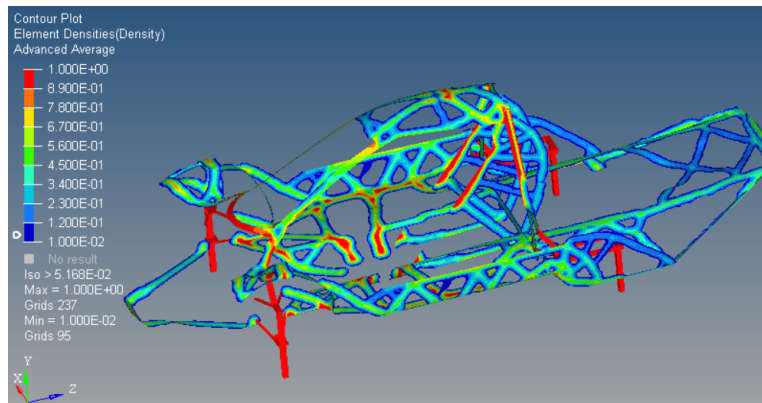


Figure 60: Topology optimization result

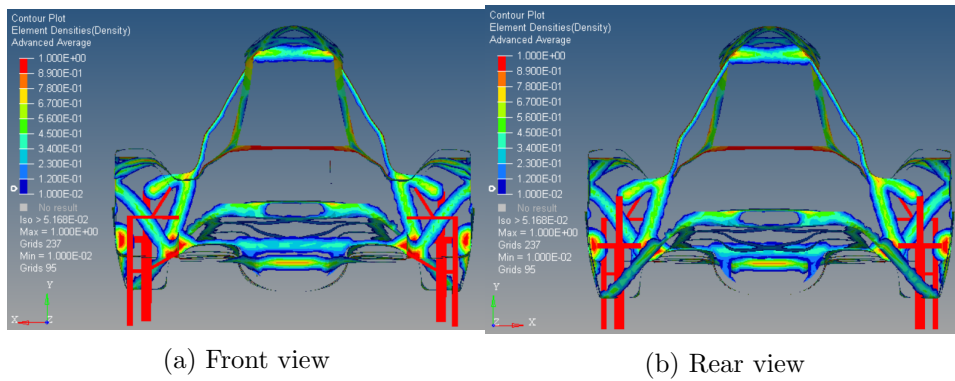


Figure 61

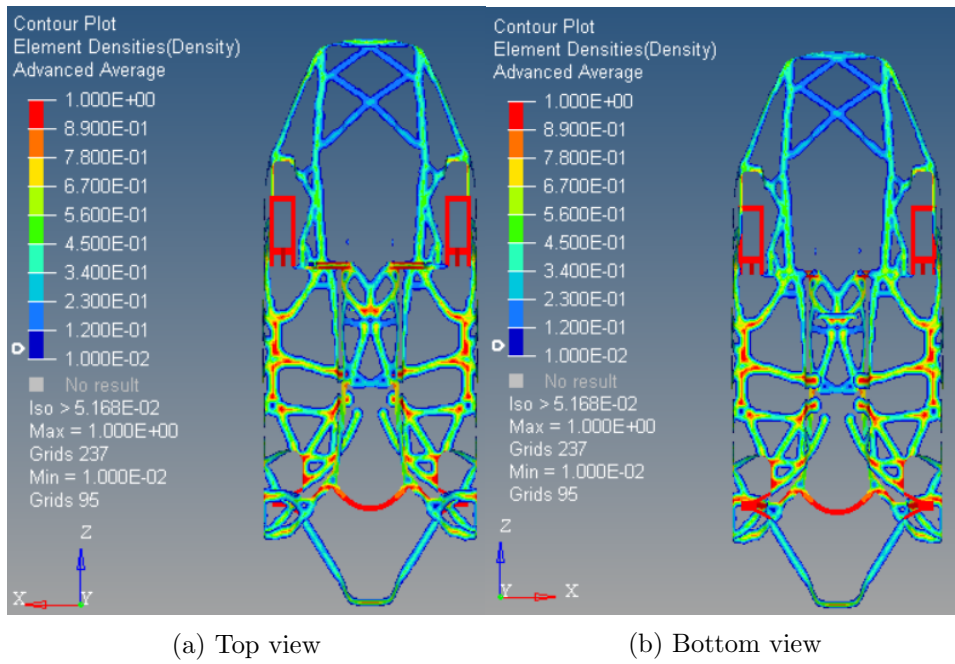


Figure 62

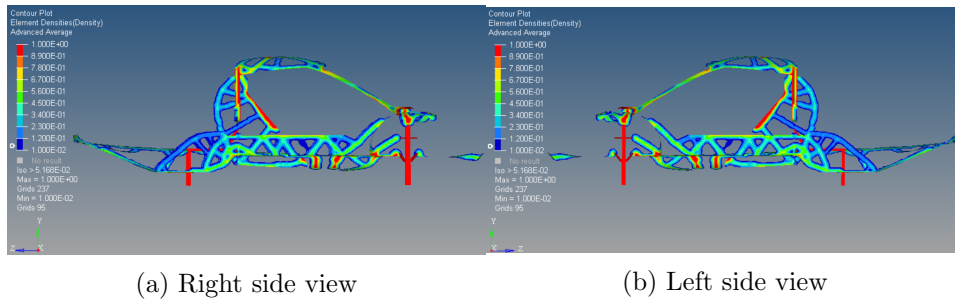


Figure 63

6.4 Composite optimization

The initial laminate design consisted of four carbon fibre plies of thickness 0.15 mm, as well as a core of thickness 10 mm. The laminate had a calculated weight of 15.3 kg. This initial weight was then further optimized.

6.4.1 Free-Size

The results from the first free-size optimization are shown in figure 64. Its goal was to determine the location of the core material. In addition, a stress analysis was done to find the location of the largest stresses and displacements. Large stresses mainly came from braking and turning done simultaneously (see appendix for all load cases). The figures below show the location of the largest stresses, as well as a simple drawing of where the core is anticipated to be. The largest stresses were calculated to be 110 MPa, and the maximum displacement was 8.2 mm, located on the roof. These two analyses constitute the foundation of the core materials location.

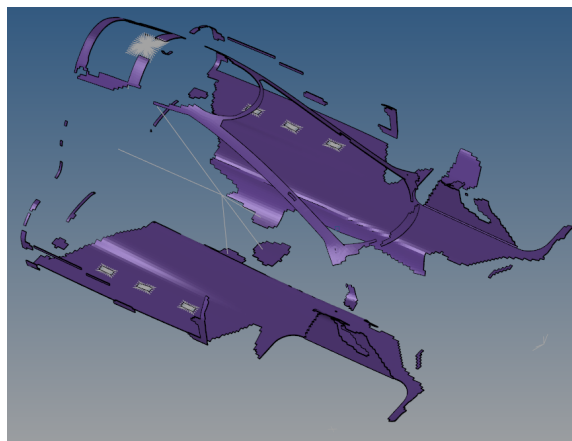
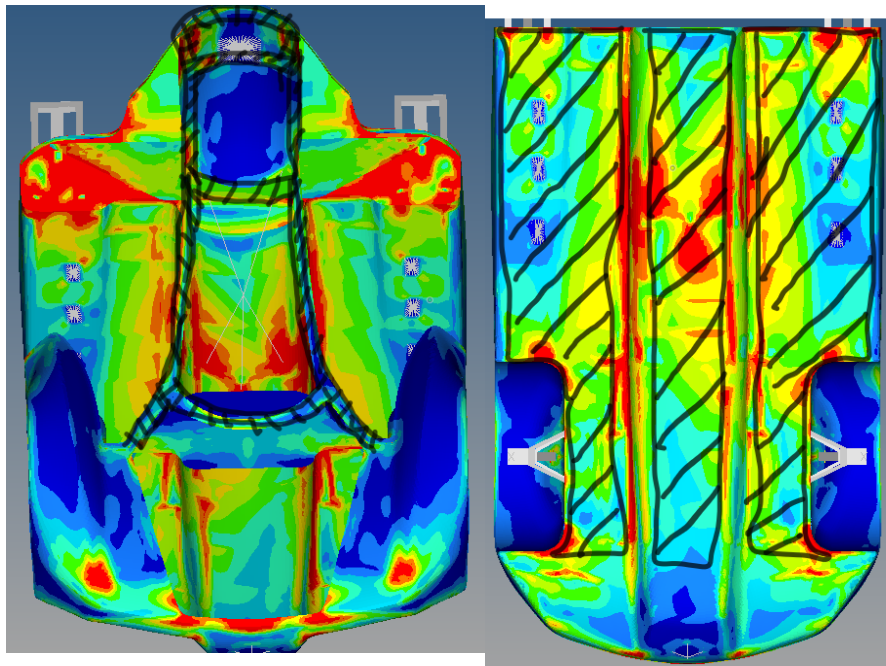
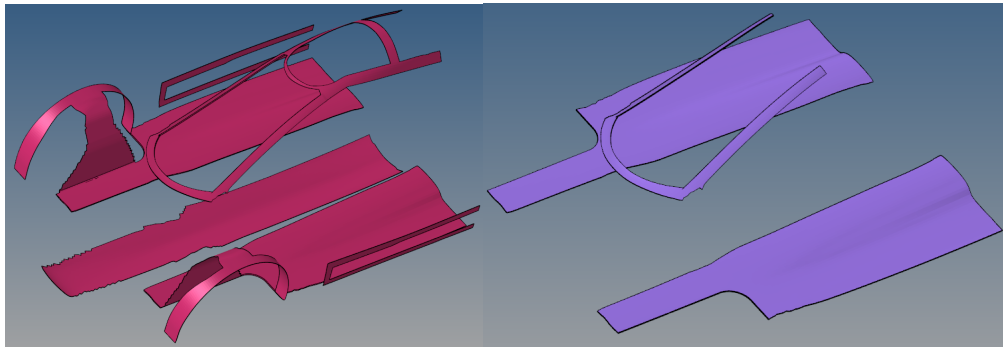


Figure 64: First free-size optimization, illustrating the shape of the core



(a) Stress plot with the core material drawing of the top (b) Stress plot with the core material drawing of the bottom

Figure 65



(a) Final design. 10 mm core that covers both the 10 mm and 20 mm area (b) 10mm core that covers only the 20 mm area, making it 20 mm in total

Figure 66

For the second free-size optimization, the design was updated with the previously calculated core location. The new weight was reduced down to 10.8 kg in total before the second optimization was completed. The second free-size optimization resulted in a laminate of 20 plies. The weight was at

this point reduced to 6.8 kg. The maximum thickness was 11.4 mm, and the thinnest laminate created was 0.6 mm, which was the constraint in the free-size design variable. To get an idea of the variation the optimization generates, the thicknesses of the laminate can be observed below.

Define laminate:							
Name	Id	Color	Material	Thickness	Orientation	IP	Result
Ply 1	7100	■	Carbon Fibre	0.05816	0.0	0	yes
Ply 2	7200	■	Carbon Fibre	0.02657	0.0	0	yes
Ply 3	7300	■	Carbon Fibre	0.04970	0.0	0	yes
Ply 4	7400	■	Carbon Fibre	0.01557	0.0	0	yes
Ply 5	8100	■	Carbon Fibre	0.05816	90.0	0	yes
Ply 6	8200	■	Carbon Fibre	0.02657	90.0	0	yes
Ply 7	8300	■	Carbon Fibre	0.04970	90.0	0	yes
Ply 8	8400	■	Carbon Fibre	0.01557	90.0	0	yes
Ply 9	3100	■	Carbon Fibre	0.05341	45.0	0	yes
Ply 10	3200	■	Carbon Fibre	0.04241	45.0	0	yes
Ply 11	3300	■	Carbon Fibre	0.02518	45.0	0	yes
Ply 12	3400	■	Carbon Fibre	0.07901	45.0	0	yes
Ply 13	4100	■	Carbon Fibre	0.05341	-45.0	0	yes
Ply 14	4200	■	Carbon Fibre	0.04241	-45.0	0	yes
Ply 15	4300	■	Carbon Fibre	0.02518	-45.0	0	yes
Ply 16	4400	■	Carbon Fibre	0.07901	-45.0	0	yes
Ply 17	5100	■	Diab 45H	1.04009	180.0	0	yes
Ply 18	5200	■	Diab 45H	2.04118	180.0	0	yes
Ply 19	5300	■	Diab 45H	1.69813	180.0	0	yes
Ply 20	5400	■	Diab 45H	0.22061	180.0	0	yes

Figure 67: Table showing the thicknesses of each individual ply in the laminate [mm]

Another FEM-analysis was completed to verify the results from the free-size optimization. The maximum displacements and stresses from all the loads acting on the monocoque are presented in the summary below.

- **Subcase 1 - Load_Roof_-Y**
 - Maximum displacement is 2.05 at grid 63008.
 - Maximum 2-D element stress is 33.3 in element 72406.
- **Subcase 2 - Load_Roof_X**
 - Maximum displacement is 8.23 at grid 62394.
 - Maximum 2-D element stress is 24.1 in element 62154.
- **Subcase 3 - Load_Roof_-X**
 - Maximum displacement is 8.23 at grid 62394.
 - Maximum 2-D element stress is 24.1 in element 62154.
- **Subcase 4 - Load_Roof_Z**
 - Maximum displacement is 1.90 at grid 28475.
 - Maximum 2-D element stress is 18.5 in element 72406.
- **Subcase 5 - Load_Roof_-Z**
 - Maximum displacement is 1.90 at grid 28475.
 - Maximum 2-D element stress is 18.5 in element 72406.
- **Subcase 6 - Load_Hook**
 - Maximum displacement is 2.46 at grid 19961.
 - Maximum 2-D element stress is 104. in element 50425.
- **Subcase 8 - Load_BreakingFront**
 - Maximum displacement is 1.76 at grid 7855.
 - Maximum 2-D element stress is 23.3 in element 72406.
- **Subcase 9 - Load_BreakingBack**
 - Maximum displacement is 1.73 at grid 7855.
 - Maximum 2-D element stress is 22.1 in element 72406.
- **Subcase 10 - Load_BreakingAll**
 - Maximum displacement is 1.37 at grid 7855.
 - Maximum 2-D element stress is 18.4 in element 72406.
- **Subcase 11 - Load_TurningLeft**
 - Maximum displacement is 1.79 at grid 8735.
 - Maximum 2-D element stress is 22.2 in element 30580.
- **Subcase 12 - Load_TurningRight**
 - Maximum displacement is 1.79 at grid 42729.
 - Maximum 2-D element stress is 25.3 in element 72406.
- **Subcase 13 - Load_BreakingAndTurningRight**
 - Maximum displacement is 3.11 at grid 7855.
 - Maximum 2-D element stress is 42.4 in element 72406.
- **Subcase 14 - Load_BreakingAndTurningLeft**
 - Maximum displacement is 3.03 at grid 7855.
 - Maximum 2-D element stress is 37.3 in element 30868.
- **Subcase 15 - Load_Gravity_-Y**
 - Maximum displacement is 1.88 at grid 7855.
 - Maximum 2-D element stress is 21.7 in element 72406.
- **Subcase 16 - Load_Bump**
 - Maximum displacement is 3.77 at grid 7855.
 - Maximum 2-D element stress is 43.4 in element 72406.
- **Subcase 17 - Load_StepIn**
 - Maximum displacement is 5.95 at grid 50044.
 - Maximum 2-D element stress is 66.9 in element 49131.

Figure 68: Maximum stresses and displacements for all loads after second free-size optimization

As previously mentioned, free-size optimization creates several plies with non-manufacturable shapes and thicknesses. These were later modified element by element to obtain feasible designs and thicknesses. The figure below shows the transformation from a raw ply to a modified ply that can be manufactured. The other modified plies are found in the appendix. The total weight after editing every ply and removing two core plies (ply number 19 and 20) that were created during the second free-size was calculated to be 6.3 kg.

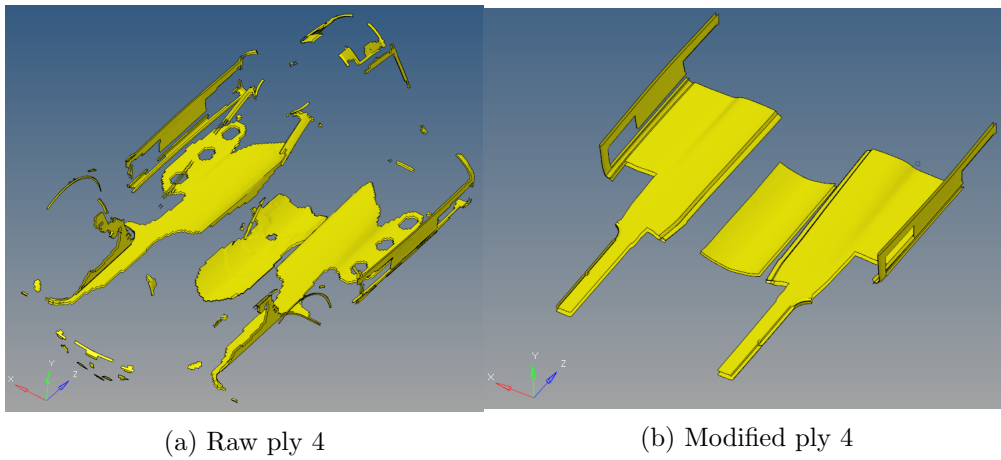


Figure 69

6.4.2 Sizing

By constraining each ply to a thickness of 0.15 mm, as well as modifying each ply, the total weight increased. However, some plies were also removed during the sizing-optimization process due to their thickness. The weight increased to 10.4 kg. The sizing optimization resulted in a decrease from 20 to 14 plies with thicknesses of 0.15 mm for the carbon fibre plies and 5 mm for the two core plies. The figure below shows the result of the thickest laminate in the monocoque, which includes two 5 mm core plies and eight 0.15 mm carbon fibre plies.

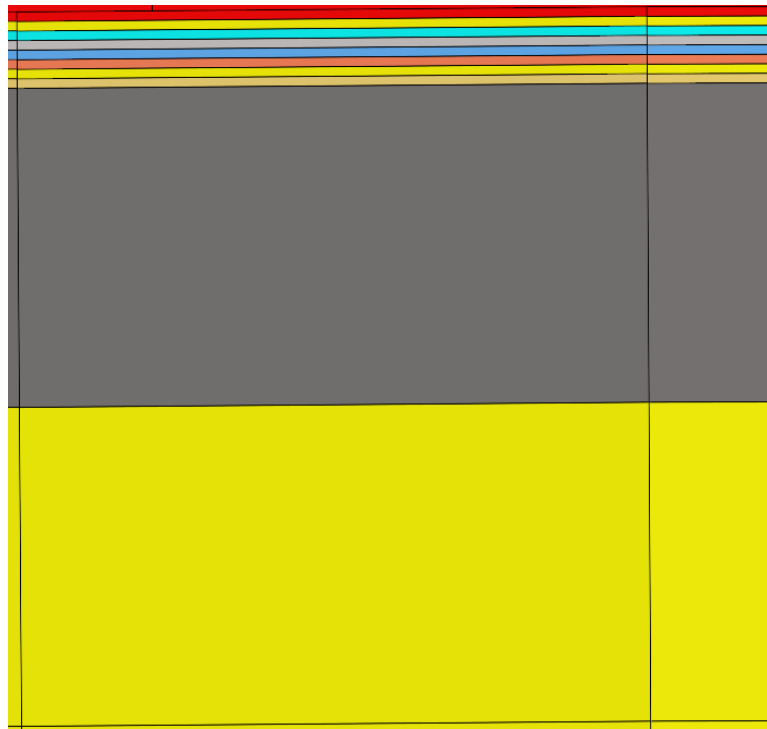


Figure 70: One half of the thickest laminate, two 5 mm core in addition to eight 0.15 mm carbon fibre plies on each side of the centre line

The maximum stresses and displacements from the FEM-analysis are listed below.

- **Subcase 1 - Load_Roof_-Y**
 - Maximum displacement is 1.75 at grid 63004.
 - Maximum 2-D element stress is 32.3 in element 72406.
- **Subcase 2 - Load_Roof_-X**
 - Maximum displacement is 7.01 at grid 62395.
 - Maximum 2-D element stress is 32.6 in element 62231.
- **Subcase 3 - Load_Roof_-X**
 - Maximum displacement is 7.01 at grid 62395.
 - Maximum 2-D element stress is 32.6 in element 62231.
- **Subcase 4 - Load_Roof_-Z**
 - Maximum displacement is 1.49 at grid 28458.
 - Maximum 2-D element stress is 17.3 in element 72406.
- **Subcase 5 - Load_Roof_-Z**
 - Maximum displacement is 1.49 at grid 28458.
 - Maximum 2-D element stress is 17.3 in element 72406.
- **Subcase 6 - Load_Hook**
 - Maximum displacement is 5.76 at grid 26775.
 - Maximum 2-D element stress is 309. in element 16749.
- **Subcase 8 - Load_BreakingFront**
 - Maximum displacement is 1.46 at grid 7855.
 - Maximum 2-D element stress is 17.5 in element 75821.
- **Subcase 9 - Load_BreakingBack**
 - Maximum displacement is 1.51 at grid 7855.
 - Maximum 2-D element stress is 19.7 in element 31356.
- **Subcase 10 - Load_BreakingAll**
 - Maximum displacement is 1.18 at grid 26776.
 - Maximum 2-D element stress is 18.1 in element 30580.
- **Subcase 11 - Load_TurningLeft**
 - Maximum displacement is 1.73 at grid 6142.
 - Maximum 2-D element stress is 23.7 in element 30580.
- **Subcase 12 - Load_TurningRight**
 - Maximum displacement is 1.73 at grid 40136.
 - Maximum 2-D element stress is 23.7 in element 64256.
- **Subcase 13 - Load_BreakingAndTurningRight**
 - Maximum displacement is 2.70 at grid 42729.
 - Maximum 2-D element stress is 38.9 in element 30580.
- **Subcase 14 - Load_BreakingAndTurningLeft**
 - Maximum displacement is 2.38 at grid 60769.
 - Maximum 2-D element stress is 37.7 in element 30868.
- **Subcase 15 - Load_Gravity_-Y**
 - Maximum displacement is 1.44 at grid 7855.
 - Maximum 2-D element stress is 18.4 in element 75821.
- **Subcase 16 - Load_Bump**
 - Maximum displacement is 2.88 at grid 7855.
 - Maximum 2-D element stress is 36.7 in element 75821.
- **Subcase 17 - Load_Steplin**
 - Maximum displacement is 3.69 at grid 50235.
 - Maximum 2-D element stress is 52.5 in element 32096.

Figure 71: Maximum stresses and displacements for each load case after sizing optimization

6.4.3 Shuffling

The weight was not changed in this optimization. However, the stacking sequence was shuffled in the desired order. Plies oriented at 45 and -45 degrees were paired, and plies with the same orientation were not stacked on top of each other, except for core plies. Pairing 0 and 90 degrees oriented plies is not a constraint feature in Hyperworks, however, the simulation managed to create 0 and 90 degree plies together. The full stacking sequence illustrated in the figure below shows 45 and -45 degrees paired together, and 0 and 90 degrees paired together. The result shows one half of the laminate since it is symmetrical. The 180-degree plies are the foam core.

Iteration 0	Iteration 1	Iteration 2	Iteration 3	Iteration 4	Legend
1	1	1	1	1	-45.0 degrees
2	5	5	5	5	45.0 degrees
3	2	9	9	9	0.0 degrees
4	6	13	12	13	90.0 degrees
5	3	2	2	2	180.0 degrees
6	7	6	6	6	45.0 degrees
7	4	10	10	10	0.0 degrees
8	8	14	14	14	90.0 degrees
9	9	3	3	3	-45.0 degrees
10	17	7	7	7	45.0 degrees
11	10	11	17	11	0.0 degrees
12	13	15	13	15	90.0 degrees
13	11	4	4	4	-45.0 degrees
14	14	8	8	8	45.0 degrees
15	12	12	15	12	0.0 degrees
16	18	19	19	16	90.0 degrees
17	15	17	11	17	0.0 degrees
18	19	18	18	18	180.0 degrees
19	16	16	16	19	90.0 degrees
20	20	20	20	20	180.0 degrees

Figure 72: Stacking sequence with respective orientations

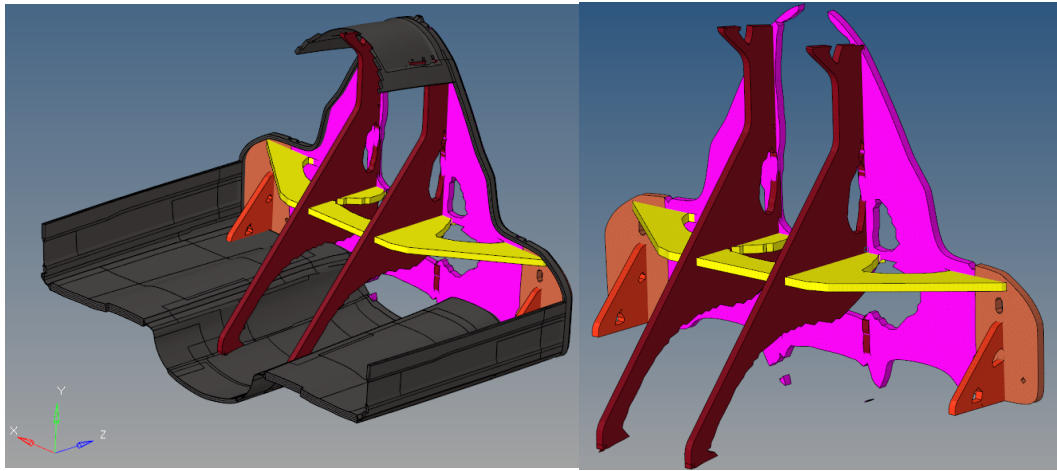
The FEM-analysis of the new design created from the shuffling is shown below.

- **Subcase 1 - Load_Roof_-Y**
 - Maximum displacement is 1.13 at grid 63005.
 - Maximum 2-D element stress is 17.8 in element 63242.
- **Subcase 2 - Load_Roof_X**
 - Maximum displacement is 4.81 at grid 28398.
 - Maximum 2-D element stress is 21.0 in element 62231.
- **Subcase 3 - Load_Roof_-X**
 - Maximum displacement is 4.81 at grid 28398.
 - Maximum 2-D element stress is 21.0 in element 62231.
- **Subcase 4 - Load_Roof_Z**
 - Maximum displacement is 1.07 at grid 28447.
 - Maximum 2-D element stress is 13.0 in element 72406.
- **Subcase 5 - Load_Roof_-Z**
 - Maximum displacement is 1.07 at grid 28447.
 - Maximum 2-D element stress is 13.0 in element 72406.
- **Subcase 6 - Load_Hook**
 - Maximum displacement is 0.945 at grid 19961.
 - Maximum 2-D element stress is 48.4 in element 50425.
- **Subcase 8 - Load_BreakingFront**
 - Maximum displacement is 1.03 at grid 7855.
 - Maximum 2-D element stress is 12.9 in element 32755.
- **Subcase 9 - Load_BreakingBack**
 - Maximum displacement is 1.07 at grid 7855.
 - Maximum 2-D element stress is 16.7 in element 65032.
- **Subcase 10 - Load_BreakingAll**
 - Maximum displacement is 0.770 at grid 7855.
 - Maximum 2-D element stress is 15.8 in element 64256.
- **Subcase 11 - Load_TurningLeft**
 - Maximum displacement is 1.36 at grid 6142.
 - Maximum 2-D element stress is 18.7 in element 30580.
- **Subcase 12 - Load_TurningRight**
 - Maximum displacement is 1.36 at grid 40136.
 - Maximum 2-D element stress is 18.6 in element 64256.
- **Subcase 13 - Load_BreakingAndTurningRight**
 - Maximum displacement is 1.94 at grid 42729.
 - Maximum 2-D element stress is 32.4 in element 30580.
- **Subcase 14 - Load_BreakingAndTurningLeft**
 - Maximum displacement is 1.74 at grid 6142.
 - Maximum 2-D element stress is 32.8 in element 30868.
- **Subcase 15 - Load_Gravity_-Y**
 - Maximum displacement is 1.00 at grid 7855.
 - Maximum 2-D element stress is 13.0 in element 32096.
- **Subcase 16 - Load_Bump**
 - Maximum displacement is 2.01 at grid 7855.
 - Maximum 2-D element stress is 26.1 in element 32096.
- **Subcase 17 - Load_StepIn**
 - Maximum displacement is 2.79 at grid 50252.
 - Maximum 2-D element stress is 40.4 in element 32096.

Figure 73: Maximum stresses and displacements for each load case after shuffling optimization

6.5 Topology optimization of the inner structure

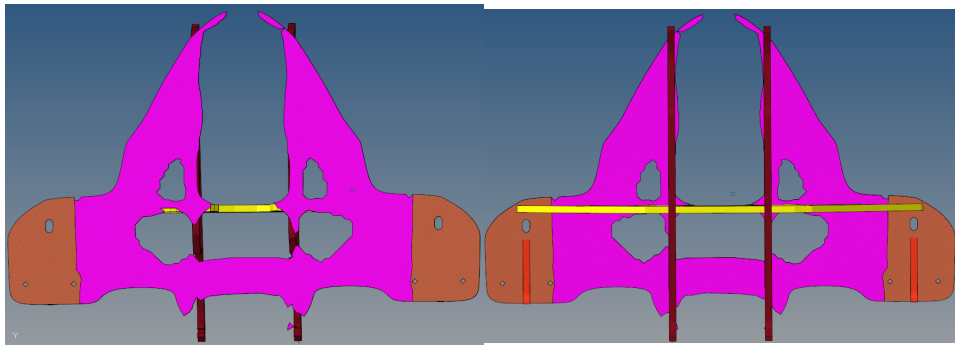
The result of the topology optimization of the inner structure is shown below. The weight was reduced to 8.1 kg after this optimization.



(a) Firewall

(b) Firewall

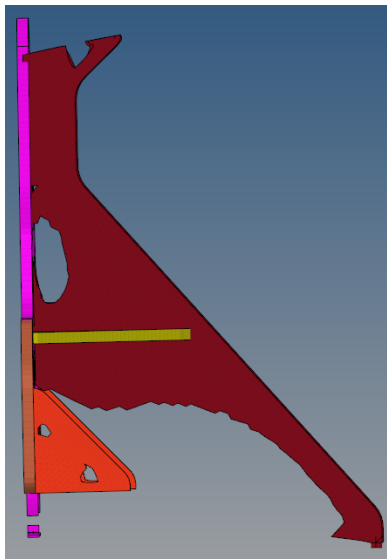
Figure 74



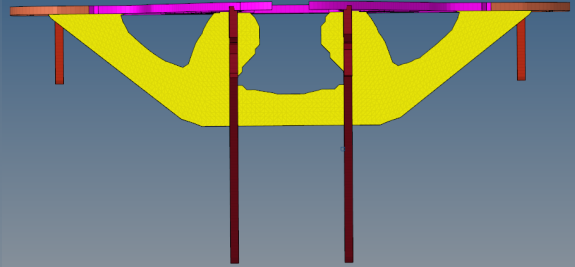
(a) Rear view of the firewall

(b) Front view of the firewall

Figure 75

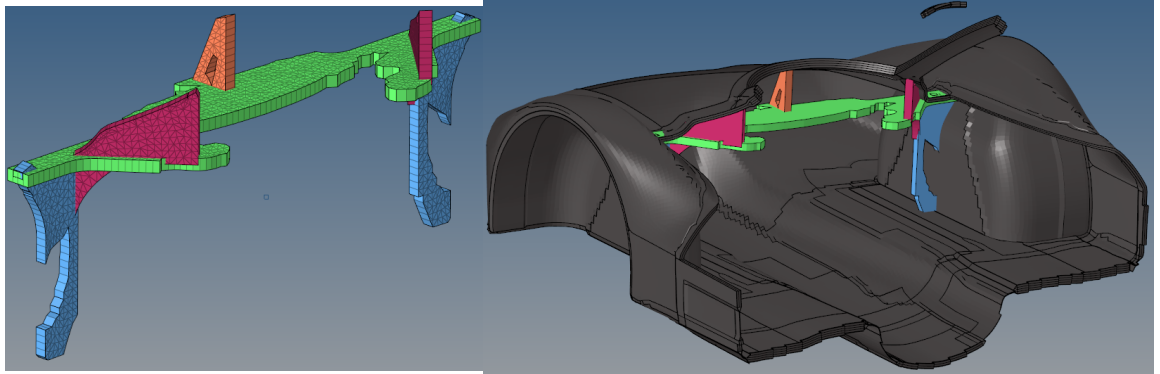


(a) Side view of the firewall



(b) Top view of the firewall

Figure 76



(a) Dashboard

(b) Dashboard

Figure 77

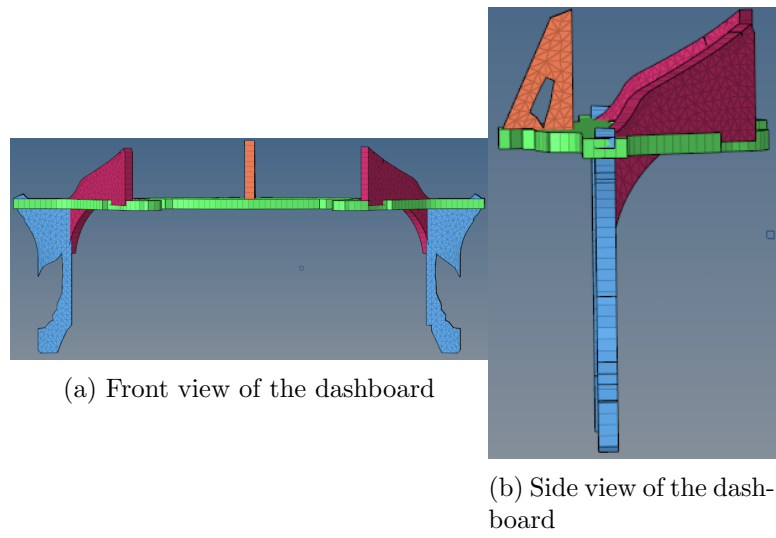


Figure 78

The results from the FEM-analysis after the topology optimization is shown below.

- **Subcase 1 - Load_Roof_-Y**
 - Maximum displacement is 1.65 at grid 63002.
 - Maximum 2-D element stress is 46.6 in element 72406.
- **Subcase 2 - Load_Roof_X**
 - Maximum displacement is 5.40 at grid 28398.
 - Maximum 2-D element stress is 26.7 in element 28555.
- **Subcase 3 - Load_Roof_-X**
 - Maximum displacement is 5.40 at grid 28398.
 - Maximum 2-D element stress is 26.7 in element 28555.
- **Subcase 4 - Load_Roof_Z**
 - Maximum displacement is 2.22 at grid 74215.
 - Maximum 2-D element stress is 41.9 in element 73058.
- **Subcase 5 - Load_Roof_-Z**
 - Maximum displacement is 2.22 at grid 74215.
 - Maximum 2-D element stress is 41.9 in element 73058.
- **Subcase 6 - Load_Hook**
 - Maximum displacement is 8.14 at grid 26774.
 - Maximum 2-D element stress is 305. in element 16749.
- **Subcase 8 - Load_BreakingFront**
 - Maximum displacement is 1.45 at grid 7855.
 - Maximum 2-D element stress is 24.7 in element 75817.
- **Subcase 9 - Load_BreakingBack**
 - Maximum displacement is 1.39 at grid 7855.
 - Maximum 2-D element stress is 22.7 in element 75817.
- **Subcase 10 - Load_BreakingAll**
 - Maximum displacement is 2.11 at grid 26774.
 - Maximum 2-D element stress is 24.2 in element 21853.
- **Subcase 11 - Load_TurningLeft**
 - Maximum displacement is 2.41 at grid 60768.
 - Maximum 2-D element stress is 32.5 in element 75821.
- **Subcase 12 - Load_TurningRight**
 - Maximum displacement is 2.40 at grid 26774.
 - Maximum 2-D element stress is 32.0 in element 73058.
- **Subcase 13 - Load_BreakingAndTurningRight**
 - Maximum displacement is 3.33 at grid 26775.
 - Maximum 2-D element stress is 46.8 in element 72406.
- **Subcase 14 - Load_BreakingAndTurningLeft**
 - Maximum displacement is 4.36 at grid 60768.
 - Maximum 2-D element stress is 54.5 in element 75821.
- **Subcase 15 - Load_Gravity_-Y**
 - Maximum displacement is 2.58 at grid 60768.
 - Maximum 2-D element stress is 27.9 in element 21853.
- **Subcase 16 - Load_Bump**
 - Maximum displacement is 5.16 at grid 60768.
 - Maximum 2-D element stress is 55.8 in element 21853.
- **Subcase 17 - Load_Steplin**
 - Maximum displacement is 3.32 at grid 52150.
 - Maximum 2-D element stress is 59.7 in element 26433.
- **Subcase 18 - Load_SeatBelt**
 - Maximum displacement is 2.04 at grid 74215.
 - Maximum 2-D element stress is 25.3 in element 75821.

Figure 79: Maximum stresses and displacements for each load case after the last topology optimization

6.6 Material selection

The table below shows a summary of the material testing.

Material testing				
Material Type	Price[NOK/m ²]	Ease of use	Draping	Weight[gram/m ²]
CF 2x2 twill weave spiderweb	110	Easy	Medium	300
CF 2x2 twill weave	280	Hard	Exceptional	200
CF unidirectional	240	Easy	Medium	250
Biaxial sewn 45/-45	210	Easy	Bad	450
Divinycell 45 10mm	60	Medium	Medium	45
Tubus Honeycomb 10mm	120	Easy	Good	60

The table below shows the results from the epoxy testing. The prices for the different epoxies were the same, 1000 NOK/kg.

Material testing		
Epoxy Type	Temperature [Degree Celsius]	Curing time [Hours]
Araldite ESR3+ESH3	20	168
	60	48
	80	24
Araldite LY1564+XB3404	20	288
	60	72
	80	48

The figure below shows how much a PVC foam test piece and a honeycomb test piece could bend after being heated by an oven and by a heat gun, respectively.

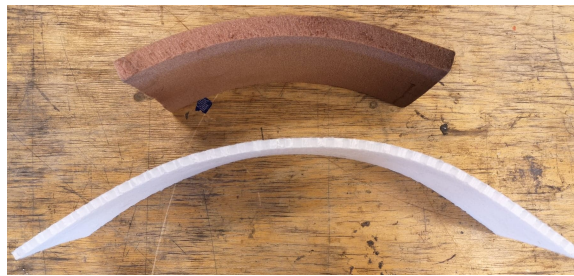


Figure 80: Bent 10 mm PVC foam and 5 mm honeycomb

The Tubus honeycomb laminate weighed approximately twice as much as the PVC foam and had two more carbon fibre plies. The PVC foam was twice as thick as the Tubus honeycomb core. The weight of the PVC foam laminate was 190 g and the Tubus honeycomb was 240 g.

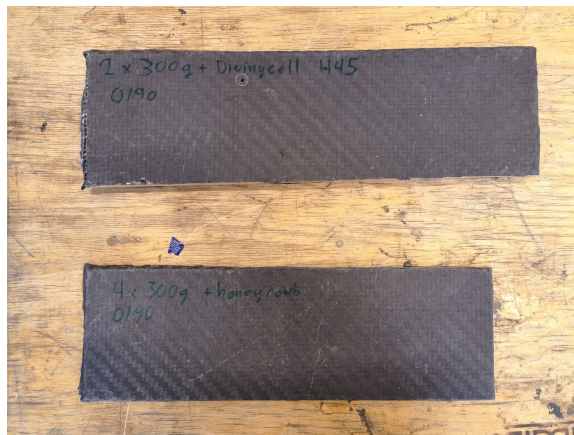


Figure 81: 2x300g/m² with foam core and 4x300g/m² with honeycomb core

6.7 Production

Total weight of the monocoque including epoxy, extensions of carbon fibre, glue, inner structure, non-adhesive spray, tail extension and foil was 22kg.

Monocoque properties	
Total weight [kg]	22
Length [mm]	3300
Width [mm]	1200
Height with wheels [mm]	1000

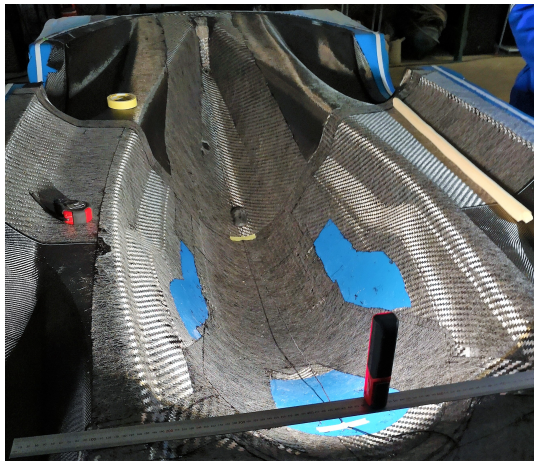


(a) 45/-45 and 0/90 carbon fibre



(b) Halfway through the first layer of the monocoque

Figure 82



(a) Layers on the upper body



(b) The core on the upper body

Figure 83

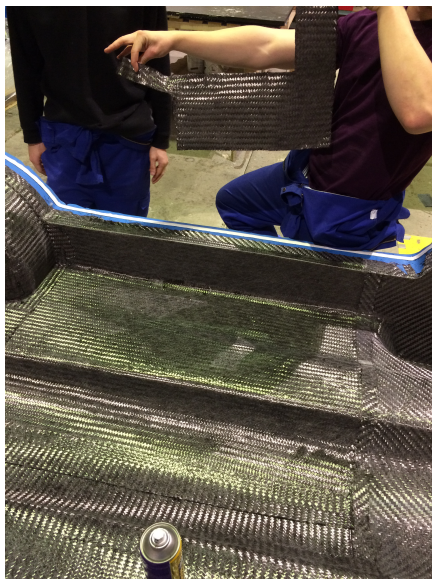


(a) The foam core on the lower body



(b) First carbon fibre layer on top of the core

Figure 84



(a) Each ply layer consisted of tens of different patches



(b) Carbon fibre layers

Figure 85

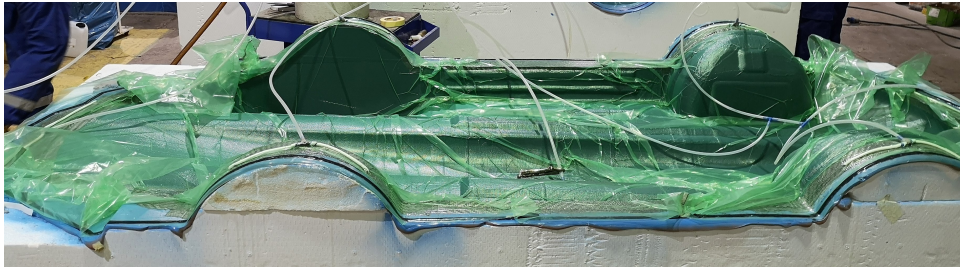


Figure 86: Set-up before vacuum infusion



(a) Monocoque after infusion



(b) Firewall. Notice the core in the corners is made denser to support the rear suspension

Figure 87



Figure 88: Monocoque without inner structure



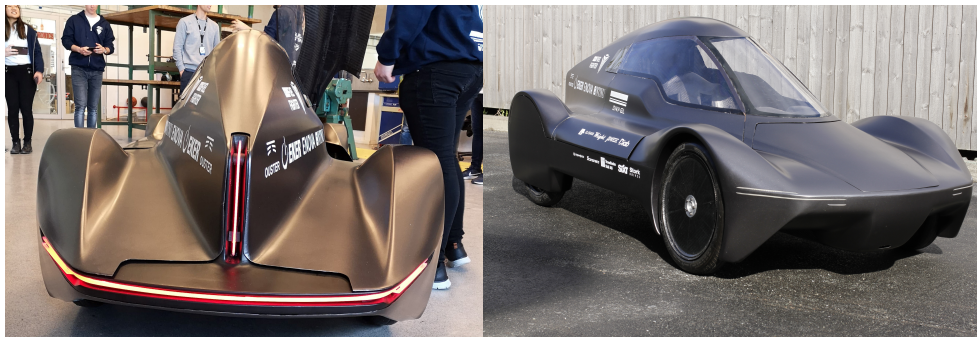
Figure 89: Top of the monocoque before post processing



Figure 90: Front view of the finished product



Figure 91: Side view of the finished product



(a) Rear view of the finished product (b) Side view of the finished product

Figure 92

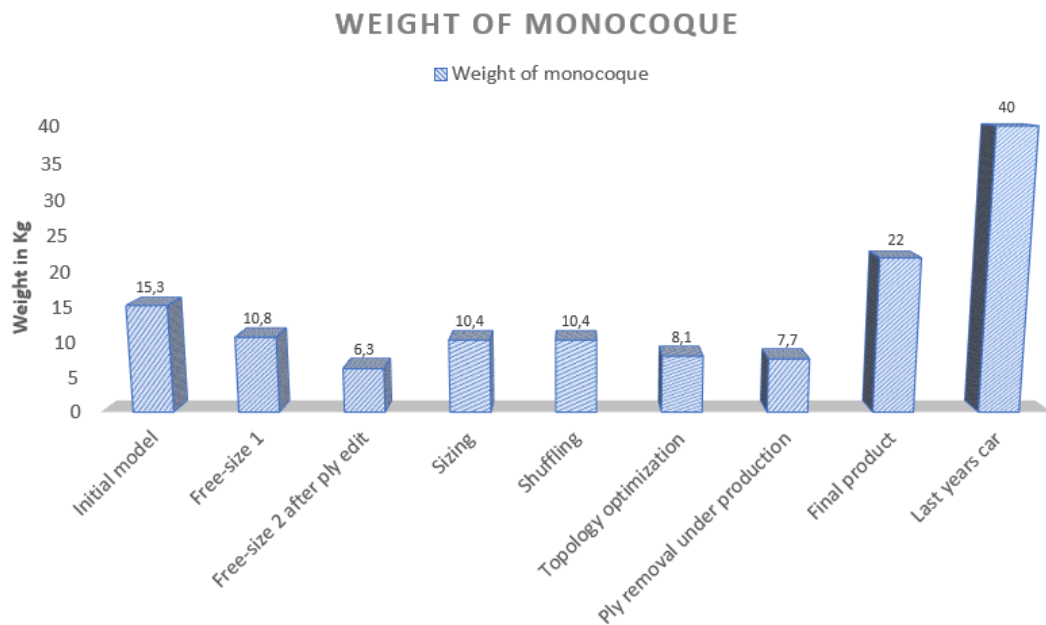


Figure 93: Graph displaying the progression of the weight of the monocoque through each optimization step

7 Discussion

7.1 Load cases

For optimizing the car, the best approach would have been to use dynamic load cases, which could better simulate situations such as braking and turning. However, dynamic load cases require huge amounts of data-power, which DNV GL Fuel Fighter does not have access to. For that reason, a quasi-static load case approach was used. This means that many static loads are applied to the car, which together simulates dynamic loads. This did pose some challenges, however. Using too many load cases that simulate similar situations will result in one feature dominating the final design. At the same time, too many load cases overall will make the final design weak in all situations, as the material will be spread out to accommodate every conceivable load instead of focusing on the most dominant forces.

The topology and composite optimizations utilized two different sets of load cases. For composite optimization, gravity loads were applied to the monocoque as a way to simulate braking and turning. For the topology optimization, there was a concern that using gravity would give misleading results, as the 3D CAD model that was to be optimized was a bulk solid with far greater mass than the intended monocoque would have. Therefore gravity would induce far greater loads than the monocoque would be required to sustain. As an alternative, braking and turning forces were applied directly on the harness fastening points.

For the composite optimization, the initial mass was 15 kg, which was a somewhat accurate estimation for the final weight of the monocoque. In addition, a point mass of 140 kg was added to compensate for the weight of the driver (70 kg), as well as components that were not yet added in the monocoque (electronics, harness, glue, suspension systems, wheels etc). This point mass was constrained with five RBE2 elements, simulating the five-point racing harness (figure 113). As mentioned in the theory section, RBE2 elements induce a stiffness that might not be desired. In reality, the seat belt would only be subjected to tensile forces, but with stiff RBE2 elements the seat belt would also be subjected to compressive forces, which is not realistic. A force of 700 N was distributed on the five harness points in the simulation because of the RBE2 elements, which in reality only happens in a frontal crash. A crash from the side would only create tension in three

of the five harness points, which would increase the forces on each point to one third of 700 N instead of one fifth. Combined with the fact that the load cases featured larger loads than anticipated, the uncertainty that the stiff RBE2 elements introduced could be accepted. A better solution might be to use spring elements that are programmed to be infinitely stiff for tensile loads while having zero stiffness for compressive loads. Due to the false stiffness that the RBE2 elements provided, the displacements behind the driver's seat would probably be somewhat larger than the simulations showed. However, the fact that the RBE2 elements were fixed to single elements means they did not provide much support to the monocoque, and as such did not affect the overall results too much.

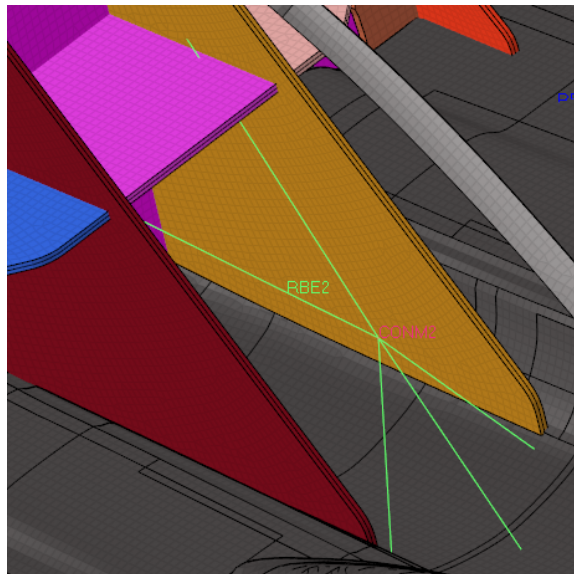


Figure 94: Point mass constrained with five RBE2 elements

After the monocoque was finished, it became apparent that some parts of the monocoque were oversized. One of these parts was the roof. Because the Shell Eco-Marathon rules state that the roof has to withstand a force of 100 N in any direction, a larger number of load cases featuring this situation might have been used. By decreasing the number of roof load cases, more material might have been placed on other, more critical spots in the car. During the composite optimization, a displacement limit of 10 mm was set. In hindsight this limit could have been increased for areas of the monocoque where small deformations would be acceptable (as long as the stresses were below the yield strength of carbon fibre).

7.2 Topology optimization

It can be observed that the optimization results have an uneven and jagged look. Some of this jaggedness stems from the limitations of the mesh, as well as the lack of a symmetry constraint, while a large part of it simply illustrates the nature of topology optimization algorithms. It is important to remember that the objective of the topology optimization was not to generate the final design but to get an idea of where the material was most critically needed. This allowed the opportunity to find geometries that could not be constructed analytically. The load paths through the structure stood out quite clearly from the optimization. This could be used to find the areas both where the material could be removed as well as where the material could be added, thus further enhancing the CAD model of the car. Topology optimization is typically used in an iterative way when designing parts, as it was in this thesis. By going back to the CAD model and refining it between optimization runs, the design was allowed to converge towards optimality.

Each iteration of topology optimization required several computational iterations to converge to a result. Each refined CAD model led to a mesh with different complexity and a total number of elements, and so the computational difficulty of optimization changed. The first two runs of 3D topology optimization required 37 iterations before convergence. The third 3D topology optimization increased that number to 42. Finally, the 2D topology optimization, featuring the most detailed model yet, required 66 iterations before convergence. This increase in iterations naturally lead to an increase in total computational time. The final 2D topology optimization took five hours to converge on a modern commercial computer. This put a limit on how detailed and complex Fuel Fighter could make their models, as the student team does not have access to supercomputers at this time.

The figures in the results section show the optimization results at a specific density threshold. While the person analyzing the results could view the entire spectrum of densities on a computer, the figures in this thesis were captured at the densities that most clearly illustrated the goal of the optimization process. In this project, the main goal was to locate the most critical load paths through the structure in order to reinforce specific parts of the monocoque, as well as detailing its interior. This information

was most clearly revealed by placing the density threshold at a percentage where the bulk of the material vanishes, leaving a truss-like structure. At what percentage this became most apparent varied greatly from model to model.

The starting point of the first optimization run was based on a 3D scanning of a clay model (figure 39). This model lacked any significant interior details. From the first iteration of topology optimization it became clear that the A-pillars stretching from the roof of the car down to the hood were subjected to high stresses. For the next model (figure 44), the dashboard was protruded further out towards the driver in order to shorten the A-pillars, and thereby prevent buckling. The space behind the driver was filled with mass, as it could be utilized for designing the car's inner structure. At the same time, the back wall was angled further back to allow more free space. After the second optimization iteration, a T-spline CAD model was made rather than basing it on a 3D scan (figure 49). At this point the aerodynamic simulations that ran parallel with the topology optimization had made huge advances, which is why the exterior of the new model looks so different. The interior of the car had also been changed. The driver's seat had been pushed forward to further exploit the space behind it for internal structure. The harness fastening points had been reshaped in order to place loads more accurately, and the point where the A-pillar meets the wheel arch had been narrowed in.

It is important to note that the changes in the CAD model between each iteration were not solely based on the results of the topology optimization. It was a combination of different considerations and developments in aerodynamics, design, ergonomics and structure working in combination. Topology optimization allowed knowledge about structural changes to be revealed whenever a design change in the CAD model was made. This way, the model could be analyzed at each step of the design process. By performing topology optimization in parallel with aerodynamic simulations, design and ergonomic considerations, it was possible to have decisions be based on all aspects of the car throughout the process.

Topology optimization techniques can be prone to local optimization of the problems they try to solve. Convergence of the results does not guarantee global optimization. In future projects, if time constraints permit it, it would be smart to introduce small, random changes in the design during the iteration process, so as to impose small perturbations that could "push"

the solution out of a local optimum[12].

7.3 Free shape optimization

The free shape optimization was completed after the third topology optimization iteration. The areas highlighted in red is where the software identified the greatest need for deformation by growing to accommodate stress concentrations, while blue means the area was shrunk to omit wasteful material. The most critical areas that stand out are the A-pillars, the roof and the upper supporting structure behind the seat. As the element size was quite low during the free shape optimization, the change in the shape of the structure would also be quite small. Therefore the result from the free shape optimization did not have a huge effect on the next redesign of the CAD model. This was to be expected, however, as this type of optimization was only meant as a fine-tuning step. The resulting structure from the free shape optimization provided the basis for the final 2D CAD model.

7.4 2D topology optimization

After the third topology optimization and subsequent free shape optimization, a 2D CAD model was made (figure 59). The results from these latest optimization runs provided the basis for the new models internal structure. By using plates in the car's interior, further optimization could be carried out after the composite optimization had been completed. At this point, the CAD model provided a satisfying starting point for the composite optimization. However, a final topology optimization was done on the 2D model. The result of this optimization did not directly affect the final design of the car. Instead it worked as a verification for the composite optimization, by observing how closely linked the stress concentrations in the topology optimization correlated with the placement of core material in the composite optimization.

7.5 Composite optimization

The simulated weight of the CAD model was only 15.3 kg before any optimizations were done on the monocoque. However, it has to be taken into account that this would not reflect the actual weight of the produced car. With vacuum infusion, the added weight from the epoxy should be estimated

to be at least 40% of the total mass, most likely 50% or more. In addition, extensions of 5 mm carbon fibre were made at the point where carbon fibre plies met. Adhesive spray used to keep plies together also increased the weight slightly. All this considered, the total weight before vacuum infusion was anticipated to be around 40 kg. When evaluating the displacements and stresses it is important to keep in mind which values are acceptable. The stresses should not approach 350 MPa, which is the yield strength of carbon fibre. The displacements should not exceed 5 mm around the wheel wells and the firewall due to the influence on the driving experience. If the surfaces where the suspension systems are fixed start to bend, it would negatively affect important properties of the wheels, such as the camber angle, toe angle, caster angle and steering axle inclination. This would in turn make the car less energy efficient when rolling (For further information on this subject, see Lars Ramstads master's thesis, [13]). Elsewhere on the car, a limit of 10 mm was set as valid values for displacements. This is in part because the car was designed to stand 110 mm above the ground, leaving some extra room above the required height of 100 mm stated by the Shell Eco-Marathon rulebook. Other areas that do not influence the driving efficiency or the distance from the ground had a maximum displacement of 10 mm. This limit could have been set higher to save weight, since it do not influence the driving efficiency.

7.5.1 Free-size optimization

It was decided that the core had to be made in advance due to difficulties in the optimization process. Because of the foams low density and high stiffness, the optimizer wanted core plies throughout the entire car, in addition to several discrete core plies reinforcing this structure. The optimizer probably chose this design because its objective was to increase the stiffness as much as possible. By increasing the thickness of the laminate with a thick core, the second moment of inertia was increased. This would be beneficial in theory, but impossible to manufacture due to the bending limits of the foam core material. The monocoque would also have an unnecessarily large amount of core, even at locations where the displacements would be close to zero. For these reasons, the free-size optimization was done separately from the other optimization runs.

The results from the first free-size optimization provided an idea of where the core should be located in order to withstand bending, see figure 64. This ply was one of the plies that did not cover the whole car. However, as the

results show, the core was evenly spread throughout the entire car, except for the front. This shape was also hard to obtain due to the bending limits of the foam core used in this project. For these reasons, it had to be modified in order to be manufacturable. The FEM analysis correlated with the free-size optimization in terms of placing core where the largest stresses were located. By combining the free-size optimization, the stress plot and manufacturing constraints, the final design of the core was made as shown in the results section. It was decided that the locations with the largest curvatures needed the thinnest core available (10 mm) to be able to drape around curves. It turned out that the greatest need for strength was located at the points where the driver would step into the car, in addition to the wheel well. At these locations a 20 mm core was used.

The model for composite optimization was reshaped with the new core design to save weight and prevent complications during the simulations. The weight was calculated in Hyperworks to be 10.8 kg, where the loss in weight came exclusively from trimming the foam core. The second free-size optimization increased the number of plies by 15, with very low thickness values. The weight was reduced to 6.8 kg, which is an unrealistically low value for the car. The low weight stems from the extremely thin plies generated under the optimization process. As the table in the results section shows, some of the thicknesses were as low as 0.01 mm. Such thicknesses were not feasible. Since the optimizer at this point had no constraints for the individual thicknesses for each ply (only for the laminate as a whole), it tried to reach its objective, which was minimizing compliance, yet satisfies its mass constraint of 8 kg. It is observed that four core plies were created (Ply 17-20, see the table in section 6.4.1), even though only two was desired. Since the core design was already made, the two new plies were deleted. The FEM analysis resulted in a maximum stress of 66.9 MPa, which is far from the yield strength of carbon fibre (350 MPa). The largest displacement from any load case was found on the roof, measuring 8.23 mm. This value was acceptable since a displacement on the roof would only happen if the car was pushed or it rolled over. It would not influence the car's driving ability during the race. The most important loads to observe are the ones generated from braking and turning. These are acting on the car at all times when driving, and only small displacements are allowed. If there is major bending of the car during the race it might influence the steering and braking system. The maximum displacements from these load cases were located around the wheel wells and in the drivers seat. However, these displacements were only

3.77 mm and were therefore not critical.

Every ply from the second free-size optimization was modified element by element to remove free-air elements and make it manufacturable. The modification consisted of adding or removing elements in each ply, which in this case resulted in a reduction of 500 g in total. The design for the ply patches were based on the optimization results, with a goal in mind to make them as square shaped as possible. Cutting carbon fibre is easiest when it is cut in squares or rectangles (because of the carbon fibre pattern), hence the designs shown in the appendix. Many plies had a small group of elements throughout the car. However, these were in most cases removed because they only complicated the manufacturing process and did not provide any substantial strength. These modifications were essential to achieve results that could be used in a practical situation.

7.5.2 Sizing

Each ply was constrained to a thickness of 0.15 mm in order to be identical to the 2x2 twill carbon fibre that Lindberg&Lund provided for DNV GL Fuel Fighter. It is important to keep in mind that each ply in this optimization project had half the thickness of the actual ply Fuel Fighter used (0.30 mm, 0/90 degree orientation). The same was true for the core material. When constraining the thickness to 0.15 mm, the monocoque would automatically be stiffer, considering the thickness was many times larger than for the ones in the free-size optimization. However, the increase in thickness resulted in an increase in weight, even though some plies were removed. This increase came solely from the thickness constraint. By evaluating the FEM analysis performed after the sizing optimization, it became apparent that the monocoque had become stiffer after the sizing step. The largest displacement from braking and turning had been reduced by approximately 0.8 mm due to the thicker plies.

7.5.3 Shuffling

As the initial design shows (iteration 0 of the shuffling optimization, figure 72) the 0, 90, 45 and -45 degree oriented plies were stacked in groups of their orientation. Having four 0 degree oriented plies on top of each other would not provide homogeneous strength since all the fibres would be pointing in the same direction. Since the actual plies used in the manufacturing process were plies with both 0 and 90 degree oriented fibres weaved into each other, having a unidirectional laminate would not be possible any-

ways. However, the possibilities for making the car stiffer and lighter would have increased if unidirectional fibres were used (given that the fabric is lightweight). This is because some points on the car were only subjected to forces in one direction. In such a particular case it would not be necessary to strengthen it in any other directions. For this project, every element on the car has fibres pointing in at least two directions. The possible orientations are either 0/90, 45/-45, or all four of these.

The shuffling optimization was done to constrain the stacking sequence rather than optimizing it. This is because it was desired to have 45/-45 paired together and 0/90 paired together. However, the optimizer was allowed to stack two plies of 0/90 or 45/-45 after each other, meaning it was not constrained to alternate between 0/90 and 45/-45. By observing iteration 4, it can be seen that the optimizer ended up alternating 45/-45 and 0/90 degree orientation. Nevertheless, it is important to notice that the stacking sequence shows 20 plies, even though only 14 plies are left after the sizing optimization. It is not obvious why the empty plies remain in the shuffling optimization, but they will not affect the results as they do not have any structural strength. This is because the plies did not exist in the model after the free-size optimization. The empty plies are ply number 2, 6, 10, 14, 19 and 20. This was one ply from each orientation plus two core plies. The same stacking sequence was therefore maintained (alternating between 0/90 and 45/-45).

By studying the FEM-results it can be seen that the displacements and stresses had been further reduced. At this point, the monocoque had a more homogeneous laminate due to the shuffling optimization, which resulted in homogeneous strength properties. The maximum displacement from braking and turning left was reduced by approximately 6 mm, which is quite a lot by just changing the stacking order. The displacing element was located between the wheel wells. The displacements in general for all load cases were reduced. The stresses also decreased in general in the monocoque. However, the stresses were not of high importance since they were far from the yield strength (350 MPa). The weight remained the same since the number of plies were unchanged.

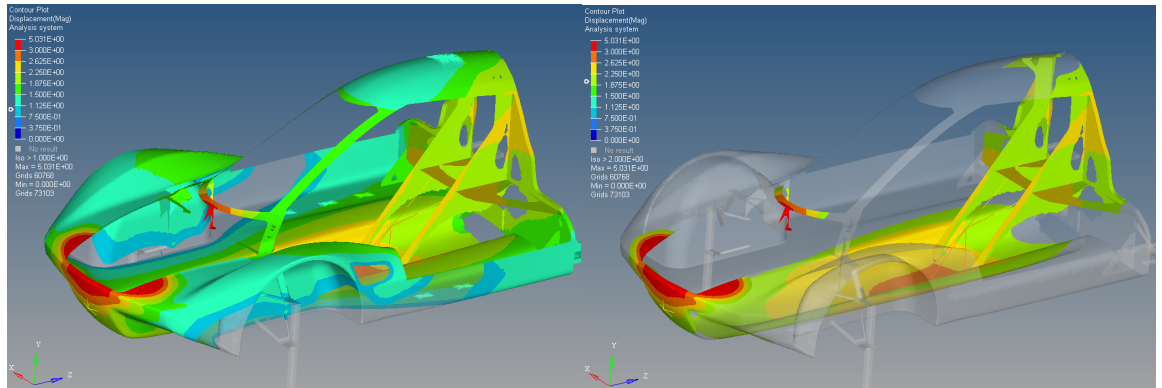
7.6 Topology optimization of the inner structure

The previous topology optimization was done to observe how the inner structure of the monocoque would look like and where additional support should be located. However, after the inner structure was implemented into the CAD-model and then imported for composite optimization, it became clear that there were spots with low stresses and displacements on the inner structure of the final design. This meant unnecessary mass. In addition, the firewall was outside the design space during the whole process because the Shell Eco-Marathon rules state that the wall needs to be one solid piece. Even so, a solution to make the firewall lighter was found. The firewall was designed with a 5 mm foam core with one 300 g carbon fibre twill weave on each side. Due to safety reasons, holes could not be made in the firewall. However, it was decided that the carbon fibre and foam material could be cut away leaving only a single layer of carbon fibre where the need for structural strength was small. With this in mind, a topology optimization was used for making the firewall lighter.

Performing a topology optimization on a composite laminate provided new challenges when dealing with material properties. As previously stated, Hyperworks does not support composite materials for topology optimization. To solve this problem, a theoretical material was made to mimic the bending properties of the composite laminate. The Altair support team was asked for guidance, but they had never looked into this way of countering the material problem. The method did however work for our purpose, and the results were good for reducing the weight while not sacrificing too much stiffness. By studying the FEM analysis results after the topology optimization, it was observed that the displacements were larger than before the topology optimization. However, none of the displacements over 5 mm were located where the suspension systems were fixed. The largest displacement of 5.03 mm, created from the car driving over a bump, was located in the front of the car, which is not critical, see figure 95a. Notice that only some parts of the car are showing, while the rest is transparent. The transparent parts show displacements smaller than 1 mm. The colored areas are displacements equal to or greater than 1 mm.

A displacement of 8.14 mm was created from the hook load in front of the car. The stress was 305 MPa, which was only 45 MPa under the carbon fibres yield strength. This was more closely analyzed, and it was found that the hook load was located on only one element. Why this happened is uncertain,

however the hook was later placed on the core material instead of the thin carbon fibre ply in front, to avoid large displacements of the thin front bumper (this decision was done under production after the simulations). The other displacement contour plots for the other load cases are found in the appendix, which show that there are little to no displacements on the wheel hubs.



(a) Displacement plot showing elements with displacements greater than 1 mm for the bump load (b) Displacement plot showing elements with displacements greater than 2 mm for the bump load

Figure 95

It is also important to notice load case number 18, which is another load simulating the seat belts. For the other optimization runs, the forces acting on the harness fastening points were simulated by fixing the point mass with five RBE2 elements. This can be seen in section 5.4.1. During last years technical inspection, the seat belt was pulled with great force to test its strength. For that reason, an individual load case for the seat belt was implemented for the topology optimization since these loads are acting on the inner structure that was to be optimized. In addition, a small safety factor was added to ensure the structure could withstand an even larger force, should the technical inspection be more strict than previous years.

By sacrificing some stiffness the topology optimization reduced the weight by 2.3 kg overall. Converting theoretical results directly into practical results were difficult, and for that reason, there were some discrepancies from theory to practice. The comparison between topology optimization and practical results is shown below. In most cases, more material was removed than the simulations suggested. This was simply because the monocoque was unnecessarily stiff according to the FEM analysis. It was therefore de-

cided to make it lighter at the cost of some stiffness, rather than heavy and oversized. For the dashboard, some beams were added to provide support for the electronics.

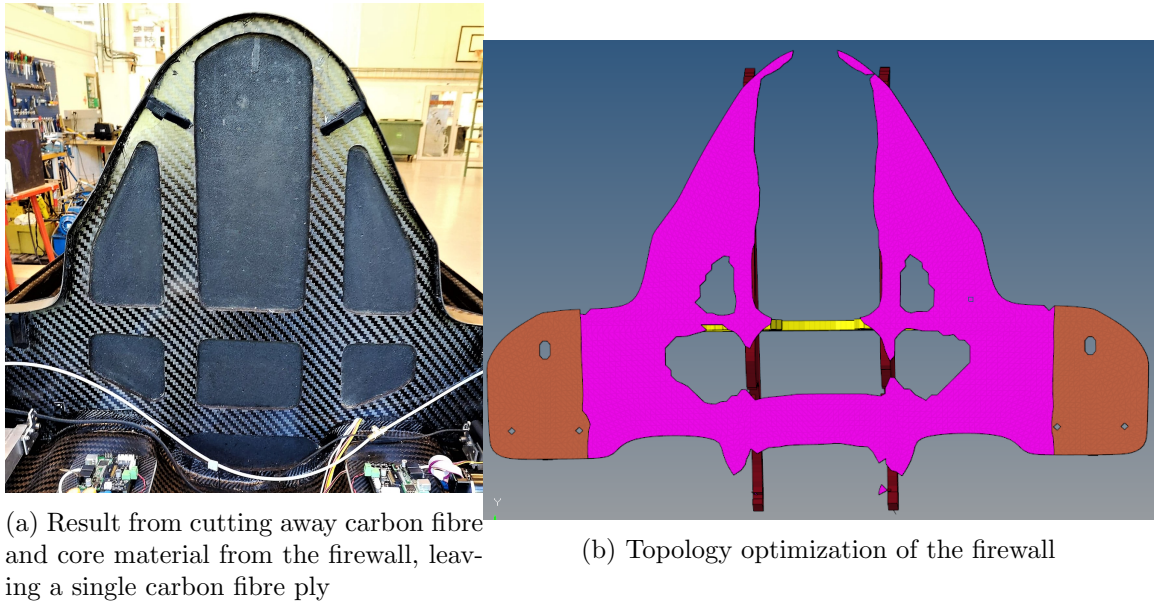


Figure 96

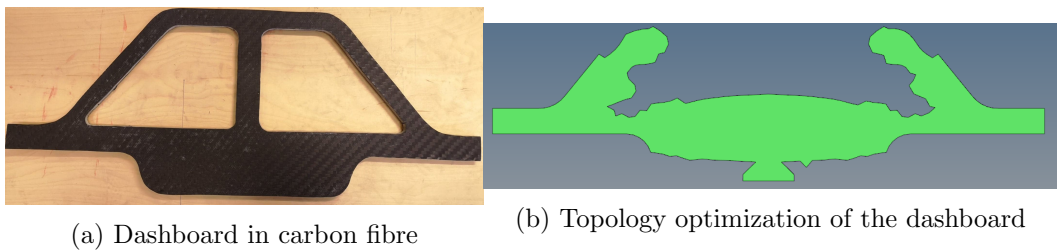


Figure 97

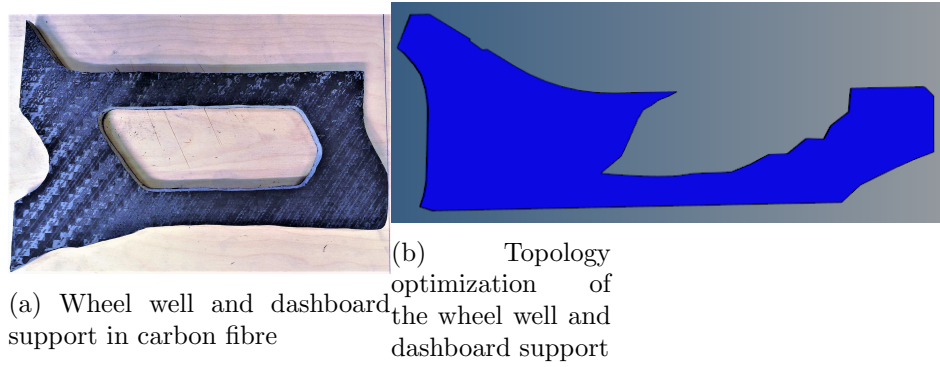


Figure 98

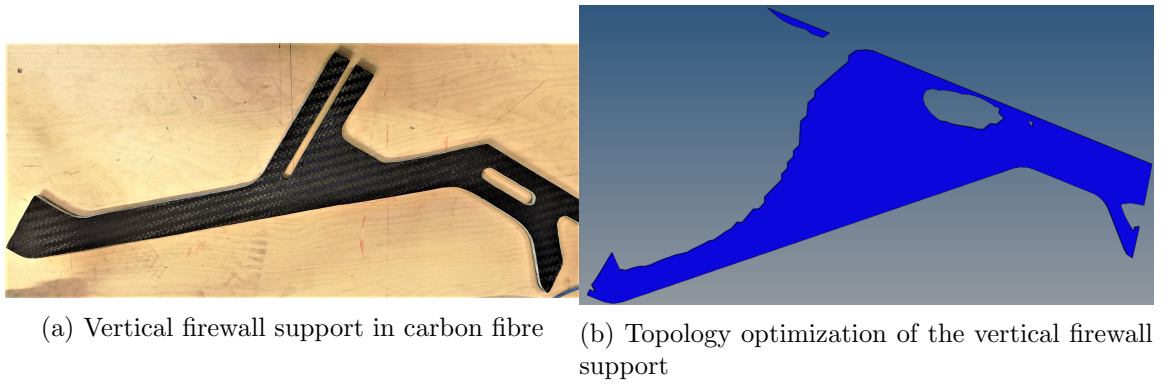


Figure 99

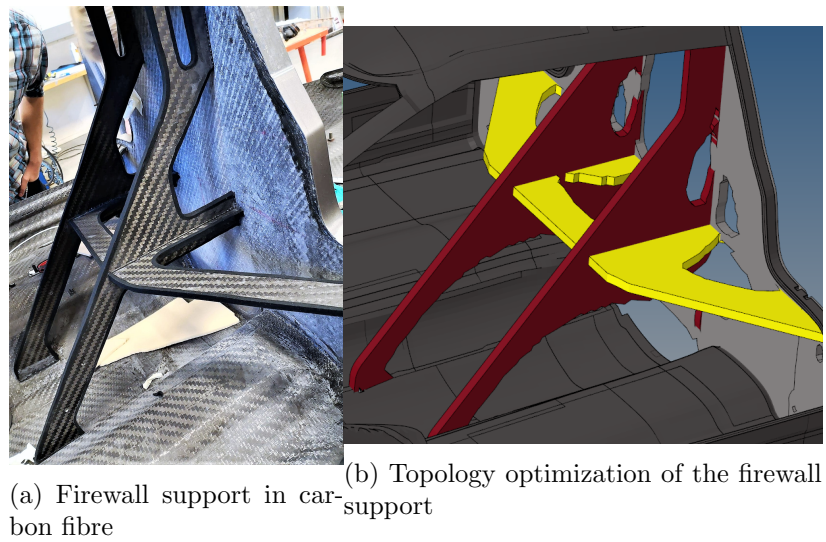


Figure 100

7.7 Material selection

The tests performed prior to the trip to HPC, Sarpsborg, helped determine the optimal material choices for the production of the monocoque. Several factors such as cost and availability weighed in on the decision alongside material properties.

Carbon fibre The unidirectional fibre available to us (250 g) was too heavy, since the material only has strength in one direction. Stacking it to get an equivalent material to a biaxial fibre would effectively double the weight of the fibre. Unidirectional fibre is also time consuming to lay. The biaxial sewn fabric (45/-45) was also considered. However, the ones available were too heavy (450 g) and did not drape easily enough around curvatures. The 1x1 carbon fibre pattern was not available for testing. However, by looking at reviews it became apparent that the stiff fabric made it difficult to handle, and therefore not suitable for use on intricate shapes. The 2x2 twill weave (300 g) was available at a cheaper price than the other carbon fibre types. The fabric had a thin sheet of spiderweb material across its surface preventing fringes at the cutting lines. In addition to making the manufacturing process a lot easier, this allowed for a smoother carbon fibre surface. This is because single fibres tend to separate and create holes in the weave of regular carbon fibres. This makes the fibre weaker and less aesthetically pleasing. By tilting the 0/90 weave by 45 degrees, a 45/-45 oriented fabric was achieved. Alternating between these two weave types resulted in a sufficiently homogeneous material. The 2x2 twill was therefore chosen as the main carbon fibre type to use on the car. Even though the fabric draped sufficiently around intricate curvatures, the spiderweb made the fabric too stiff and hard when double curvatures were present. For that reason a thinner 2x2 twill weave (200 g) without a spiderweb was also used in certain places.

Core The Tubus honeycomb was superior in its ability to bend, but after the vacuum infusion test, it became apparent that the cells in the honeycomb filled up with epoxy, thus leading to a far heavier sandwich panel than had PVC foam been used. Lindberg&Lund claimed that the thin film on top of the honeycomb should prevent this, but our tests indicated otherwise. The other available honeycomb materials were not an option due to their high prices, in addition to the added danger of the cells filling with epoxy. Had

pre-impregnated carbon fibre been used, these cores types could have been a better alternative.



Figure 101: The cells of the honeycomb were saturated with epoxy, making the core heavier than PVC foam

The PVC foam tests provided information about the materials bending limits and its ability to withstand epoxy absorption during infusion. The results showed that the foam did not bend easily with the use of a heating gun. The surface got burned, but the core of the material remained cold and was, therefore, unable to bend. Placing the core in an oven for about 15 minutes (depending on the thickness) at 100 degrees Celsius made it softer. However, it cooled down fast, and a permanent bend was difficult to maintain. After a few days of testing, it was concluded that the best method for bending PVC foam was to build moulds that the foam could bend around inside the oven.

Another observation was that the foam did not absorb any epoxy during vacuum infusion, which made it applicable for this type of manufacturing.

Resin After testing the two epoxy types at different temperatures, it was found that Araldite ESR3 epoxy combined with an ESH3 hardener had the fastest curing time, and was therefore chosen as the resin for the monocoque. According to the data sheets that followed the epoxies, the curing times were remarkably different from the experimental results. At 80 degrees the ESR3 system should harden after 60 minutes, but that was not the case during the test. The long curing times might be a result of an uneven temperature in the laboratory. The heating lamp heated some spots more than others,

which caused an uneven temperature throughout the epoxy in the laminate. In addition, students were opening the windows every now and then which also caused temperature fluctuations.

During most of the project, the ESR3/ESH3 epoxy/hardener combination was used, until the supply ran out. At that point, Araldite LY1564 epoxy combined with XB3404 hardener was used instead, as the mechanical properties were the same for the two epoxy systems, except for a slightly longer curing time for the LY1564/XB3404 system.

Manufacturing method The choice of manufacturing method was reached solely on a theoretical basis. Experience from previous Fuel Fighter teams made it apparent that manual coating often lead to heavier sandwich panels, as the amount of epoxy used is hard to control. Prepreg carbon fibre would have had the best material properties, but the price was too high for DNV GL Fuel Fighters budget. Prepreg also requires an autoclave to manufacture, and extensive experience with the material. Infusion then became a good middle ground. The manufacturing method provided good results, and the equipment needed for the process was readily available to us at NTNUs composite lab.

On the basis of the assessments above, the following were chosen for the monocoque:

Carbon fibre: 300 g 2x2 twill weave

Core material: PVC foam

Resin: Epoxy (Araldite ESR3 + ESH3)

Manufacturing method: Infusion

7.8 Production

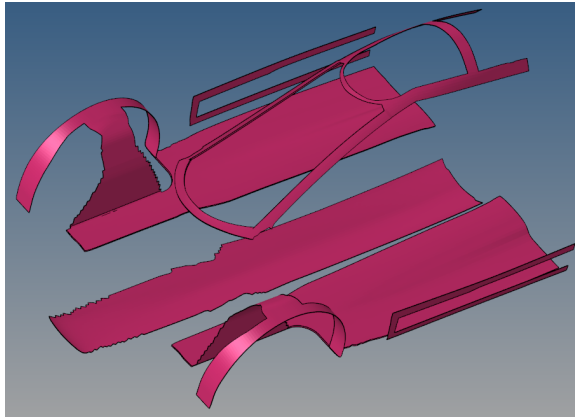
The production of the monocoque was completed at HPC without any major setbacks, in a total duration of seven days. The largest delay emerged from the shaping of the foam cores. Large pieces of 10 mm cores required a small bend to fit some of the curves of the monocoque, and this was unexpectedly hard to accomplish. The problem was that the core could get burned and brittle if it remained too long in the oven. If the core was not in the oven long enough, it would not bend at all. Finding a good middle ground was harder than anticipated, and so an entire day was needed to shape the cores. Having a pre-made mould for the 10 mm cores might have

made the job easier. The problem was solved by making a cut in the core and then place wedges to force the core to bend, see figure 102.



Figure 102: A wedge was placed in the middle of the core to bend it

The 5 mm cores bent more easily, but still required a mould inside the oven to bend around. Considering the difficulties that arose with the cores, much of the core material was removed from the actual design. There were several spots on the monocoque where the core could not be placed as the simulations had intended, because of the curvature of the mould. However, more carbon fibre was laid at these locations to ensure sufficient strength. The core on the wheel well was much denser than the typical foam core. This was done to withstand the forces acting from the front suspension. The dense foam was too stiff to bend and was therefore made in two pieces (see figure 103a). A comparison between the optimization and the actual result is shown below. The core placed on the right and left side of the upper body was done to stiffen the doors.



(a) The core proposed by the simulation



(b) The core of lower body as it was manufactured

Figure 103



Figure 104: Core of upper body as it was manufactured

For the most part, each layer of carbon fibre was shaped and placed according to the composite optimization. However, a few changes were made during manufacturing. Even after the optimization processes had stripped away a lot of material, the monocoque still retained more than enough strength. Removing an entire carbon fibre layer from both 45/-45 and 0/90 degree oriented plies would save further weight without jeopardizing the structural integrity of the monocoque. These plies were ply number 2 (-45 degrees), 6 (45 degrees), 13 (0 degrees) and 16 (90 degrees) (figure 72). Seeing as this suggestion was not based on any data, but rather a hunch, it was desirable to get an estimate of how removing a carbon fibre layer would

affect the monocoque's ability to withstand external loads. By bringing a computer to the workshop, the Hyperworks software could do strength calculations on site. Although removing the carbon fibre layer naturally lead to a weakening of the structure as a whole, this weakening, as well as the resulting additional deformation under stress, was negligible. The weight saved by this action made the change worth it. The displacements and stresses for the last design made during production at HPC can be viewed below. Most of the displacements increased by a maximum of 0.5 mm. The displacements from braking and turning even decreased by approximately 0.1 mm, which was rather surprising. However, the removed plies might not have contributed too much to the stiffness of the monocoque, instead leading to higher deformation when the car is braking and turning due to the added mass. Following this operation, the weight of the monocoque was reduced from 8.1 Kg to 7.7 Kg. The other components that was not a part of the monocoque were made out of two carbon fibre plies, each 3 mm thick. This was decided on only by testing how easily a plate of one, two and three carbon fibre plies could bend. It was concluded that two layers were extremely light, yet stiff enough as long as the ply was curved, which basically every part of the car was.

- **Subcase 1 - Load_Roof_-Y**
 - Maximum displacement is 1.71 at grid 28398.
 - Maximum 2-D element stress is 47.6 in element 72406.
- **Subcase 2 - Load_Roof_X**
 - Maximum displacement is 5.64 at grid 28398.
 - Maximum 2-D element stress is 30.8 in element 76138.
- **Subcase 3 - Load_Roof_-X**
 - Maximum displacement is 5.64 at grid 28398.
 - Maximum 2-D element stress is 30.8 in element 76138.
- **Subcase 4 - Load_Roof_Z**
 - Maximum displacement is 2.26 at grid 74215.
 - Maximum 2-D element stress is 42.5 in element 73058.
- **Subcase 5 - Load_Roof_-Z**
 - Maximum displacement is 2.26 at grid 74215.
 - Maximum 2-D element stress is 42.5 in element 73058.
- **Subcase 6 - Load_Hook**
 - Maximum displacement is 8.17 at grid 26774.
 - Maximum 2-D element stress is 305. in element 16749.
- **Subcase 8 - Load_BreakingFront**
 - Maximum displacement is 1.53 at grid 7855.
 - Maximum 2-D element stress is 26.3 in element 75817.
- **Subcase 9 - Load_BreakingBack**
 - Maximum displacement is 1.46 at grid 7855.
 - Maximum 2-D element stress is 24.2 in element 75817.
- **Subcase 10 - Load_BreakingAll**
 - Maximum displacement is 2.06 at grid 26774.
 - Maximum 2-D element stress is 24.1 in element 72406.
- **Subcase 11 - Load_TurningLeft**
 - Maximum displacement is 2.37 at grid 60768.
 - Maximum 2-D element stress is 32.2 in element 75821.
- **Subcase 12 - Load_TurningRight**
 - Maximum displacement is 2.36 at grid 26774.
 - Maximum 2-D element stress is 32.0 in element 73058.
- **Subcase 13 - Load_BreakingAndTurningRight**
 - Maximum displacement is 3.24 at grid 26775.
 - Maximum 2-D element stress is 49.5 in element 72406.
- **Subcase 14 - Load_BreakingAndTurningLeft**
 - Maximum displacement is 4.26 at grid 60768.
 - Maximum 2-D element stress is 55.0 in element 75821.
- **Subcase 15 - Load_Gravity_-Y**
 - Maximum displacement is 2.52 at grid 60768.
 - Maximum 2-D element stress is 27.4 in element 75817.
- **Subcase 16 - Load_Bump**
 - Maximum displacement is 5.03 at grid 60768.
 - Maximum 2-D element stress is 54.8 in element 75817.
- **Subcase 17 - Load_Stepln**
 - Maximum displacement is 3.77 at grid 52149.
 - Maximum 2-D element stress is 59.2 in element 26433.
- **Subcase 18 - Load_SeatBelt**
 - Maximum displacement is 2.10 at grid 74215.
 - Maximum 2-D element stress is 26.2 in element 75821.

Figure 105: Load cases after removing four additional plies (equating to two physical 3 mm plies)

Because the 2x2 twill weave with spiderweb did not drape well around some curves, the layers had to be cut into several patches to make it fit the curves. Every patch required a 5 mm overlap with the next patch. It is hard to tell how much extra weight this contributed to. For the most intricate curves on the monocoque, the expensive 200 g twill weave without spiderweb was used. This was needed on locations such as the wheel arches to make the manufacturing process easier. In addition, three non-adhesive spray bottles of 500 mL each were used. In total, this weight was estimated to be around 1 kg. Approximately 22kg of epoxy was used, although much of this was absorbed into the peel ply and infusion mesh, which was removed when the vacuum infusion was completed. However, roughly 15kg of epoxy was estimated to be infused into the car, which consists of the monocoque, the rear hatch, doors, hood and flanges. The weight of the epoxy in the monocoque is therefore somewhat lower than 15 kg.

More complications arose after the car was brought back to Trondheim.

The carbon fibre would not separate easily from the mould, despite the previous spraying and waxing. The mould was therefore broken up with crowbars, chisels and hammers. It was impossible to remove the fibre from the mould where the curvature was too intricate. A lot of the non-adhesive blue spray was left on the carbon fibre, meaning either the wax or the spray was not applied correctly. The adhesive spray could also have made the carbon fibre stick to the mould when it was laid. Slip angles were made for all surfaces, and should not be the reason for the problem.

The production of the inner structure and the firewall was hard to perform with precision. First, a 2D-model of the firewall was placed on the foam in order to cut it out with the correct dimensions. One layer of carbon fibre was placed on each side of the foam before it was vacuum infused with epoxy. After production it turned out that the firewall did not fit the upper and lower body of the monocoque perfectly, which resulted in hours of readjustments and additional glue to fill gaps. When the firewall was glued to the lower body, it had a slightly wrong angle which resulted in a bad fit with the upper body. To resolve this, the firewall was buckled up to the correct angle and then glued to the upper body. This meant that the firewall was under constant tension, but considering how strong the epoxy glue was and that the tension was small, these internal stresses were acceptable.

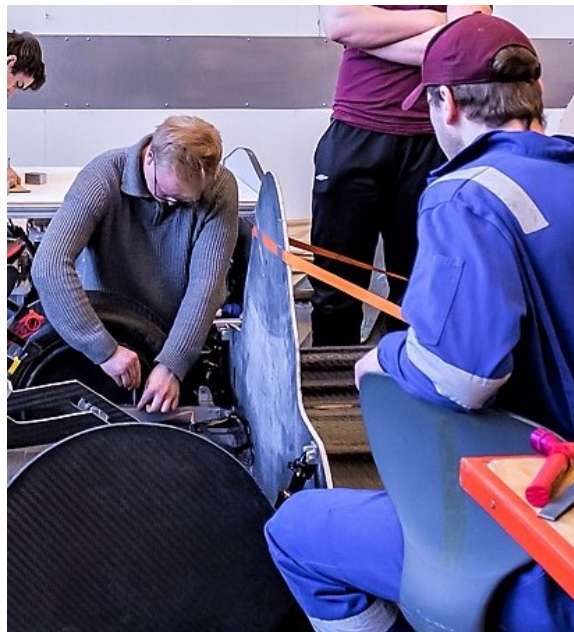


Figure 106: The firewall buckled up with straps

Another design change revolved around the dashboard. Instead of the double layered dashboard the topology optimization suggested, it was decided to only make one layer of supporting beams. This was in part to save weight, but also to allow more free space for other features such as speedometer, steering mechanisms and lights.

After the production of the firewall ended, the production of the inner structure was carried out using a different technique. A large carbon fibre plate was produced in the lab, and a 2D-drawing was placed on top of the finished plate to measure the dimensions of the inner structure. The parts were then cut with pressurized air tools. Most of the parts fit on the first try. These were then glued to the monocoque. The total amount of glue used on the car is estimated to be approximately 3 kg. This is a significant amount of glue, but it was unavoidable to get a proper assembly of the car. The glue used was Araldite 2048, which was bought from Lindberg&Lund. This glue is good for composites and had a fracture elongation of 95%, which is useful for parts that are exposed to vibrations and small displacements.

Despite the added glue (3 kg), extensions (1 kg), adhesive spray (1 kg) and epoxy (10 kg), the total weight of the monocoque ended up at 22 kg. It underwent a weight reduction of 45% compared to last years monocoque weight of 40 kg. Since last years monocoque had one less door and no detachable hood, its weight went up with the larger surface area. Even so, these parts were structural parts of the monocoque, and the added stiffness resulted in thinner plies elsewhere on the car. This years monocoque still weighed only 27 kg when the rear hatch, hood and both doors were attached.

8 Conclusion

For the 2019 Shell Eco-Marathon competition, DNV GL Fuel Fighter decided to utilize topology optimization in order to make its car more competitive. Through several iterations of optimization, along side aerodynamic simulations and design analysis, the CAD model could be shaped for optimality based on a large number of factors. The process led to an improved monocoque design that could be built lighter and stronger than previous years.

The composite optimization assisted the manufacturing process greatly by determining the exact number of carbon fiber plies needed, as well as their shapes, thicknesses, orientations and stacking sequence. The optimization process also determined how best to utilize a foam core in the most efficient way possible. After all this effort, the monocoque might still be oversized at certain locations. Further research with the use of Hyperworks might improve the monocoques weight and strength even more.

The material tests performed prior to building the monocoque revealed vital information for making the right material choices. Failing to physically verify the behaviour of each material during manufacturing could have resulted in major setbacks, costing the Fuel Fighter team both time and money. The manufacturing process was a success, and the combined effort of optimization and careful material choices led to a weight reduction of the monocoque by 45% compared to last years model.

When looking at the final product, it is obvious that the time and resources dedicated to this lengthy optimization process was a good investment. It was a project with large uncertainties, where neither the master students nor professors had any prior experience with the subject matter, or the optimization program itself. However, DNV GL Fuel Fighters goal of creating a highly efficient car was the perfect candidate for the type of optimization technology that Altair provided. Optimizing the monocoque using generative design might be the most important and decisive improvement DNV GL Fuel Fighter made this year. Combined with extensive material tests and research, an extremely light yet stiff monocoque was able to be built, providing the 2019 DNV GL Fuel Fighter team with their most competitive car design yet.

References

- [1] Rainer Rauch Erke Wang, Thomas Nelson. Back to elements - tetrahedra vs. hexahedra. 2004.
- [2] Sreeram Polavarapu. Topology and free-size optimization with multiple loading conditions for light weight design of die cast automotive backrest frame. 2008.
- [3] M. Shakeri S. Nikbakt, S. Kamarian. A review on optimization of composite structures part i: Laminated composites. *Composite Structures*, 195:158–185, 2018.
- [4] Tim Bull Chris Bailey and Aaron Lawrence. The bending of beams and the second moment of area. *The Plymouth Student Scientist*, page 328–339, 2013.
- [5] Mirabel Cerqueira Rezende Jane Maria Faulstich de Paiva, Sérgio Mayer. Comparison of tensile strength of different carbon fabric reinforced epoxy composites. *Scielo Analytics*, 9:83–89, 2005.
- [6] Nasrin Ferdous Reashad Bin Kabir. Kevlar-the super tough fiber. *International Journal of Textile Science*, 1:78–83, 2012.
- [7] Madhu Bajpai Prashant Gupta. Development of siliconized epoxy resins and their application as anticorrosive coatings. 2011.
- [8] Shipra Jaswal and Bharti Gaur. New trends in vinyl ester resins. *Reviews in Chemical Engineering*, 2014.
- [9] Richard Powe Ed Collings Kerry Kirwan James Meredith, Edvard Bilson. A performance versus cost analysis of prepreg carbon fibre epoxy energy absorption structures. *Composite Structures*, 124:206–213, 2015.
- [10] Eirik Evjan Furuholmen. Master thesis. 2019.
- [11] Daniel Tidman Anton Olason. Methodology for topology and shape optimization in the design process. 2010.
- [12] G.P. Steven O.M. Querin and Y.M. Xie. Evolutionary structural optimisation (eso) using a bidirectional algorithm. *Engineering Computations*, 15:1031–1048, 1998.
- [13] Lars Ramstad. Steering system and suspension development in dnv gl fuel fighter. 2019.

Websites

- [14] J. D. Laukkonen. <http://www.crankshift.com/monocoque>, 2013.
- [15] S. Sriram. <https://www.cars24.com/blog/body-on-frame-vs-unibody-suvs>, 2018.
- [16] Altair. https://connect.altair.com/CP/SA/training/self_paced/aero_v13/PDF/chapter7_demonstr
- [17] Altair. <https://insider.altairhyperworks.com/opt-laminate-composite/>, 2011.
- [18] Altair. https://altairuniversity.com/wp-content/uploads/2013/07/Skateboard_tutorial_Prakash_MGJuly1.pdf, 2018.
- [19] bmwblog. <https://www.bmwblog.com/2014/09/19/guide-understanding-carbon-fiber-weaves-fabrics/>, 2014.
Visited: 2018-14-11.
- [20] Carbon.ee. <https://www.carbon.ee/en/n/carbon-fiber-all-patterns-explained>, 2015.
Visited: 2018-14-11.
- [21] Easy Composites. <https://www.easycomposites.co.uk/!/fabric-and-reinforcement/reinforcement-fabric-samples/carbon-fibre-biax-300g-1m-SAMPLE.html>, 2018.
- [22] Easy Composites. <http://www.easycomposites.co.uk/!/composites-tutorials/carbon-fibre-cloth-explained>, 2015.
Visited: 2018-14-11.
- [23] Colan. <http://www.colan.com.au/compositereinforcement/woven-fabrics/carbon-fibre/carbon-woven-fabric-plain-200g-m2-500mm.html>, 2015.
Visited: 2018-14-11.
- [24] Net Composites. <https://netcomposites.com/guide-tools/guide/core-materials/>, 2018.
- [25] Gurit David Cripps. <https://netcomposites.com/guide-tools/guide/core-materials/>, 2018.
Visited: 2018-15-11.
- [26] DiabGroup. <https://netcomposites.com/guide-tools/guide/core-materials/pvc-foam/>, 2018.
Visited: 2018-15-11.

- [27] Gurit David Cripps. <https://netcomposites.com/guide-tools/guide/core-materials/honeycomb-cores/>, 2018.
Visited: 2018-15-11.
- [28] TubusWaben. <http://www.tubus-waben.de/en/ausfuehrungen.html>, 2018.
Visited: 2018-15-11.
- [29] Gurit David Cripps. <https://netcomposites.com/guide-tools/guide/resin-systems/>, 2018.
Visited: 2018-16-11.
- [30] SollerComposites. <http://www.sollercomposites.com/EpoxyResinChoice.html>, 2018.
Visited: 2018-15-11.
- [31] Hexcel. <https://www.hexcel.com/innovation/Documents/Prepreg%20and%20Infusion%20%20P>, 2018.
Visited: 2018-18-11.
- [32] Shell. https://www.shell.com/energy-and-innovation/shell-ecomarathon/_jcr_content/par/toptasks_1617110573.stream/1535524274245/90098d1f799999284eco-marathon-2019-global-rules-chapter-I.pdf, 2018.

Appendices

A Calculations for braking and turning forces

Input:			All four wheels braking:	
m	150	kg	Output:	
l	1,7	m	N_f	554 N
l_f	0,7	m	N_b	182 N
h	0,4	m	F_f	388 N
my	0,7	N/N	F_b	127 N
g	9,80665	m/s ²	Front wheels only:	
			Output:	
			N_f	518 N
			N_b	218 N
			F_f	363 N
			F_b	0 N
			Rear wheels:	
			Output:	
			N_f	475 N
			N_b	260 N
			F_f	0 N
			F_b	182 N

Figure 107: Spreadsheet for calculating loads on wheels

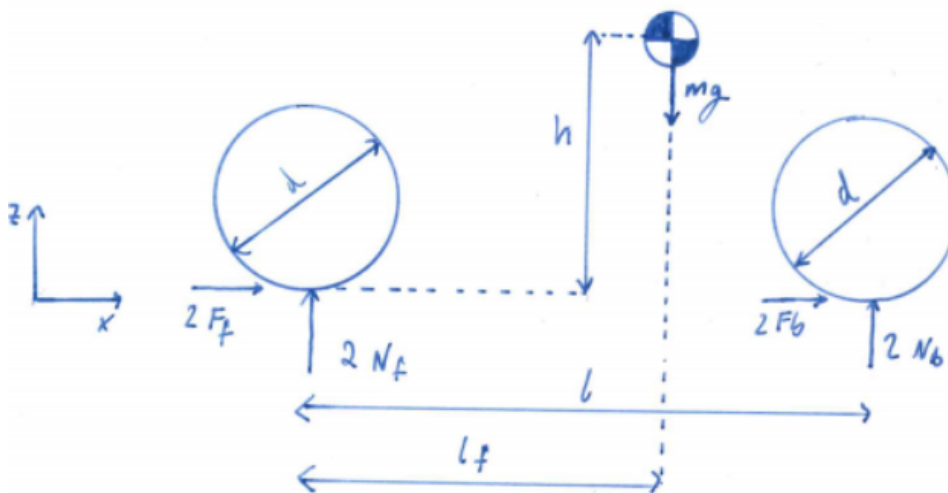
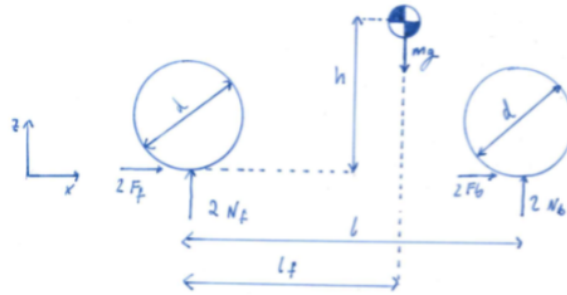


Figure 108: Explanation of terms in a spreadsheet



$$\Sigma F_x = F_{brakes} = mg\mu = 2(N_b + N_f)\mu = 2(F_b + F_f) = ma$$

$$\Sigma F_g = 0$$

$$mg = 2(N_b + N_f)$$

$$N_f = \frac{mg}{2} - N_b$$

$$\Sigma M_{cm} = 0 = 2(F_b + F_f)h + 2N_b(l - l_f) - 2N_f l_f$$

$$0 = 2\mu(N_b \frac{mg}{2} - N_b)h + 2N_b(l - l_f) - 2(\frac{mg}{2} - N_b)l_f$$

$$0 = mg\mu h - mgl_f + 2N_b(l - l_f) + 2N_b l_f$$

$$0 = mg(\mu h - l_f) + 2N_b l$$

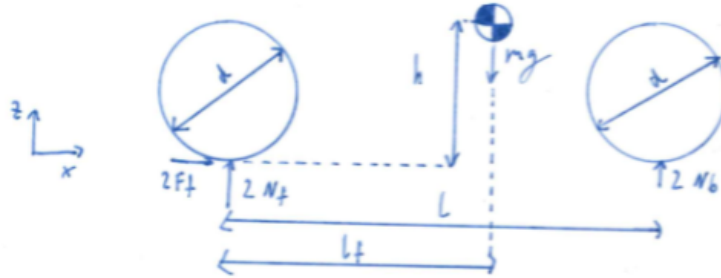
$$N_b = \frac{mg(l_f - \mu)h}{2l}$$

$$N_f = \frac{mg}{2} - N_b$$

$$F_b = N_b \mu$$

$$F_f = (\frac{mg}{2} - N_b)\mu$$

Figure 109: Braking - all four wheels



$$\Sigma F_x = F_{brakes} = 2N_f\mu = 2F_f = ma$$

$$\Sigma F_y = 0$$

$$mg = 2(N_b + N_f)$$

$$N_b = \frac{mg}{2} - N_f$$

$$\Sigma M_{cm} = 0 = 2F_f h + 2N_b(l - l_f) - 2N_f l_f$$

$$0 = 2N_f h\mu + 2\left(\frac{mg}{2} - N_f\right)(l - l_f) - 2N_f l_f$$

$$0 = 2N_f(h\mu - (l - l_f) - l_f) + mg(l - l_f)$$

$$0 = 2N_f(h\mu - l) + mg(l - l_f)$$

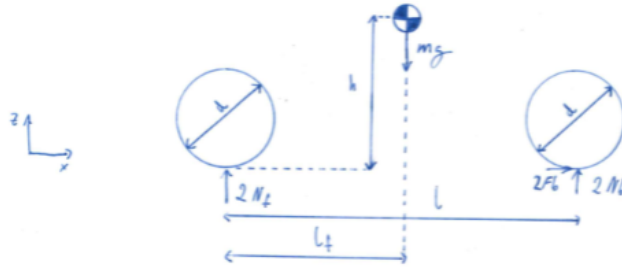
$$N_f = \frac{mg(l - l_f)}{2(l - h\mu)}$$

$$N_b = \frac{mg}{2} - N_f$$

$$F_f = N_f\mu$$

$$F_b = 0$$

Figure 110: Braking - front wheels only



$$\Sigma F_x = F_{brakes} = 2N_b\mu = 2F_b = ma$$

$$\Sigma F_y = 0$$

$$mg = 2(N_b + N_f)$$

$$N_f = \frac{mg}{2} - N_b$$

$$\Sigma M_{cm} = 0 = 2F_b h + 2N_b(l - l_f) - 2N_f l_f$$

$$0 = 2N_b h\mu + 2N_b(l - l_f) - 2\left(\frac{mg}{2} - N_b\right)l_f$$

$$0 = 2N_b(h\mu + (l - l_f) + l_f) - mgl_f$$

$$0 = 2N_b(h\mu + l) - mgl_f$$

$$N_b = \frac{mgl_f}{2(h\mu + l)}$$

$$N_f = \frac{mg}{2} - N_b$$

$$F_b = N_b\mu$$

$$F_f = 0$$

Figure 111: Braking - rear wheels only

All wheels:
$$\frac{388 * 2 + 127 * 2}{150 * 9.81} = 0.7G$$

Front wheels:
$$\frac{363 * 2}{150 * 9.81} = 0.5G$$

Rear wheels:
$$\frac{182 * 2}{150 * 9.81} = 0.25G$$

Turning: 14 m radius turn at 30 km/h top speed

$$a = \frac{v^2}{r} = \frac{\frac{30}{3.6^2}}{14} = 4.95 \frac{m}{s^2}$$

$$\frac{4.95}{9.81} = 0.5G$$

Figure 112: Calculations for braking and turning

$$v = v_0 + at$$

$$m = 70kg, t = 1s, v_0 = 30 \frac{km}{h} = 8.33 \frac{m}{s}, v = 0$$

$$a = -\frac{v_0}{t} = -\frac{8.33}{1} = -8.33 \frac{m}{s^2}$$

$$F = ma = -70 * 8.33 = 583.1N$$

Number of harness points = 5

$$F_h = \frac{F}{5} = \frac{-583.1}{5} = 116.62N$$

Figure 113: Calculations for forces acting on the harness

B Stress contour plots after the first free-size optimization

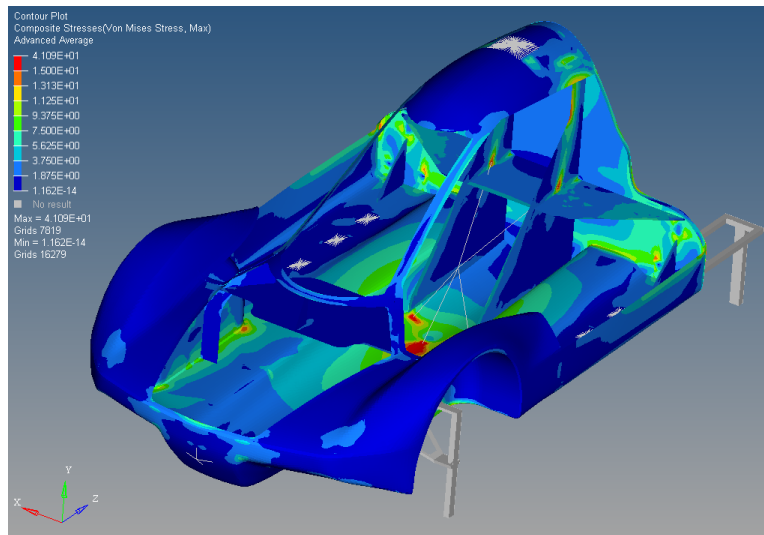


Figure 114: Stress contour plot, braking all wheels

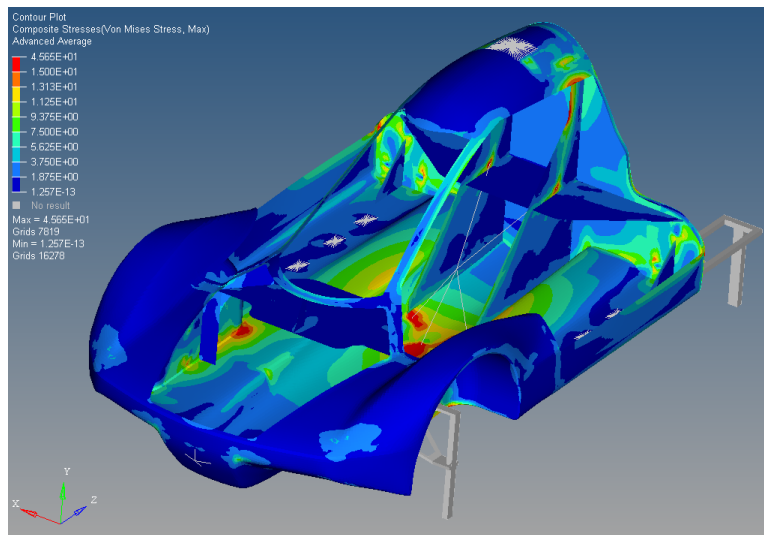


Figure 115: Stress contour plot, braking front wheels

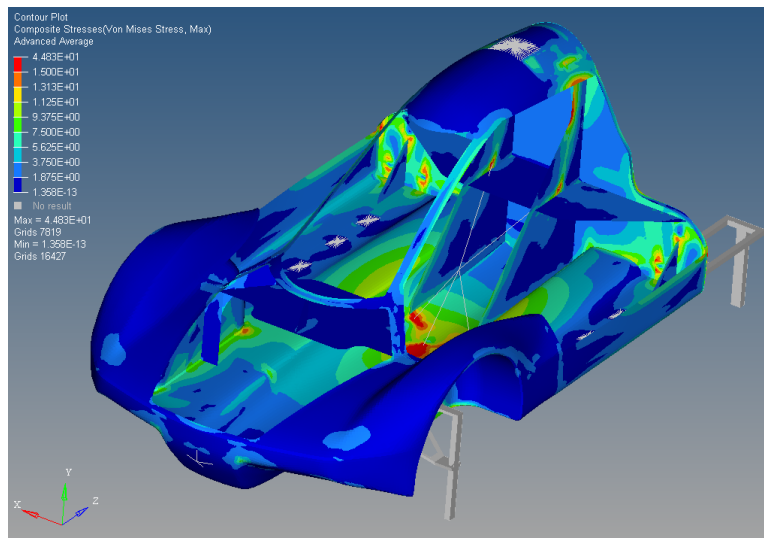


Figure 116: Stress contour plot, braking back wheels

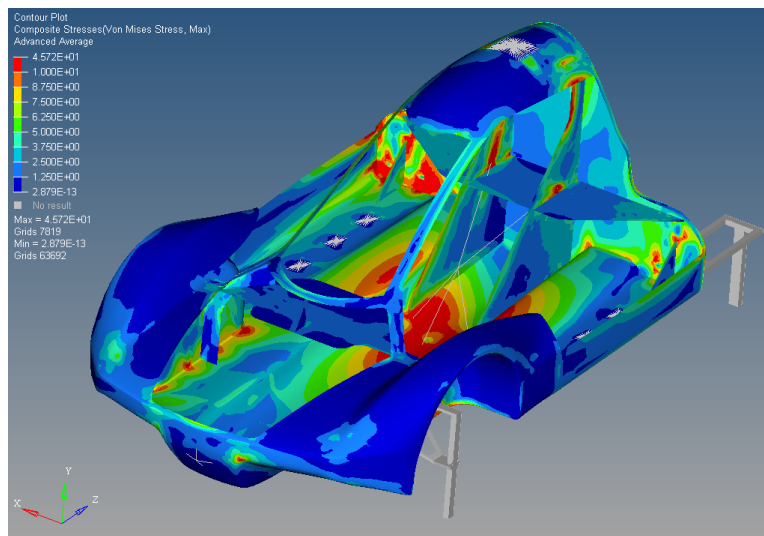


Figure 117: Stress contour plot, turning left

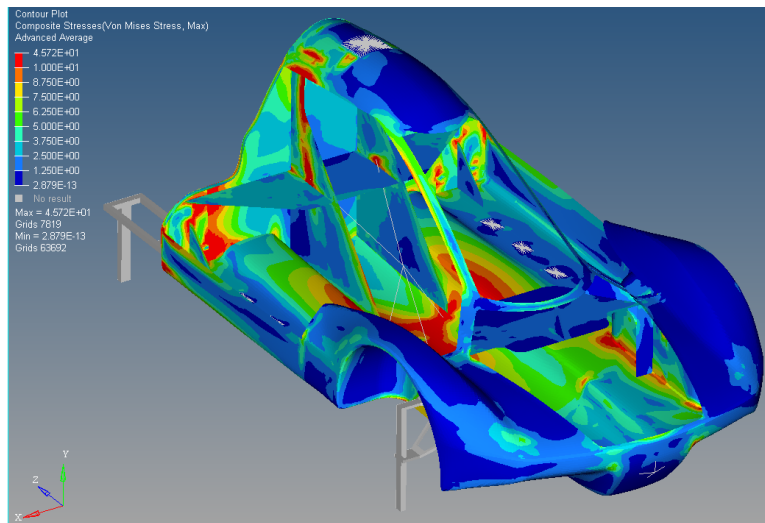


Figure 118: Stress contour plot, turning left

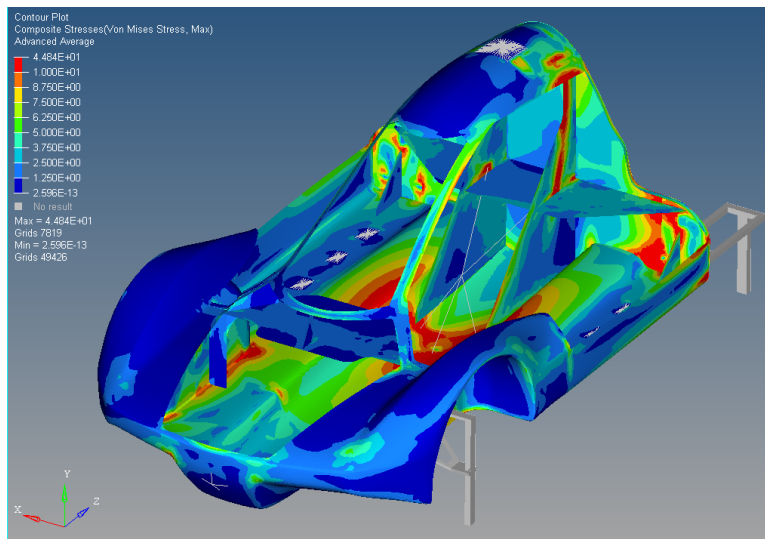


Figure 119: Stress contour plot, turning right

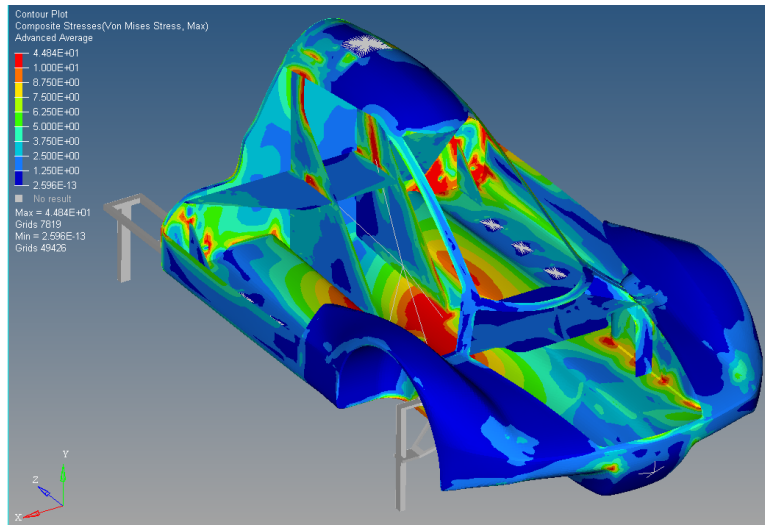


Figure 120: Stress contour plot, turning right

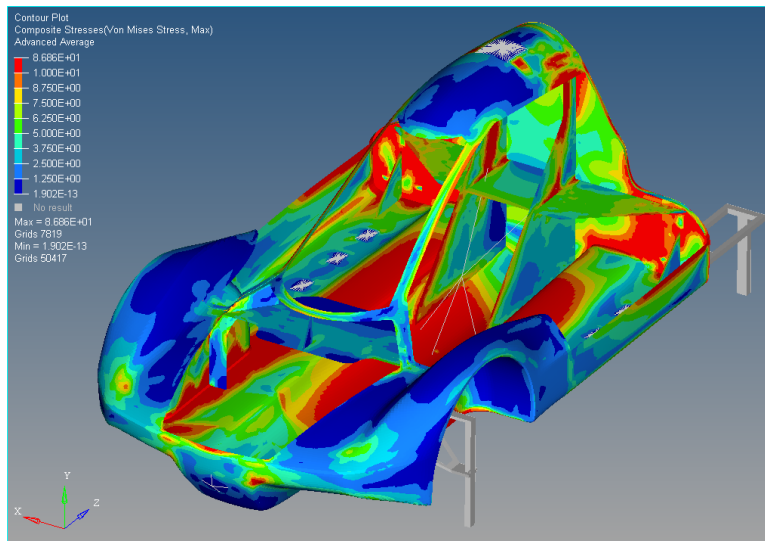


Figure 121: Stress contour plot, braking and turning left

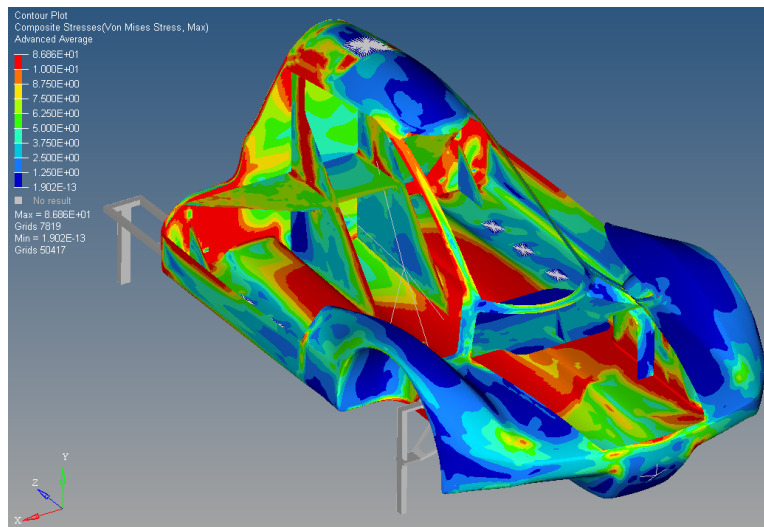


Figure 122: Stress contour plot, braking and turning left

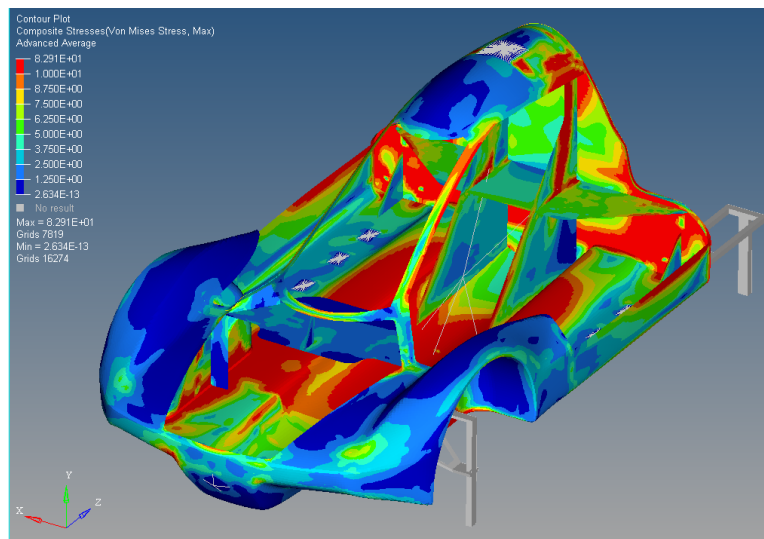


Figure 123: Stress contour plot, braking and turning right

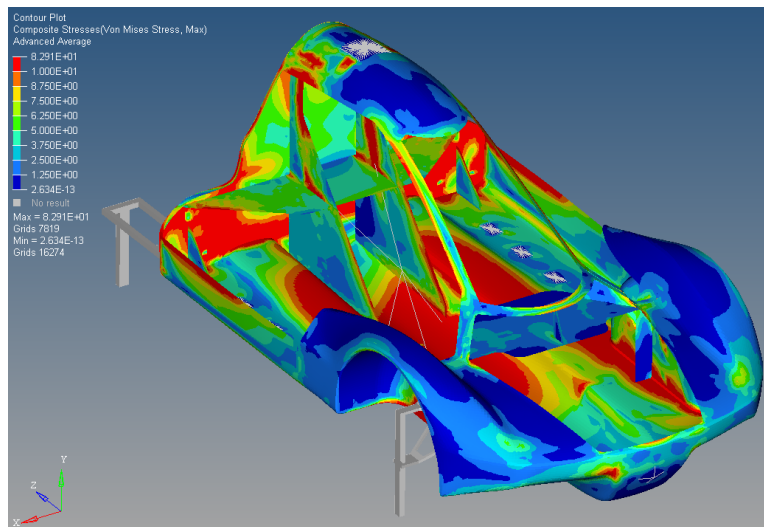


Figure 124: Stress contour plot, braking and turning right

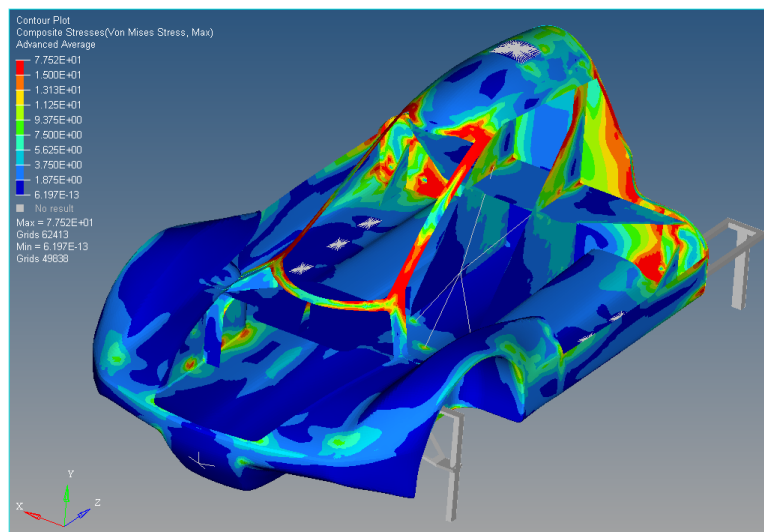


Figure 125: Stress contour plot, roof load in the X direction (same in the -X direction)

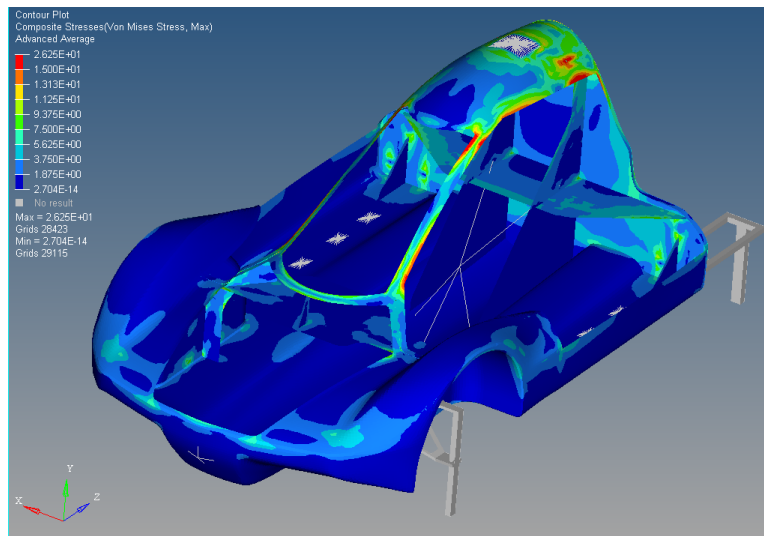


Figure 126: Stress contour plot, roof load in the -Y direction

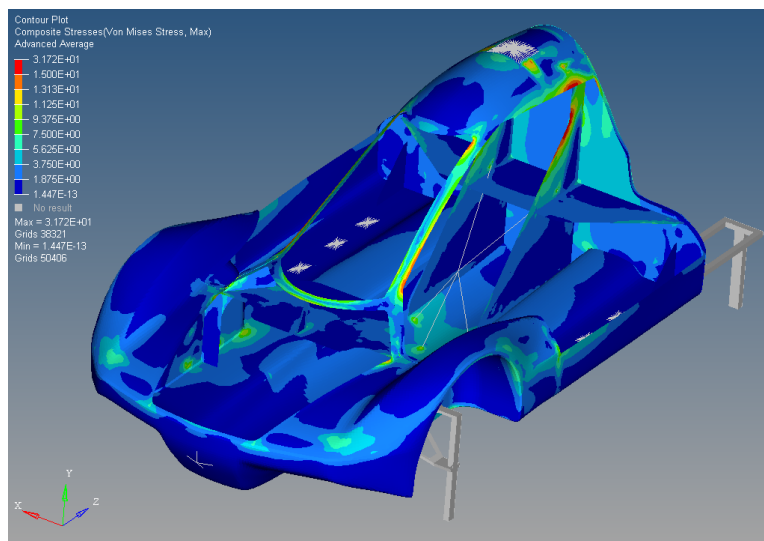


Figure 127: Stress contour plot, roof load in the -Z direction

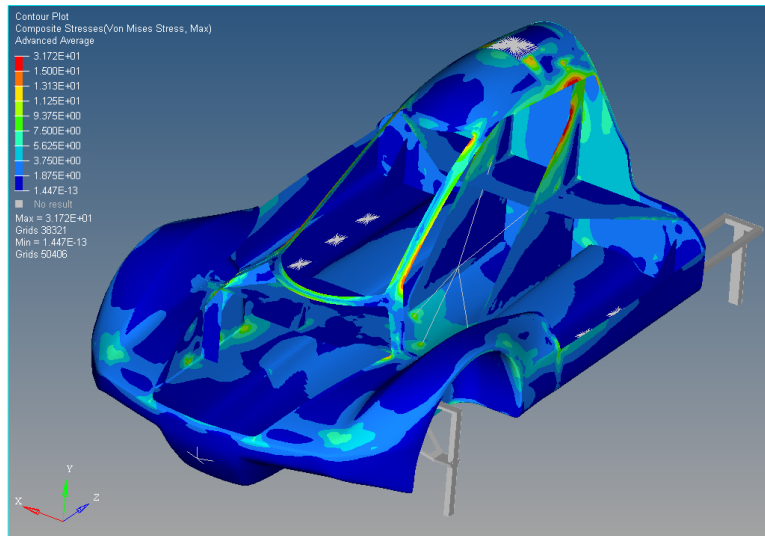


Figure 128: Stress contour plot, roof load in the Z direction

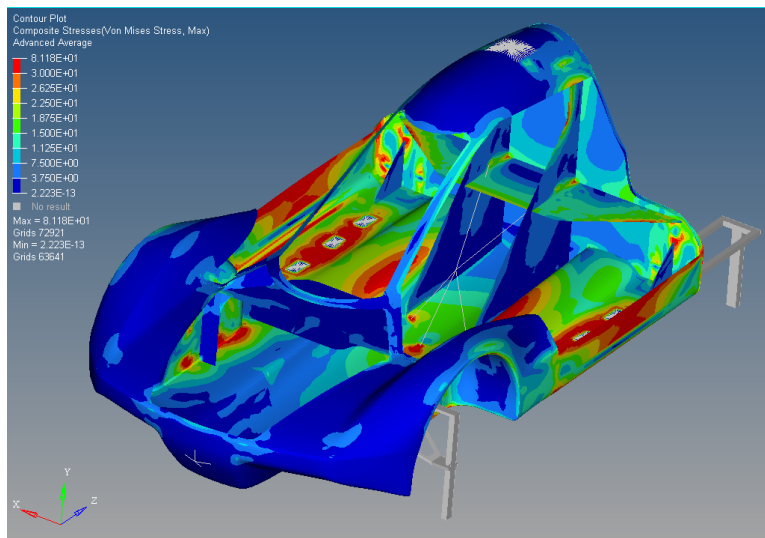


Figure 129: Stress contour plot, step into the carload

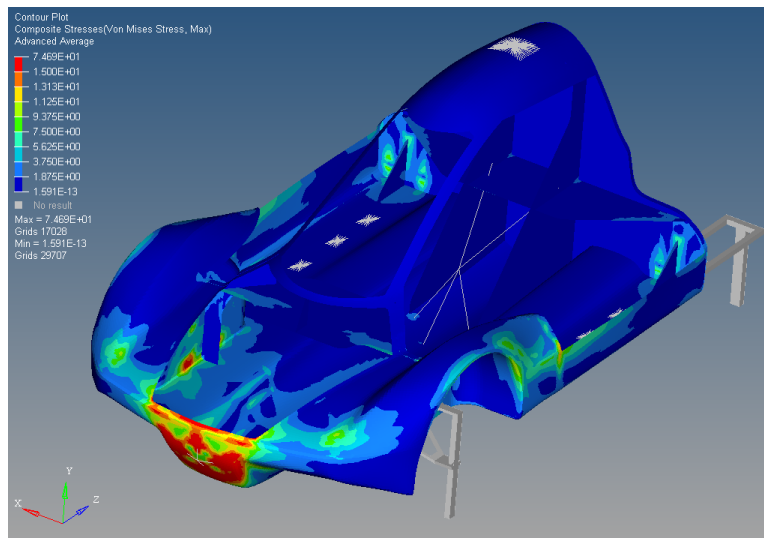


Figure 130: Stress contour plot, hook load

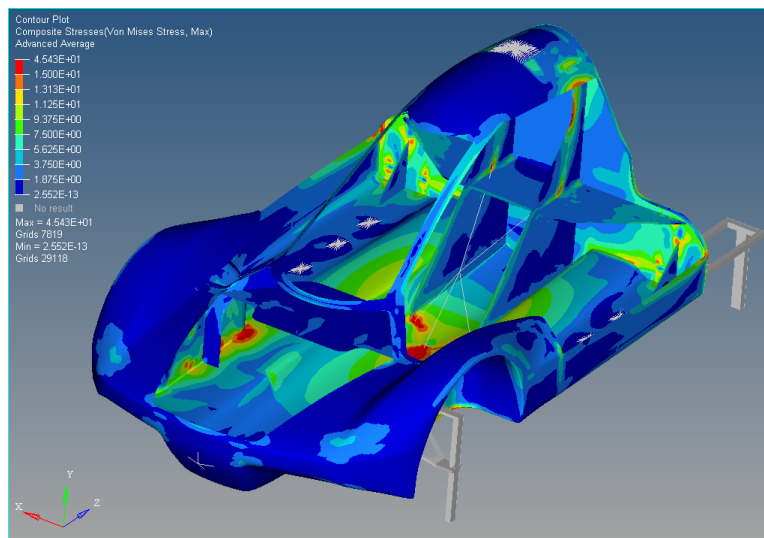


Figure 131: Stress contour plot, gravity in the negative Y direction

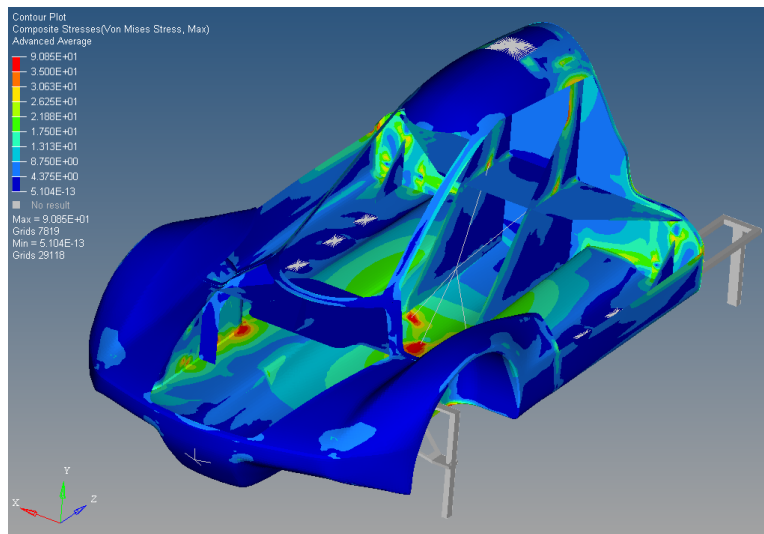
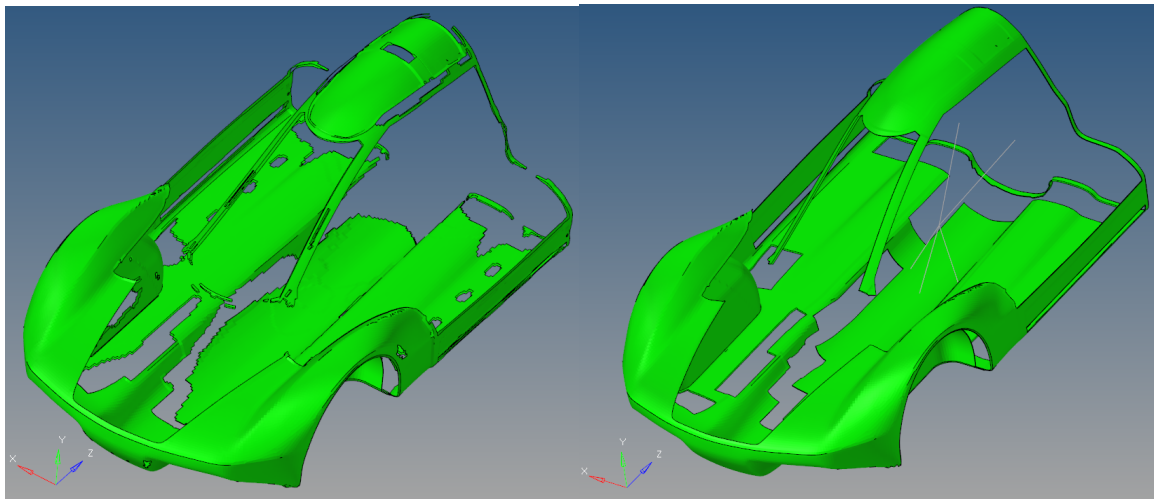


Figure 132: Stress contour plot, bump load

C Ply shapes

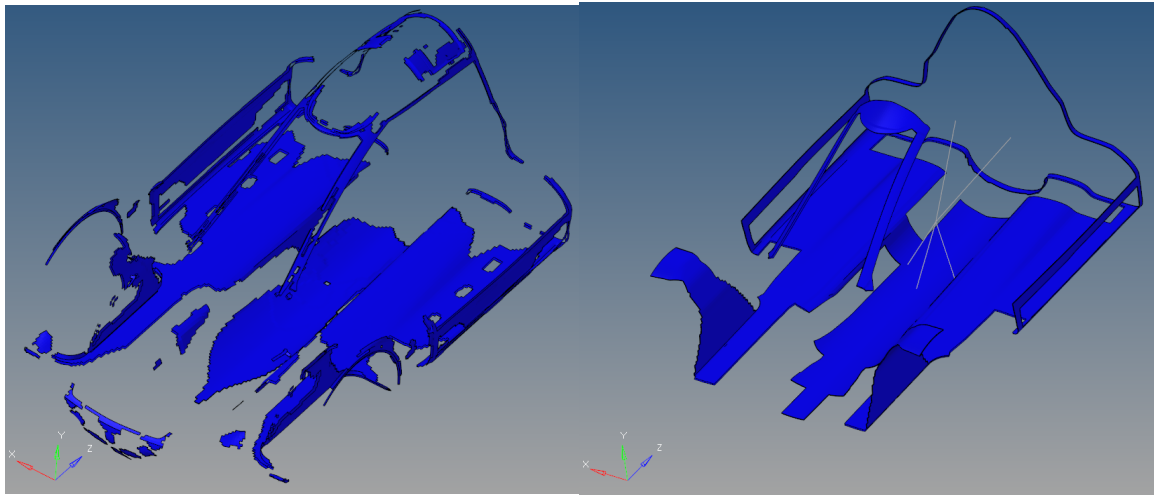
The figures below shows all ply shapes except the plies that cover the whole car. Ply 19 and 20 are the deleted cores, for that reason they are not observed here.



(a) Raw ply 2, 0 degrees

(b) Modified ply 2, 0 degrees

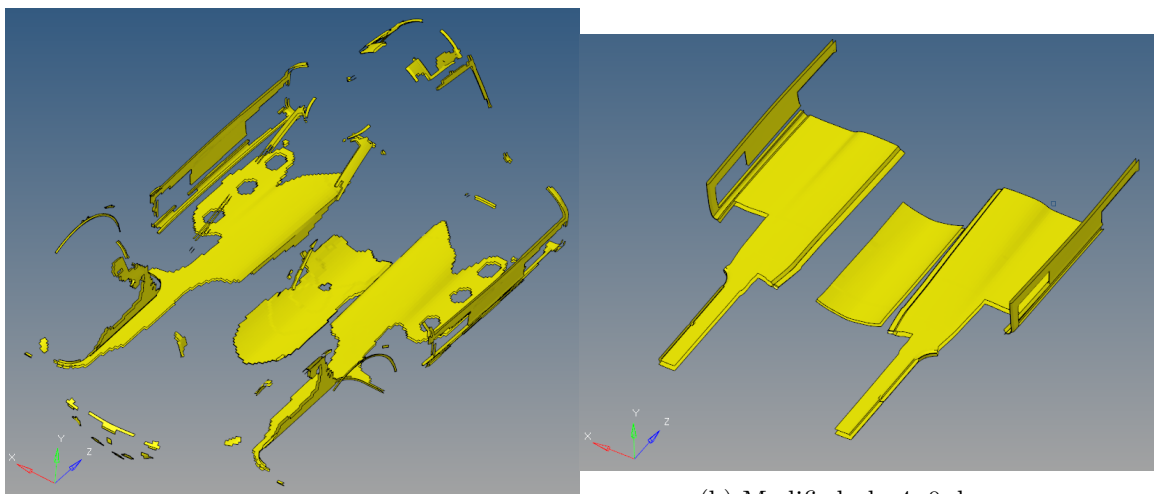
Figure 133



(a) Raw ply 3, 0 degrees

(b) Modified ply 3, 0 degrees

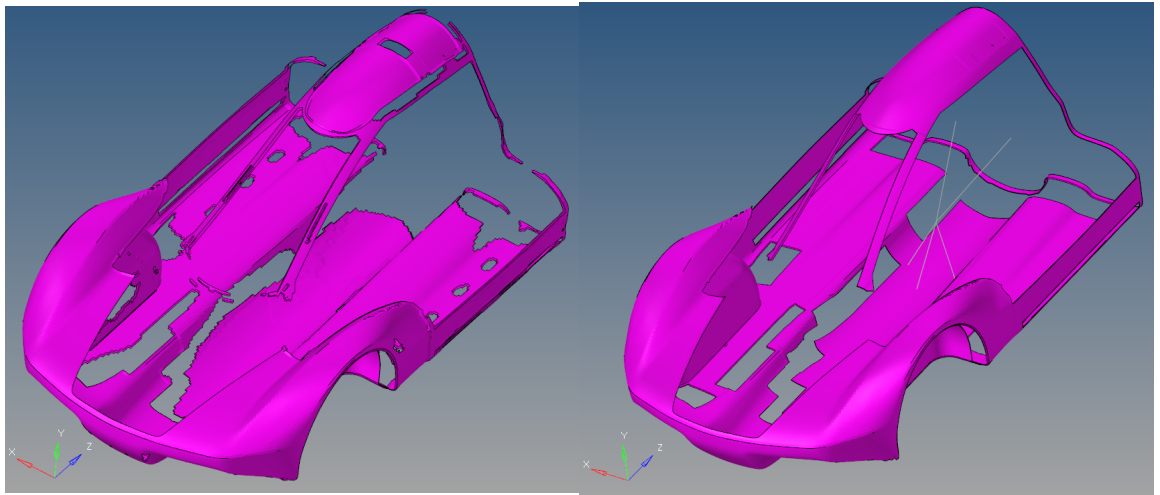
Figure 134



(a) Raw ply 4, 0 degrees

(b) Modified ply 4, 0 degrees

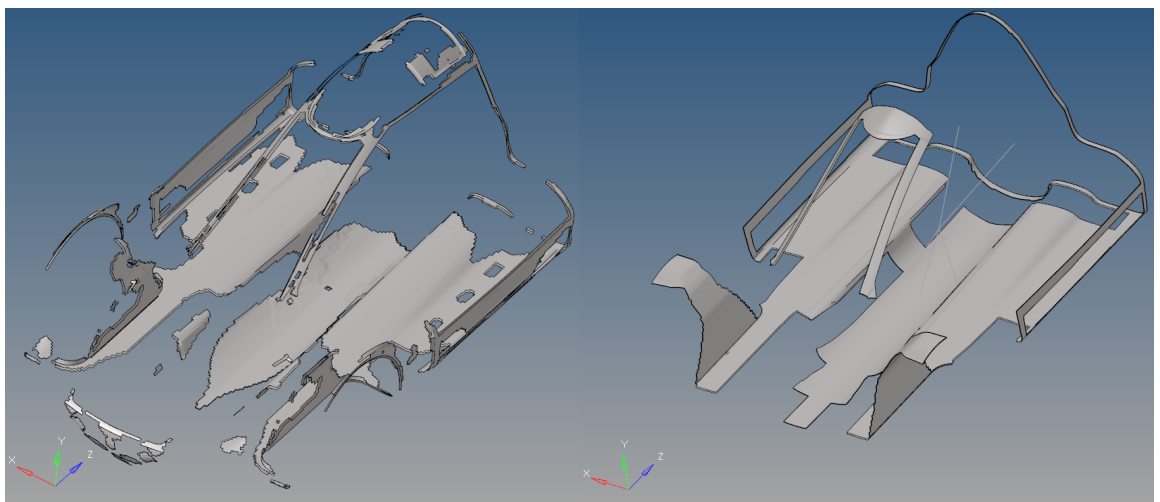
Figure 135



(a) Raw ply 6, 90 degrees

(b) Modified ply 6, 90 degrees

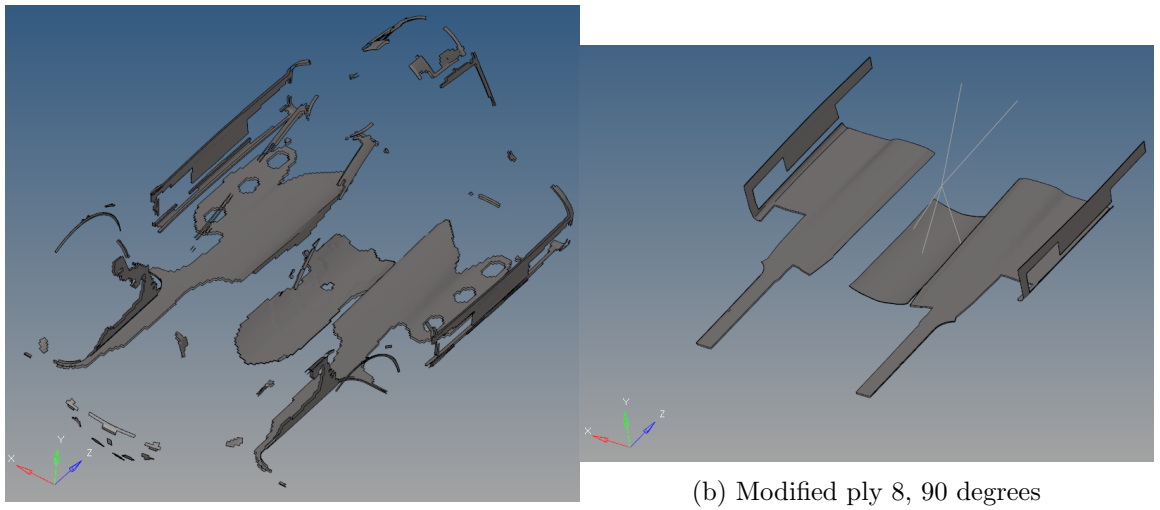
Figure 136



(a) Raw ply 7, 90 degrees

(b) Modified ply 7, 90 degrees

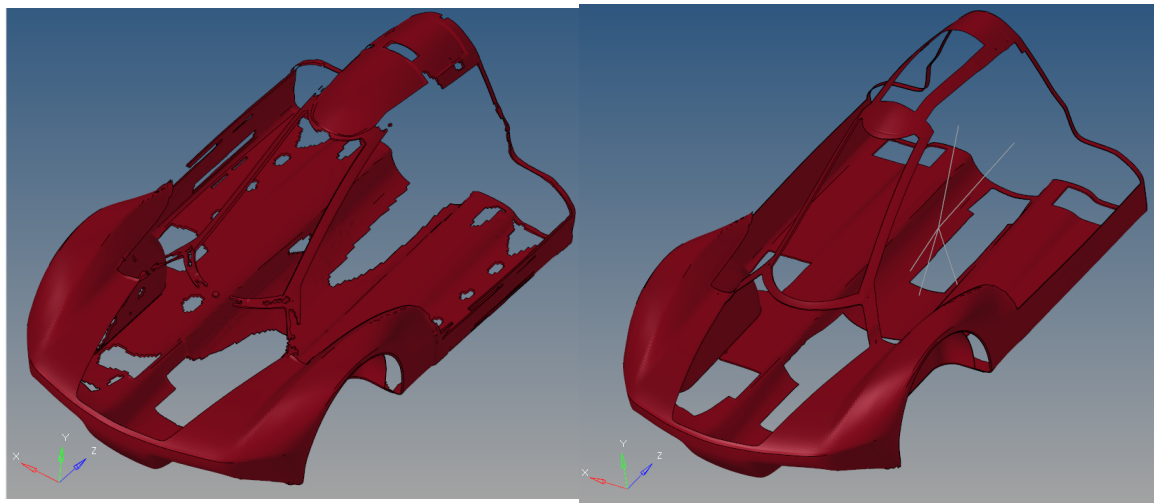
Figure 137



(a) Raw ply 8, 90 degrees

(b) Modified ply 8, 90 degrees

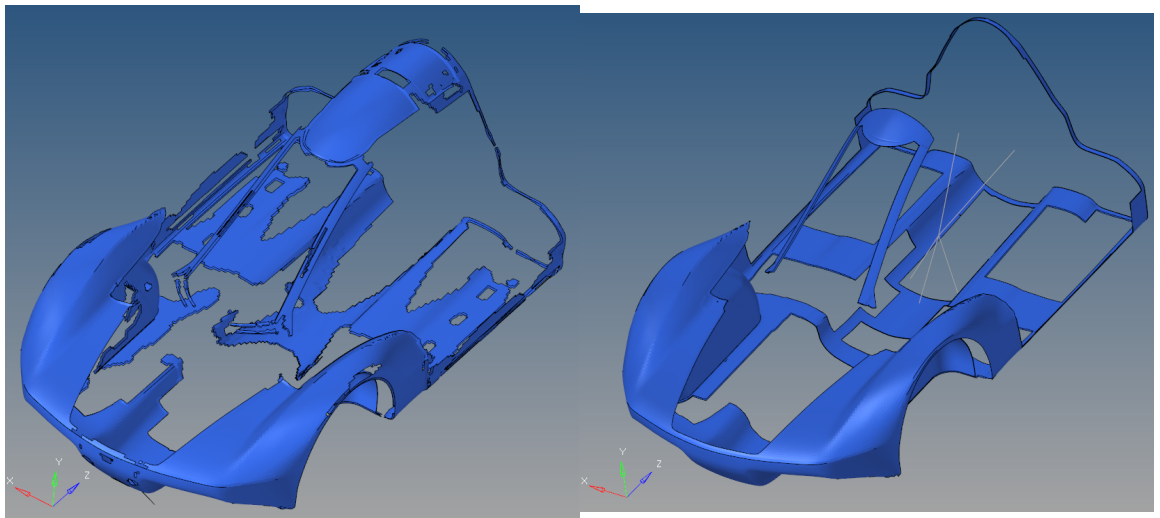
Figure 138



(a) Raw ply 10, 45 degrees

(b) Modified ply 10, 45 degrees

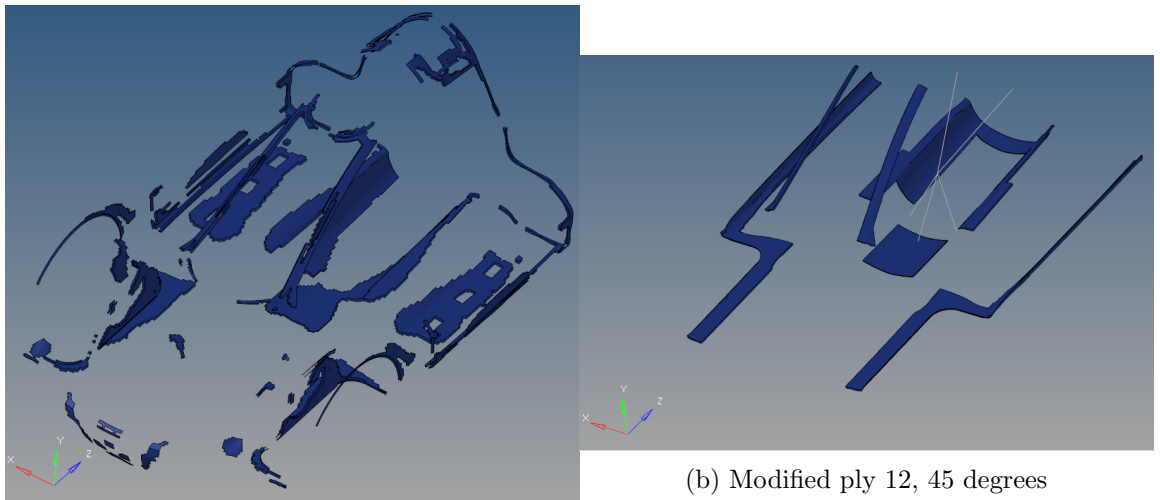
Figure 139



(a) Raw ply 11, 45 degrees

(b) Modified ply 11, 45 degrees

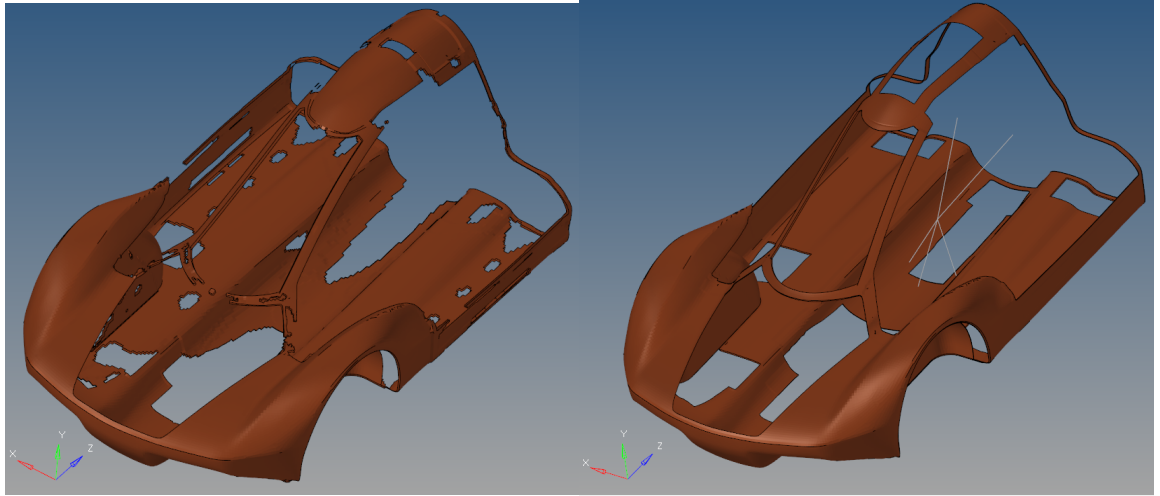
Figure 140



(a) Raw ply 12, 45 degrees

(b) Modified ply 12, 45 degrees

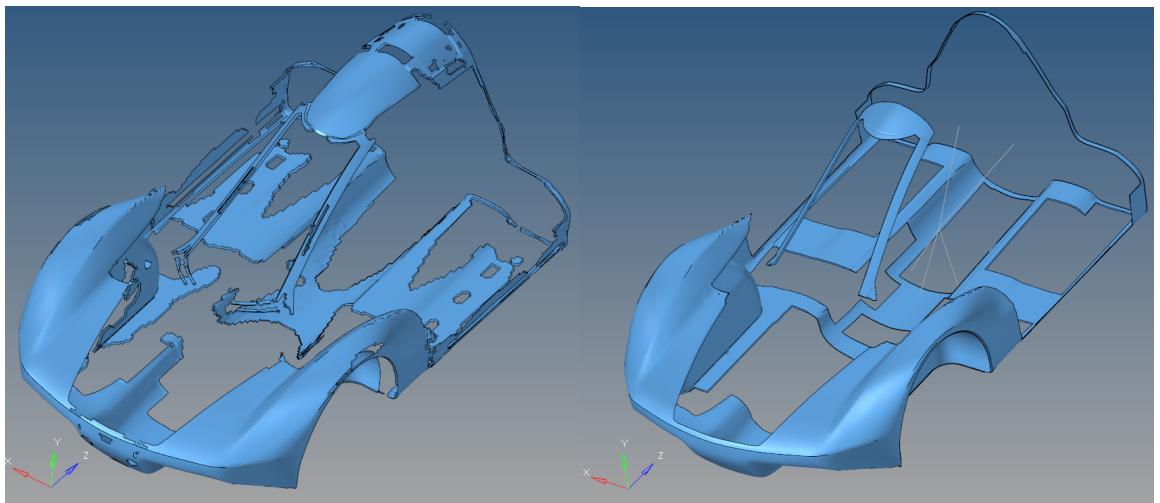
Figure 141



(a) Raw ply 14, -45 degrees

(b) Modified ply 14, -45 degrees

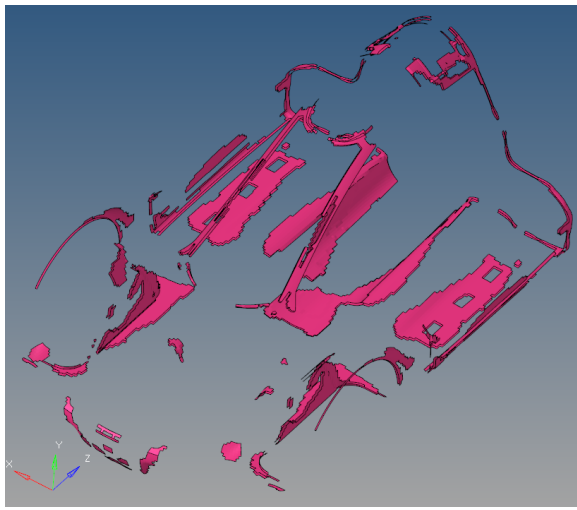
Figure 142



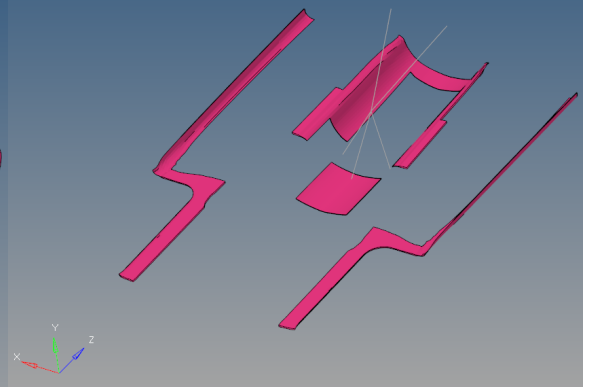
(a) Raw ply 15, -45 degrees

(b) Modified ply 15, -45 degrees

Figure 143

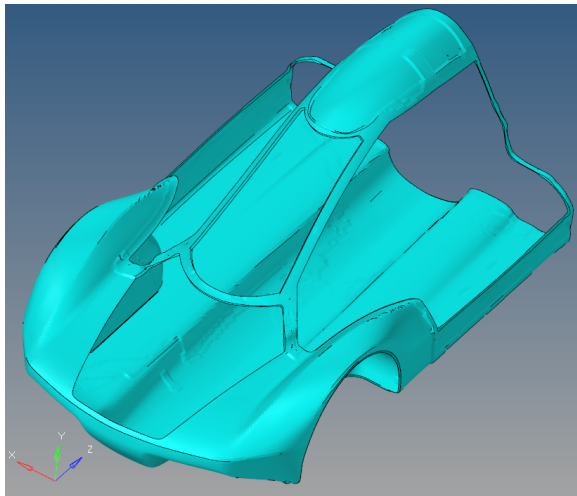


(a) Raw ply 16, -45 degrees

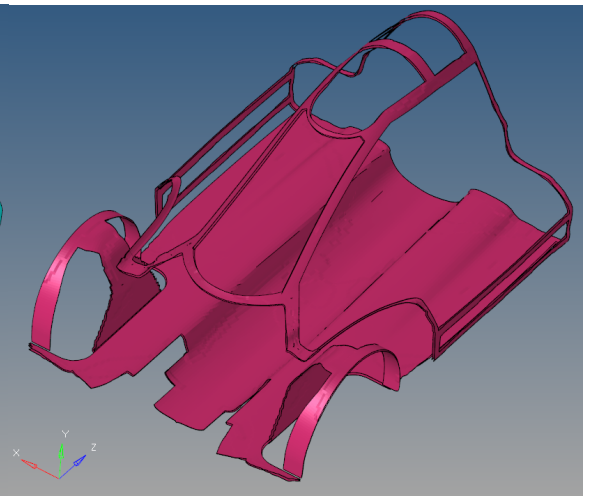


(b) Modified ply 16, -45 degrees

Figure 144



(a) Raw core, ply 17



(b) Modified core, ply 17, 5mm

Figure 145

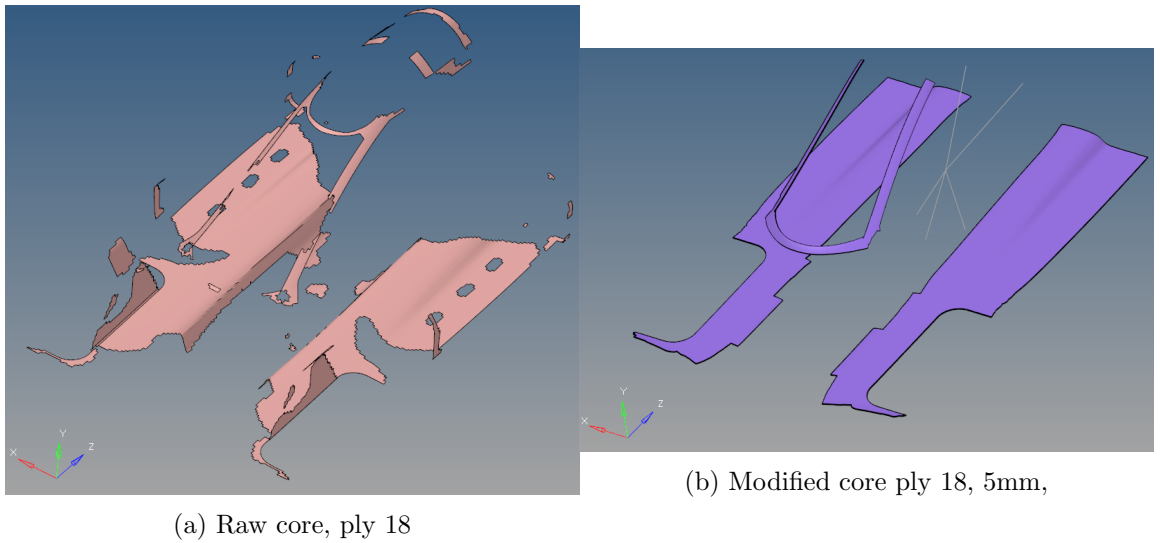


Figure 146

D Displacements for the final design

The figures below show the displacements after the last topology optimization that was done on the inner structure. Notice that only some parts of the car are showing, while the rest is transparent. The transparent parts shows displacements smaller than 1 mm. The colored areas show displacements equal to or greater than 1 mm. This tells how small displacements that exist on the monocoque.

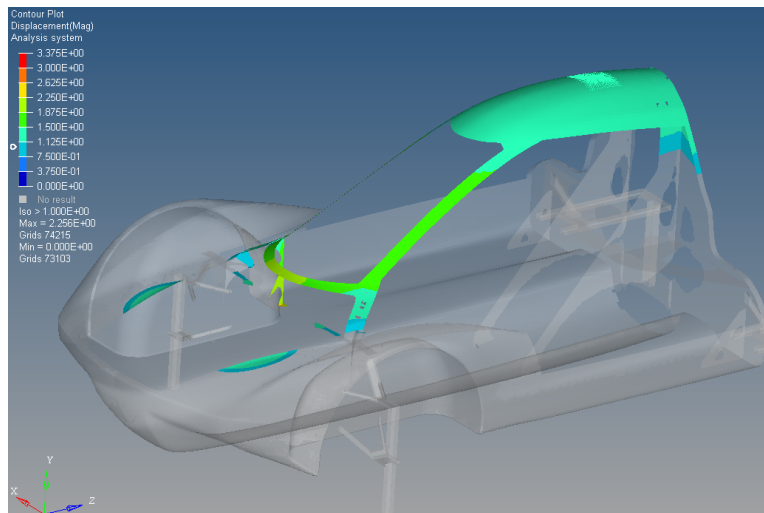


Figure 147: Displacement, roof load Z-direction

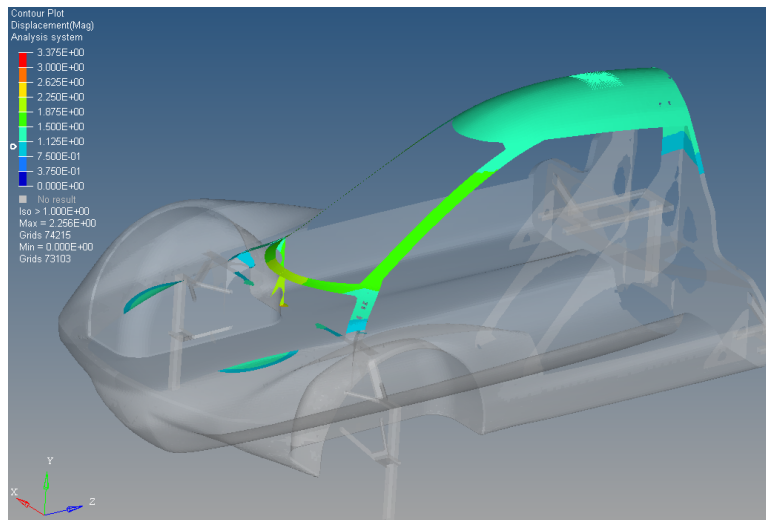


Figure 148: Displacement, roof load negative Z-direction

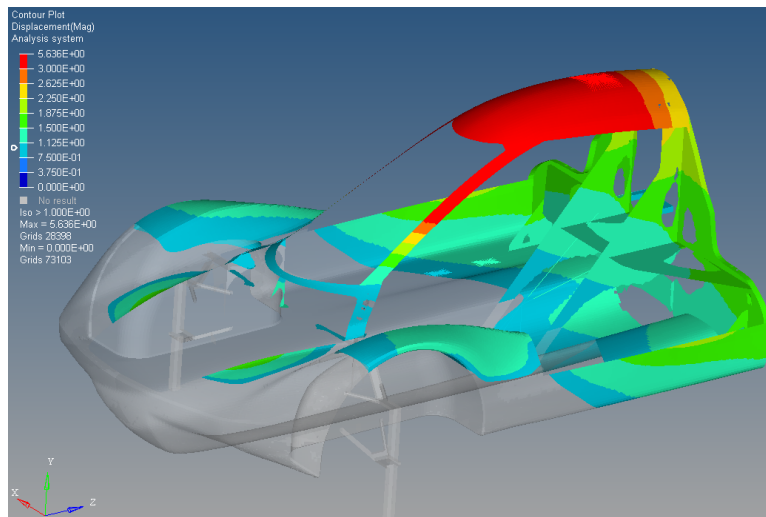


Figure 149: Displacement, roof load X-direction

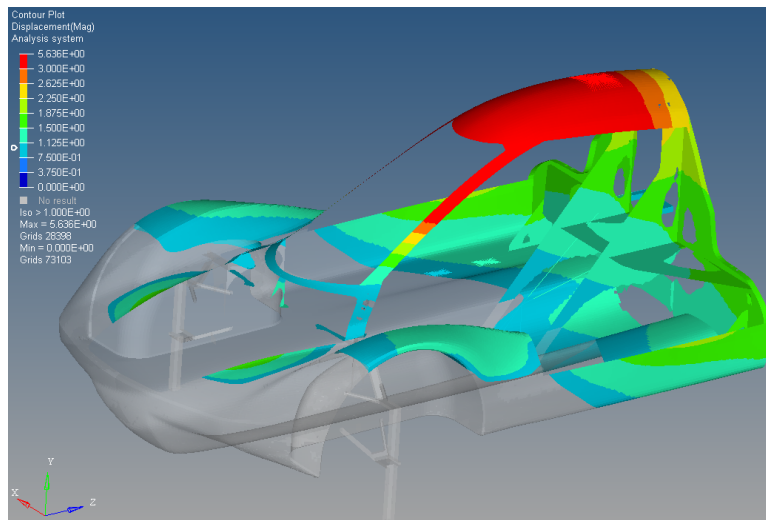


Figure 150: Displacement, roof load negative X-direction

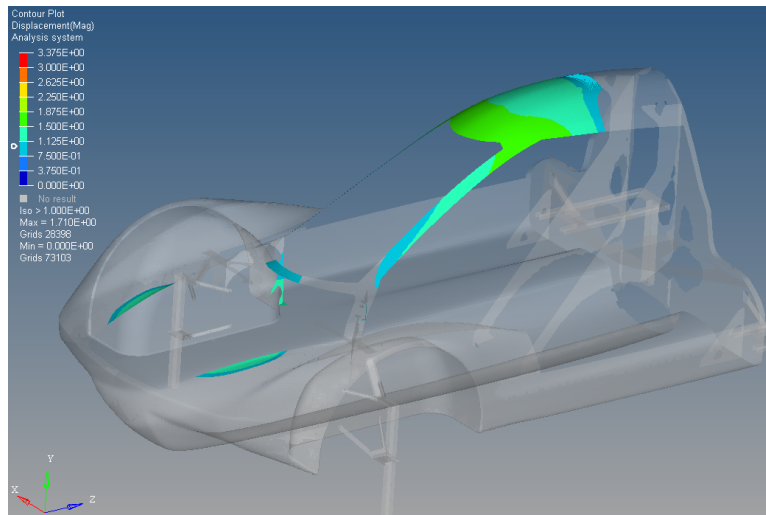


Figure 151: Displacement, roof load negative Y-direction

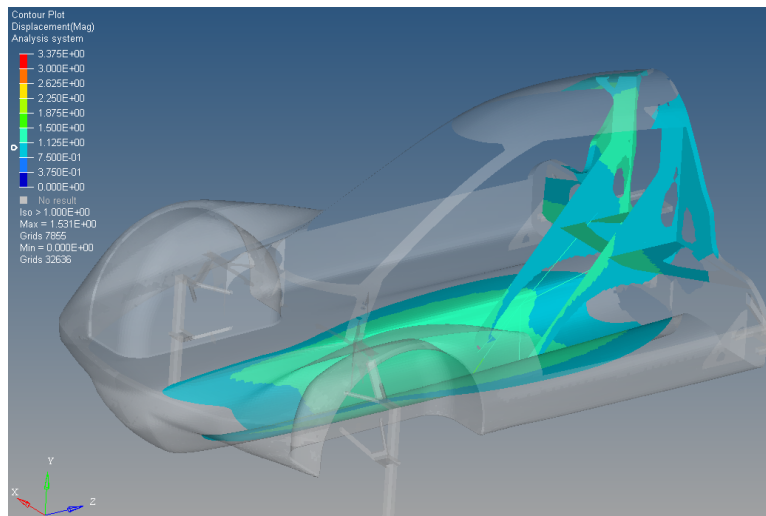


Figure 152: Displacement, braking front

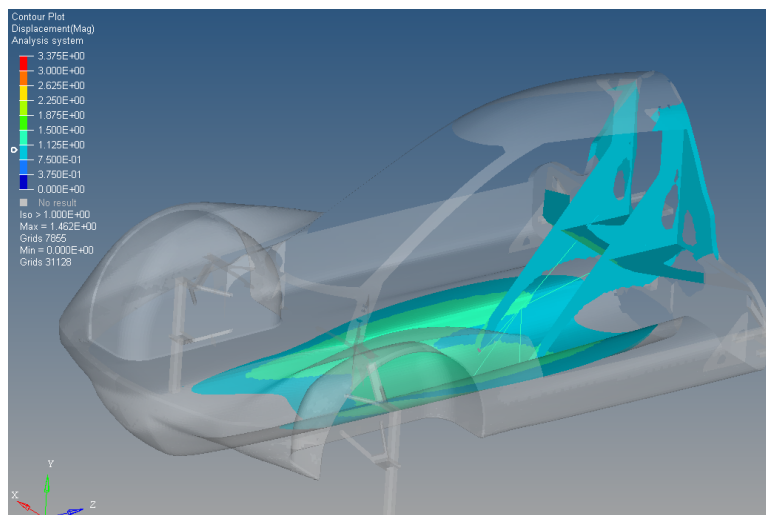


Figure 153: Displacement, braking back

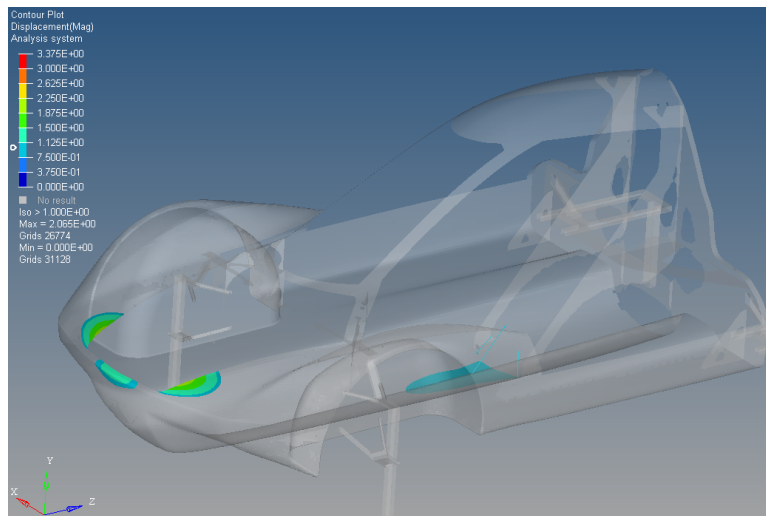


Figure 154: Displacement, braking all

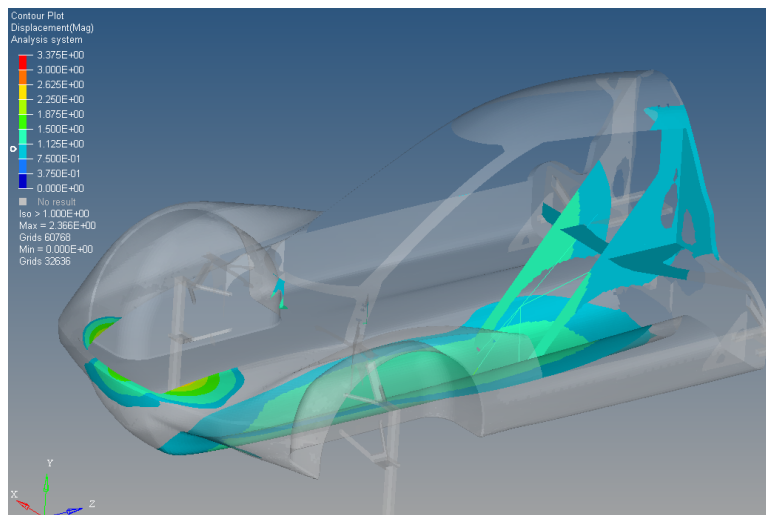


Figure 155: Displacement, turning left

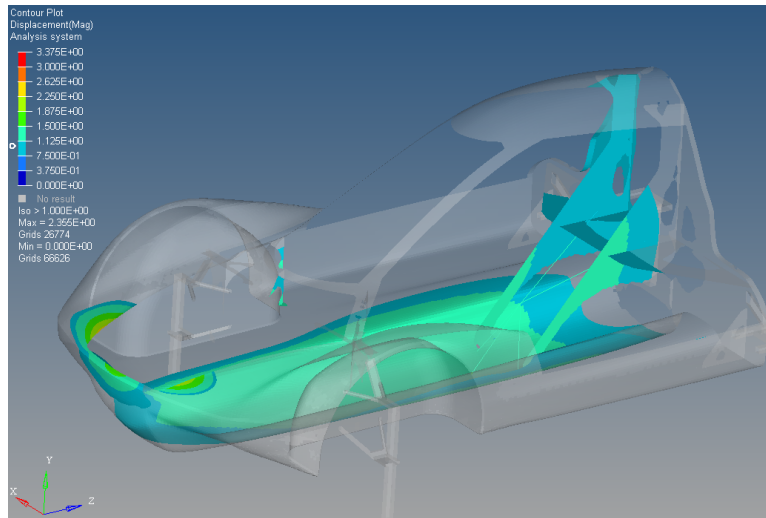


Figure 156: Displacement, turning right

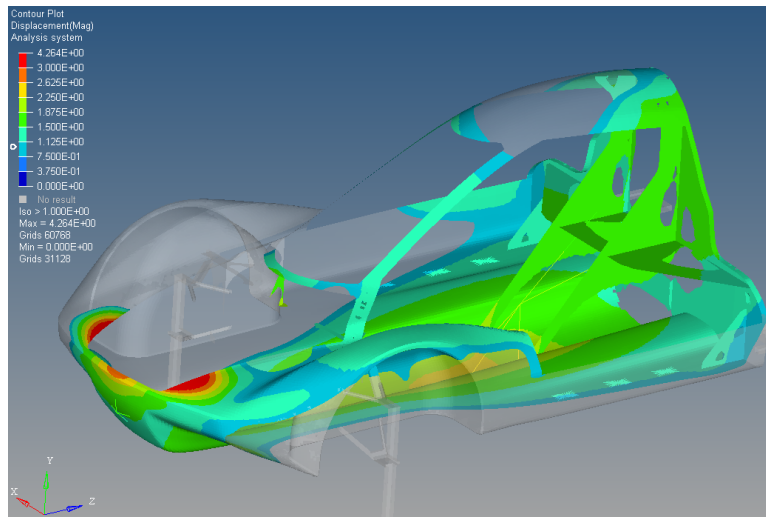


Figure 157: Displacement, braking and turning left

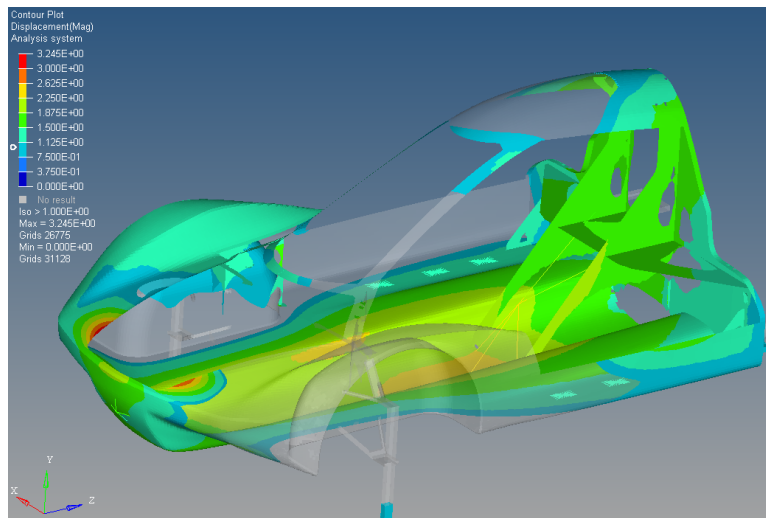


Figure 158: Displacement, braking and turning right

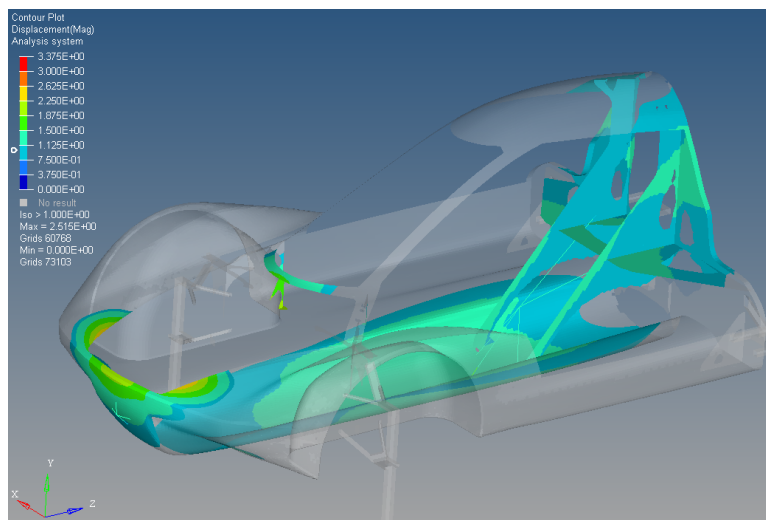


Figure 159: Displacement, gravity

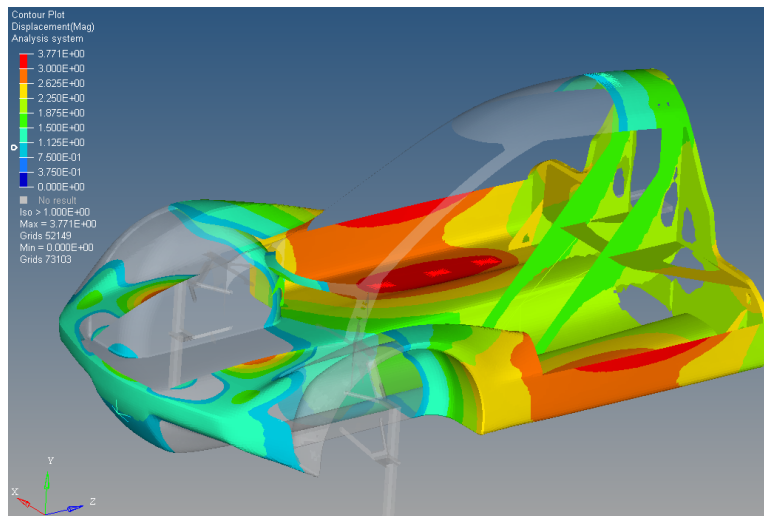


Figure 160: Displacement, step into the car

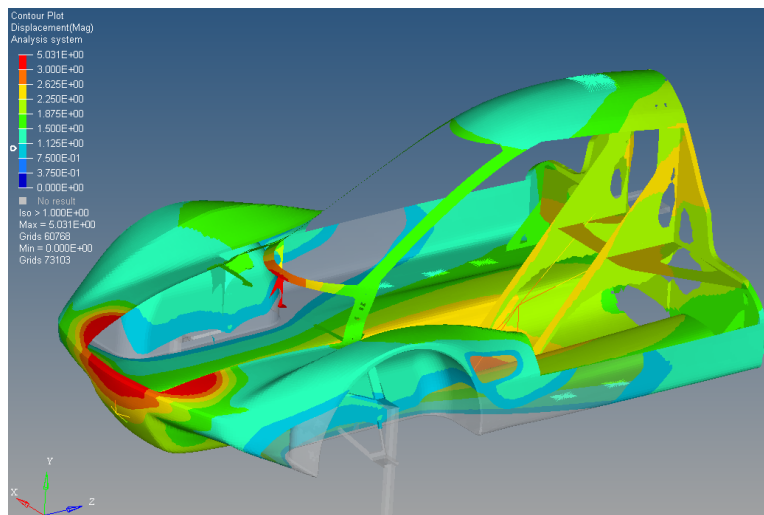


Figure 161: Displacement, bump

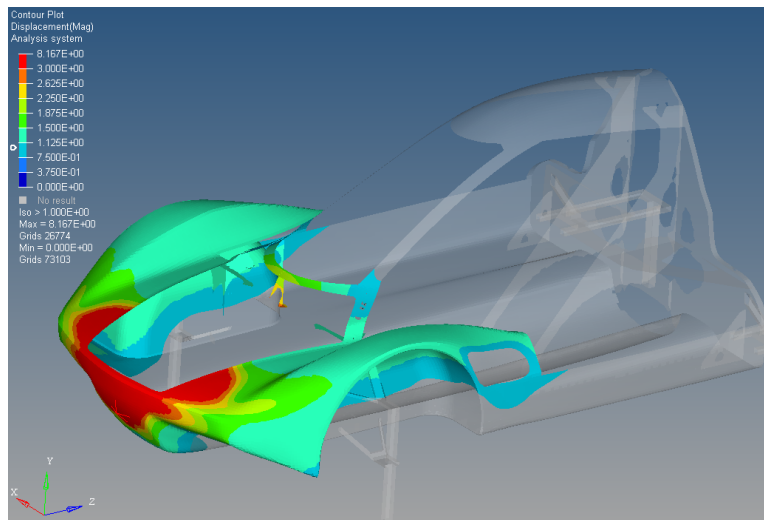


Figure 162: Displacement, hook

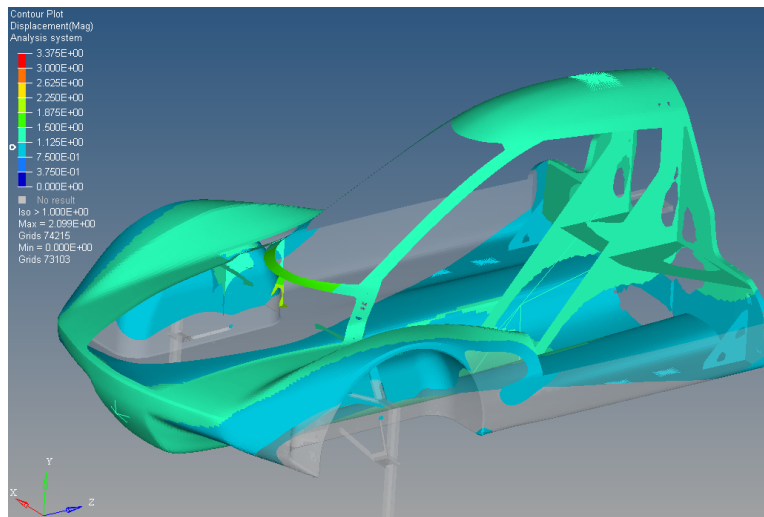


Figure 163: Displacement, seat belt

E Risk assessment

Detaljert Risikoreport

ID	33430	Status	Dato
Risikoområde	Risikovurdering: Helse, miljø og sikkerhet (HMS)	Opprettet	09.06.2019
Opprettet av	David Forrestad Swensen	Vurdering startet	10.06.2019
Ansvarlig	David Forrestad Swensen	Tiltak besluttet	
		Avsluttet	10.06.2019

Risikovurdering:
Støping av karbonfiber

Gyldig i perioden:
2/2/2019 - 6/9/2022

Sted:
NTNU Trondheim og HPC Sarpsborg

Mål / hensikt
Målet med risikovurderingen er å bli bevisst på eventuelle faremomenter som kan oppstå under støping av karbonfiber.

Bakgrunn
Bakgrunnen for risikoanalysen er at masteroppgaven som gjennomføres på NTNU har et krav om at en risikoanalyse skal gjennomføres

Beskrivelse og avgrensninger
NTNU Trondheim:
Flere to timers økter i uken i tre måneder
Antall personer for hver økt er ca. to, samtidig som det er andre studenter i rommet som kan bli påvirket av forsøkene

HPC
Varighet i en uke, 10 timers dager
Fem studenter fra NTNU, samt to ansatte hos HPC

Forutsetninger, antakelser og forenklinger
Det er forutsatt at det er god ventilasjon, da det er vifter som går i alle rom hvor karbonfiberstøpingen foregår.

Vedlegg
[Ingen registreringer]

Referanser
[Ingen registreringer]

16-19 

Norges teknisk-naturvitenskapelige universitet (NTNU)	Utskriftsdato:	Utskrift foretatt av:	Side:
Unntatt offentlighet jf. Offentlighetsloven § 14	10.06.2019	David Forrestad Swensen	1/16

Figure 164: Risk assessment

Oppsummering, resultat og endelig vurdering

I oppsummeringen presenteres en oversikt over farer og uønskede hendelser, samt resultat for det enkelte konsekvensområdet.















Farekilde:	Gassutslipp		
Uønsket hendelse:	Gass		
Konsekvensområde:	Helse Ytre miljø	Risiko før tiltak:  Risiko etter tiltak:  Risiko før tiltak:  Risiko etter tiltak: 	
Farekilde:	Kuttskader fra skarpe gjenstander		
Uønsket hendelse:	Saks		
Konsekvensområde:	Helse	Risiko før tiltak:  Risiko etter tiltak: 	
Farekilde:	Løse karbonfiber		
Uønsket hendelse:	Løse karbonfiber		
Konsekvensområde:	Helse	Risiko før tiltak:  Risiko etter tiltak: 	
Farekilde:	Karbonfiberstøv		
Uønsket hendelse:	Karbonfiberstøv		
Konsekvensområde:	Helse	Risiko før tiltak:  Risiko etter tiltak: 	
Farekilde:	Kompressor		
Uønsket hendelse:	Kompressor		
Konsekvensområde:	Helse	Risiko før tiltak:  Risiko etter tiltak: 	
Farekilde:	Varmelampe		
Uønsket hendelse:	Varmelampe		
Konsekvensområde:	Helse	Risiko før tiltak:  Risiko etter tiltak: 	

Figure 165: Risk assessment



Farekilde: Epoxy

Uønsket hendelse: Epoxy

Konsekvensområde: Helse

Risiko før tiltak: ● Risiko etter tiltak: ●

Endelig vurdering

Det er ingen kjent restrisiko etter denne vurderingen, og vurderingen er basert på få personer.

Figure 166: Risk assessment

Involverte enheter og personer

En risikovurdering kan gjelde for en, eller flere enheter i organisasjonen. Denne oversikten presenterer involverte enheter og personell for gjeldende risikovurdering.

Enhet /-er risikovurderingen omfatter

- NTNU

Deltakere

Lesere

[Ingen registreringer]

Andre involverte/interessenter

Kristoffer Tallaug Sydnes har et like stort ansvar som David Forrestad Swensen, da vi skriver masteroppgave sammen.

Følgende akseptkriterier er besluttet for risikoområdet Risikovurdering: Helse, miljø og sikkerhet (HMS):



Figure 167: Risk assessment

Oversikt over eksisterende, relevante tiltak som er hensyntatt i risikovurderingen

I tabellen under presenteres eksisterende tiltak som er hensyntatt ved vurdering av sannsynlighet og konsekvens for aktuelle uønskede hendelser.

Farekilde	Uønsket hendelse	Tiltak hensyntatt ved vurdering
Gassutslipp	Gass	Tiltak ved gassutslipp
Kuttskader fra skarpe gjenstander	Saks	Tiltak ved kuttskader
Løse karbonfiber	Løse karbonfiber	Tiltak ved løse karbonfiber
Karbonfiberstøv	Karbonfiberstøv	Tiltak mot innånding av karbonfiberstøv
	Karbonfiberstøv	Tiltak mot innånding av karbonfiberstøv
Kompressor	Kompressor	Tiltak mot feilbruk av kompressor
	Kompressor	Tiltak ved brann
	Kompressor	Tiltak ved brann
	Kompressor	Tiltak mot feilbruk av kompressor
Varmelampe	Varmelampe	Tiltak ved brann
	Varmelampe	Tiltak mot feilbruk av varmelampe
	Varmelampe	Tiltak ved brann
	Varmelampe	Tiltak mot feilbruk av varmelampe
Epoxy	Epoxy	Tiltak ved søl av epoxy
	Epoxy	Tiltak ved søl av epoxy

Eksisterende og relevante tiltak med beskrivelse:

Tiltak ved gassutslipp

God ventilasjon som fjerner gassen

Tiltak ved søl av epoxy

Bruk av neoprenhansker som beskytter hendene mot eventuelt søl av epoxy

Tiltak ved løse karbonfiber

Bruk av labfrakker eller heldekkene uniformer som hindrer karbonfiber i å feste seg på kropp

Tiltak ved kuttskader

Informere brukerne om hvor man kan finne førstehjelpsutstyr, samt lære brukerne opp i hvordan skarpe gjenstander skal håndteres

Tiltak ved brann

Orienterere brukerne om hvor brannslukningsapparatet og rømningsveier er plassert

Tiltak mot feilbruk av varmelampe

Opplæring på hvordan varmelampene skal brukes og hvordan de skal vedlikeholdes.

Tiltak mot feilbruk av kompressor

Opplære brukerne om hvordan kompressoren skal opereres

Figure 168: Risk assessment



Tiltak mot innånding av karbonfiberstøv
Bruk av heldekkende vernemasker og gode rutiner.

Figure 169: Risk assessment

Risikoanalyse med vurdering av sannsynlighet og konsekvens

I denne delen av rapporten presenteres detaljer dokumentasjon av de farer, uønskede hendelser og årsaker som er vurdert. Innledningsvis oppsummeres farer med tilhørende uønskede hendelser som er tatt med i vurderingen.

Følgende farer og uønskede hendelser er vurdert i denne risikovurderingen:

- **Gassutslipp**
 - Gass
- **Kuttskader fra skarpe gjenstander**
 - Saks
- **Løse karbonfiber**
 - Løse karbonfiber
- **Karbonfiberstøv**
 - Karbonfiberstøv
- **Kompressor**
 - Kompressor
- **Varmelampe**
 - Varmelampe
- **Epoxy**
 - Epoxy

Figure 170: Risk assessment

Detaljert oversikt over farekilder og uønskede hendelser:

Farekilde: Gassutslipp

Innånding av farlige gasser dannet av epoxy

Uønsket hendelse: Gass

Kan føre til skader i indreorganer ved store mengder av innånding

Årsak: Gassutslipp

Beskrivelse:
Dersom viftene slutter å fungere

Sannsynlighet for hendelsen (felles for alle konsekvensområder): **Svært lite sannsynlig (1)**

Kommentar:
Gode vifter som går hele tiden

Konsekvensområde: Helse

Vurdert konsekvens: **Stor (3)**

Kommentar: Skader på indre organer som kan gi varige skader

Risiko:



Konsekvensområde: Ytre miljø

Vurdert konsekvens: **Middels (2)**

Kommentar: Forurensning av miljøet

Risiko:



Figure 171: Risk assessment

Førekilde: Kuttskader fra skarpe gjenstander

Ved klipping av karbonfiber kan man kutte seg selv

Uønsket hendelse: Saks

Ved uforsiktig bruk kan man klippe seg selv i fingeren med en saks som brukes til å kutte fiber.

Årsak: Saks

Beskrivelse:

Man er ukonsentrert og kutter seg på fingeren

Sannsynlighet for hendelsen (felles for alle konsekvensområder):

Lite sannsynlig (2)

Kommentar:

Det finnes gode rutiner for karbonfiber kutting.

Konsekvensområde: Helse

Vurdert konsekvens: Liten (1)

Kommentar: Et kutt på en finger har ingen stor konsekvens

Risiko:



Figure 172: Risk assessment

Farekilde: Løse karbonfiber

Løse karbonfiber kan feste seg på kroppen til personene som jobber med fiberen

Unsket hendelse: Løse karbonfiber

Løse karbonfiber kan feste seg på kroppen til personer når karbonfiber kutting gjennomføres.

Årsak: Løse karbonfiber

Beskrivelse:

Ved klipping av karbonfiber vil det alltid løsne noen fiber som vil feste seg fast på kroppen til personene som utgjør klippingen

Sannsynlighet for hendelsen (felles for alle konsekvensområder): Svært sannsynlig (5)

Kommentar:

Karbonfiber vil alltid løsne når man kutter i karbonfiber

Konsekvensområde: Helse

Vurdert konsekvens: Liten (1)

Kommentar: Det vil kle i en dag, og bli borte ved en god dusj

Risiko:



Figure 173: Risk assessment

